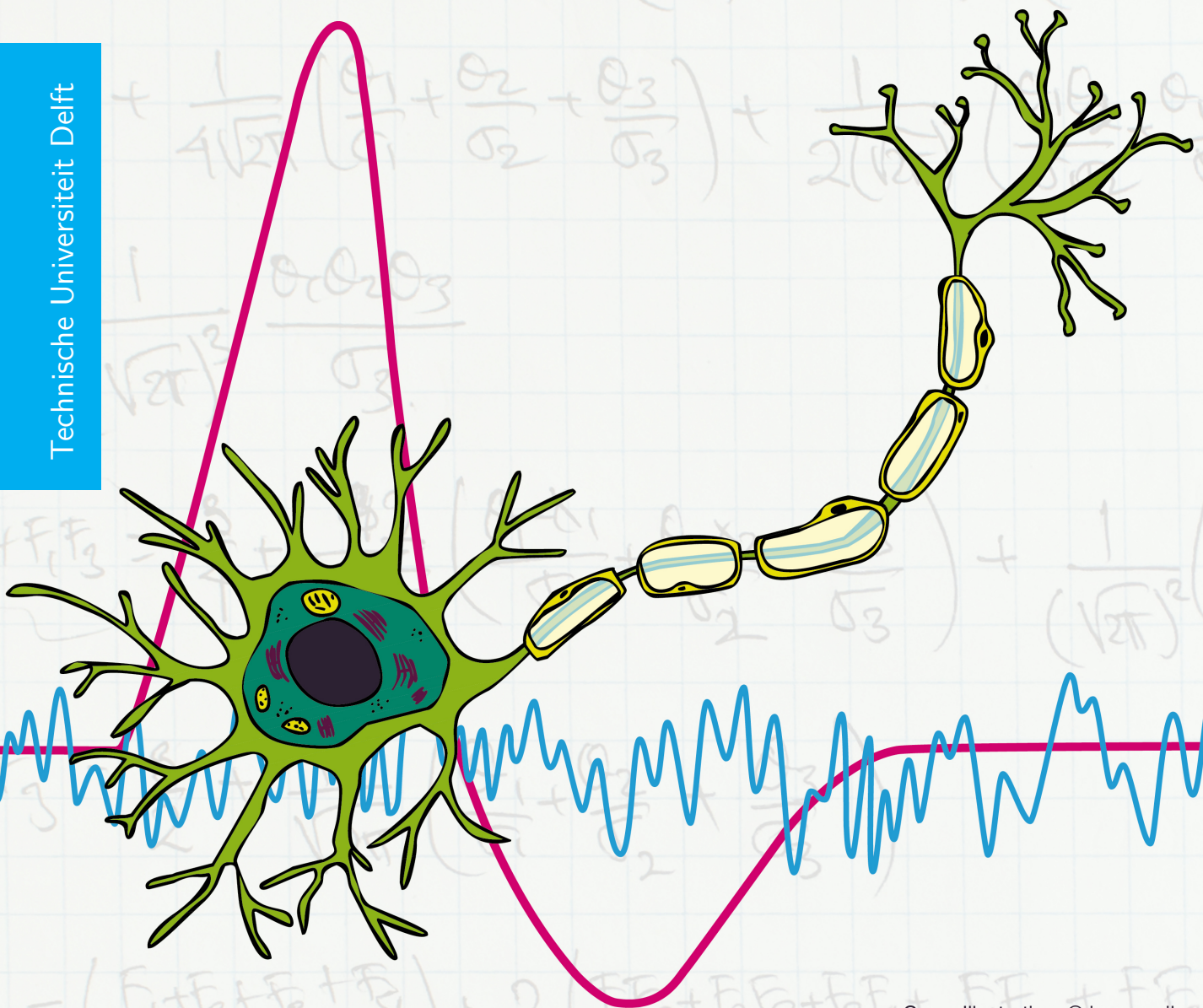# System Building Blocks for Mathematical Operators Using Stochastic Resonance

Application in an Action Potential Detection System

Insani Abdi Bangsa

TUDelft
Delft
University of
Technology

System Building Blocks for Mathematical Operators Using Stochastic Resonance

Application in an Action Potential Detection System

MASTER OF SCIENCE THESIS

for the degree of Master of Science in Biomedical Engineering
at Delft University of Technology

Insani Abdi Bangsa

October 25, 2017

Student number: 4491424
Thesis committee: Prof. dr. ir. W. A. Serdijn,   TU Delft (EE), supervisor
                    Dr. ir. J. H. Weber,   TU Delft (M)
                    Dr. D. M. J. Tax,   TU Delft (CS)

Faculty of Mechanical, Maritime and Materials Engineering (3mE)
Delft University of Technology

Abstract

Stochastic resonance (SR) is a phenomenon where the performance of a nonlinear system subjected to noise is better than it is without noise. This phenomenon can be found both in natural and artificial systems, especially in threshold-based systems such as comparators or a population of neurons. As noise always exists and interacts with the system, it is advantageous to design a system that purposefully uses SR to boost its performance.

One possible use of SR is in the signal reconstruction. In this application, noise is added to the input signal and is processed by a comparator to produce a 1-bit output signal. This output can be averaged to recover the amplified input signal.

In this thesis, three challenges regarding the use of SR in signal reconstruction are addressed. Firstly, to use SR not only to reconstruct the original signal, but also to implement mathematical operators, specifically a multiplier and an adder, that take two or more input signals. Secondly, to define the relevant metric(s) that can be used to measure the performance of the operators. Lastly, to build a system out of the proposed SR-based operators.

The SR-based mathematical operators are implemented on the system level with a comparator as its fundamental building block. To analyze the behavior of the operators, formulas for noise and distortion power are derived. MATLAB simulation is then used to verify the theoretical analysis. Finally, these SR-based mathematical operators are used to build a Teager Energy Operator (TEO) for action potentials (APs) detection.

An SR-based multiplier and adder can be implemented with the use of an XNOR logic gate and a binary half adder, respectively. The theoretical formulas are successful in predicting the noise and distortion behavior of the operators. In conclusion, it is possible to implement mathematical operators, specifically multipliers and adders, which use noise to boost their performance. The noise and distortion behavior of these operators can be predicted mathematically. Signal-to-noise ratio (SNR) and signal-to-noise-and-distortion ratio (SNDR) are used to measure the performance of the operators. Systems, specifically a TEO, can be built using the SR-based operators.

Keywords: stochastic resonance (SR), multiplier, adder, Teager Energy Operator (TEO)

Table of Contents

List of Figures

List of Tables

Acknowledgements

All praise be to Allah, for his blessing has allowed me to survive and complete my study in this university. At last, this project has come to an end. I officially started this in December 2016, although the project itself has been slowly built since May 2016. I am very grateful that I challenged myself to this strange new topic that I had never heard before. The experience of doing a curiosity-driven research, shaping my own goals and grasping for solutions in the dark sea of knowledge, surely will be beneficial for me in the future.

Firstly, I would like to thank my one and only supervisor, Prof. Wouter Serdijn, who has given me this amazing opportunity to work under his supervision and guide me through all my problems. I would also like to thank my research partner, Dieuwert Mul, for all the discussions, ideas, and inspirations. Special thanks are given to noise, especially Gaussian and uniform white noise, who are kind enough to collaborate with us and help me produce this wonderful thesis.

Secondly, I would like to thank the rest of my thesis committee, Dr. Jos Weber and Dr. David Tax, for willing to evaluate my work which I am not even sure they have heard about before. My thanks are also to the people with whom I had discussions: Jos Weber, Mario Negrello, Freek Hoebeek, and Patrick Forbes.

Thirdly, I would like to thank my parents and sister for their constant cheerings and obvious acting of understanding and being interested in my research. Next to them is all my Indonesian friends—PPI Delft, especially my BME friends: Affan, Dito, Irna, BJ, Hanif, Dika, and Niko, for all the studying and other activities we did together. Also, thanks to all the members in Bioelectronics Section, who have given me so much to learn during my study, and Irene Cécile, for helping me with the cover illustration.

Last but not least, I would like to express my gratitude to the Indonesia Endowment Fund (LPDP RI) scholarship for giving me the opportunity to actually study abroad and experience this unforgettable two years of learning in one of the greatest technical university in the world.

I hope this research does not end with me graduating, but can be continued to push the limit of electronics and signal processing fields.

Delft, University of Technology   Insani Abdi Bangsa
October 25, 2017

"Rather than make them our enemies, why not embrace them?"

Chapter 1

Introduction

Noise has been mostly considered as something undesirable in the world of signal processing. When mixed with a signal, it is thought to obstruct the extraction of information contained in the signal. However, the occurrence of a phenomenon called stochastic resonance shows that the presence of noise can improve the performance of a system.

1-1   Background

Stochastic resonance (SR) is a phenomenon where the contribution of noise to a nonlinear system can improve its performance. This phenomenon is found in various systems, both natural and artificial. Inspired by SR in neurons, where noise is used to improve the information transmission in neural circuits, various attempts to do signal reconstruction in threshold-based systems were made. Research found that by exploiting this phenomenon, the quality of information going through a "poor" system can be boosted. In the field of electronics engineering, this is an advantage in itself since these threshold-based systems can act as both an amplifier and a 1-bit analog-to-digital converter (ADC). Figure 1-1 shows the block diagram of an SR-based amplifier. The idea is to add noise (η) to the input signal (x) and process it with a threshold-based device, which implements a signum function, such as a clocked comparator to produce a 1-bit output signal (y_o). This output can then be averaged to recover the amplified input signal (y_{out}).
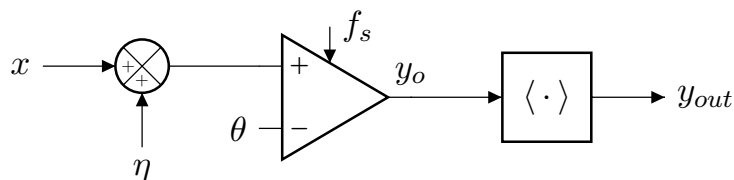
Figure 1-1: Block diagram of SR-based amplifier.

1-2   Research Questions

As mentioned in Section 1-1, SR can be used to improve the quality of signal information going through a system. This leads to the question whether the preserved signal information can be manipulated while still producing a 1-bit digital output. Therefore, the main research question of this thesis is:

"Is it possible to use the stochastic resonance (SR) phenomenon to manipulate information that is contained in the output signal?"

There are many ways to manipulate signals, the most obvious one is to perform mathematical operations on them. Therefore, this research question leads to three subquestions:

1. **Is it possible to implement mathematical operators using SR?**
   From so many mathematical operators, this thesis focuses on developing an alternative for multipliers and adders on the system level. Thus, to answer this question, this thesis develops a system-level alternative for signal multipliers and adders using SR.

2. **How can one define and predict the performance of the operators?**
   To examine the quality of the operators, it is necessary to define how to measure their performances. This thesis provides several performance metrics that are commonly used in SR research based on literatures. From these, one metric that is the most suitable for measuring the performance of the operators is chosen. After that, mathematical formulas are provided to predict the performance.

3. **Is it possible to build a system out of the SR-based math operators?**
   The proposed SR-based operators are used to implement the Teager Energy Operator (TEO), an energy operator that can function as an action potential (AP) detection system. The performance of the system is then examined.

1-3   Thesis Organization

The remainder of the thesis is organized as follows. In Chapter 2, a literature study on SR and TEO is presented. In Chapter 3, the SR-based multiplier is proposed. The theoretical background and its performance are also provided and analyzed. In Chapter 4, the SR-based adder is proposed, as well as its theoretical background and performance. In Chapter 5, the SR-based multiplier and adder are used to implement the TEO. In Chapter 6, the conclusions and recommendations for future work are described.

Stochastic Resonance and Teager Energy Operator: Definition and Properties

The purpose of this chapter is to describe and explain the stochastic resonance (SR) phenomenon and Teager Energy Operator (TEO) based on the conducted literature review. This chapter is mainly divided into two sections. In Section 2-1, the literature review of SR is discussed. The section covers the SR definition in Section 2-1-1, different types of SR in threshold-based systems in Section 2-1-2, the commonly used performance metrics in Section 2-1-3, and the performance comparison in Section 2-1-4 which discusses the best type of SR. Based on the literature study, the most suitable performance metric is chosen in Section 2-1-5. Section 2-2 discusses the review of a TEO. This consists of a definition of a TEO (Section 2-2-1), the operator's properties (Section 2-2-3), examples of well-known signals when processed by a TEO (Section 2-2-2), the effect of noise on the TEO (Section 2-2-4), its implementation (Section 2-2-5), and how a TEO can be used to detect action potentials (APs) in neurons (Section 2-2-6). Lastly, the conclusions are summarized in Section 2-3.

2-1 Stochastic Resonance (SR)

2-1-1 Definition of Stochastic Resonance

The term stochastic resonance (SR) was first introduced by Benzi et al. in [4] to explain the temperature "jump" between glacial and interglacial periods of approximately 10 K in an ice age. While the period directly correlates to the earth's orbital parameters, no existing model could reproduce this drastic change in temperature using the external periodic forces alone. The proposed model added a stochastic parameter based on a Wiener process in the commonly-thought deterministic energy-balanced model. The model proved that the drastic

temperature change is produced by the combination of external deterministic and internal stochastic forces.

Several attempts have been made to examine the occurrence of SR in different systems. Realizing that the system in [4] was modeled as a double-well potential, or in other words a bistable system, early research tended to look for SR in bistable systems, such as a Schmitt trigger [5] and a bidirectional ring laser [6]. It was not until 1993 when an SR occurrence was found in a single mechanoreceptor cell of a crayfish (*Procambarus clarkii*) [7]. The research was then taken further to prove that SR can occur in excitable systems [8]. In 1995, SR is discovered in aperiodic subthreshold signals [9]. Moreover, by using different measures of performance, it can also occur for aperiodic signal inputs which are strong enough to cross the threshold of the system, i.e. a suprathreshold signal [2].

Although Benzi et al. argued that the term "resonance" is indeed relevant in this situation, the use of the term has been thought as misleading due to the lack of resonant frequency as commonly understood in electrical engineering and signal processing [4, 5, 10]. However, McDonnell and Abbott in [11] pointed out that the term SR has been broadened and "resonance" should not be interpreted as it is in the classical term. Considering the fact that SR occurs not only in bistable systems with subthreshold periodic signals, a definition is proposed as "a phenomenon where the performance of a nonlinear system subjected by noise is better than it is without noise" [11]. The difference between the classical and stochastic resonance is illustrated in Figure 2-1.

(a) Classical Resonance   **(b)** Stochastic Resonance
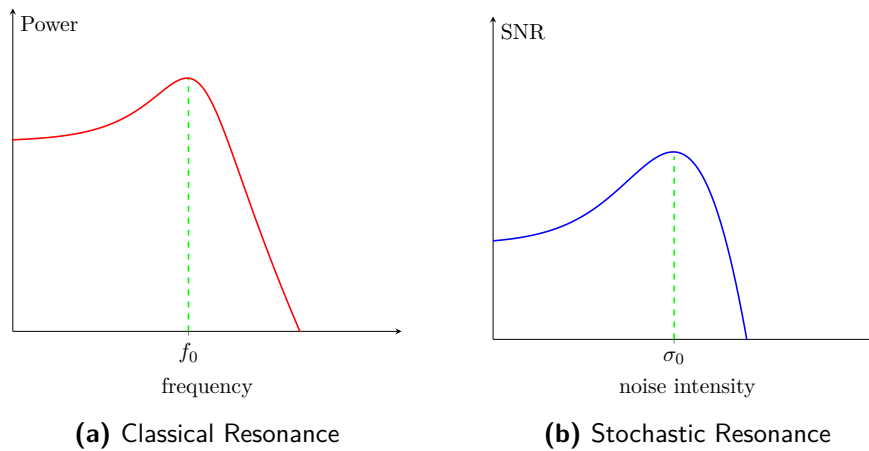
Figure 2-1: The difference between classical and stochastic resonance. (a) The classical resonance where the maximum power of the output signal is achieved for a specific resonant frequency. (b) The stochastic resonance where the optimal performance, in this case measured by the SNR, is achieved for a specific amount of noise.

2-1-2   Stochastic Resonance in Threshold-Based Systems

Biological excitable systems (i.e. neurons) found in nature work with the same principle as simple comparators to some extent. They both have low and high states, where the changes in the states happen when the input signal crosses a predetermined threshold level. However, comparators cannot mimic the refractory period characteristics of excitable systems. Despite
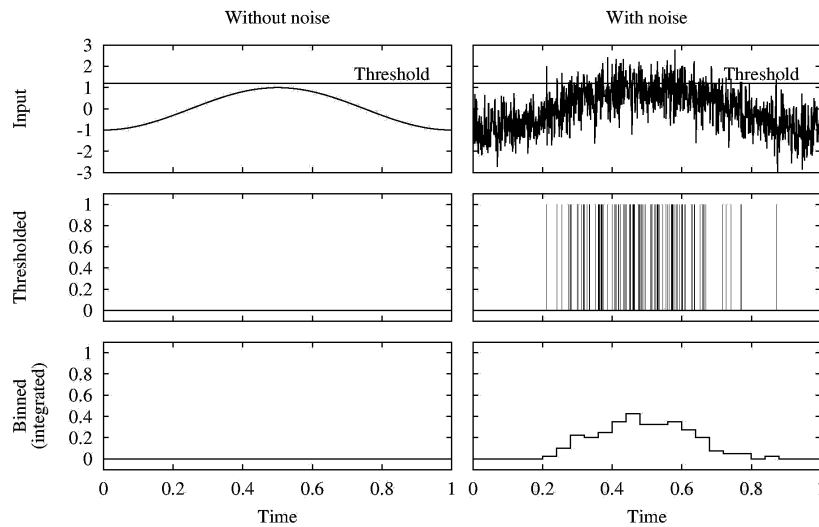
Figure 2-2: Illustration of subthreshold SR. Without noise, the output remains constantly in the low state. By adding noise, there are threshold-crossings happening when the signal is near the threshold level resulting in changes between the high and low state. (Figure taken from [1].)

the difference, it is interesting that SR has been found to occur in both systems for both subthreshold and suprathreshold signals [5, 7, 8, 9, 12].

Subthreshold Stochastic Resonance

Subthreshold SR occurs when a signal that is too small to cross the threshold level is subjected to noise at the input of the system [13]. Obviously the signal contribution alone will not produce anything (i.e. the change in states). However, the addition of noise, especially a strong enough noise, can help the signal to cross the threshold level when it is near the maximum value. This results in higher performance than that of a noiseless system. An illustration of subthreshold SR can be seen in Figure 2-2.

Similar to other bistable systems (i.e. having double-well potential function), simple comparators have the average time required for the signal to travel from one stable point to the other and back to the original point called Kramers time. The Kramers time, τ_k, is known to be proportional to the exponent of both the height of the potential barrier and the reciprocal of the noise variance [5, 13]. Mathematically,

$$\tau_k = \nu_k \propto \exp\left(\frac{\Delta U}{\sigma^2}\right),\tag{2-1}$$

where $\nu_k, \Delta U$, and σ are the Kramers rate, the height of the potential barrier, and the noise standard deviation, respectively. For a single sinusoidal input, the maximum signal-to-noise ratio (SNR) occurs when the Kramers rate and the input frequency are in the same order [5].

Suprathreshold Stochastic Resonance

Suprathreshold SR occurs when a suprathreshold signal is subjected to noise in arrays of threshold devices or a filtered threshold system, as illustrated in Figure 2-3. It was originally thought that SR could not occur for signals that already have enough power to cross the threshold [2]. However, Stocks in [14] showed that the switching of states due to the addition of the noise near the threshold can maximize the performance of the overall system. It was also shown that the maximum performance is reached when all the threshold values are set to the mean of the signal. An illustration of suprathreshold SR can be seen in Figure 2-4.

2-1-3   Performance Metrics of Stochastic Resonance

To indicate the occurrence of SR, it is necessary to decide on the performance metrics of the system. A system might display different SR behaviors for different performance metrics. It is also important to choose the metrics that really make sense in determining the performance of the system.

Signal-to-Noise Ratio (SNR)

Signal-to-noise ratio (SNR) is a performance metric used to measure how corrupted a signal in a system is compared to the perturbing noise. It is calculated by dividing the power of the signal by its noise, usually expressed in decibel (dB) [15]. Mathematically,

$$
\begin{aligned}
\mathrm{SNR}_{\mathrm{dB}} &= 10 \log_{10}\left(\frac{P_{\mathrm{signal}}}{P_{\mathrm{noise}}}\right) \\
&= 20 \log_{10}\left(\frac{A_{\mathrm{signal}}}{A_{\mathrm{noise}}}\right),
\end{aligned}
\tag{2-2}
$$

where P_{signal} and P_{noise} are signal and noise power, while A_{signal} and A_{noise} are root-mean-square (RMS) amplitude of the signal and noise, respectively, over the signal bandwidth.

In the history of SR, SNR is the most frequently used metric to measure the performance of the observed systems [5, 7, 8]. This comes simply from the fact that the signal used in the experiments are mostly a single period sinusoid. The occurrence of SR implies that there can be an SNR gain by adding noise to the system. This does not come as a surprise, since the nonlinearity of the system will spread out the power of noise over other frequencies, making the noise power in the bandwidth smaller than it would be in a linear system.

Though widely used in the electronics field, SNR gains are not necessarily effective in many signal processing fields. For instance, it does not always give the information on how closely the output signal resembles the input in terms of their shapes, which is important in signal reconstruction. One method to accommodate this pitfall is to use signal-to-noise-and-distortion ratio (SNDR), where the distortion signifies how different the output signal is with the ideal signal. Similar to SNR, SNDR is calculated by taking the quotient of the signal power with the "undesired" power, in this case the noise power and the power contributed by the distortion. Mathematically, it is formulated as

$$
\mathrm{SNDR}_{\mathrm{dB}} = 10 \log_{10}\left(\frac{P_{\mathrm{signal,\ ideal}}}{P_{\mathrm{noise}} + P_{\mathrm{distortion}}}\right),
\tag{2-3}
$$
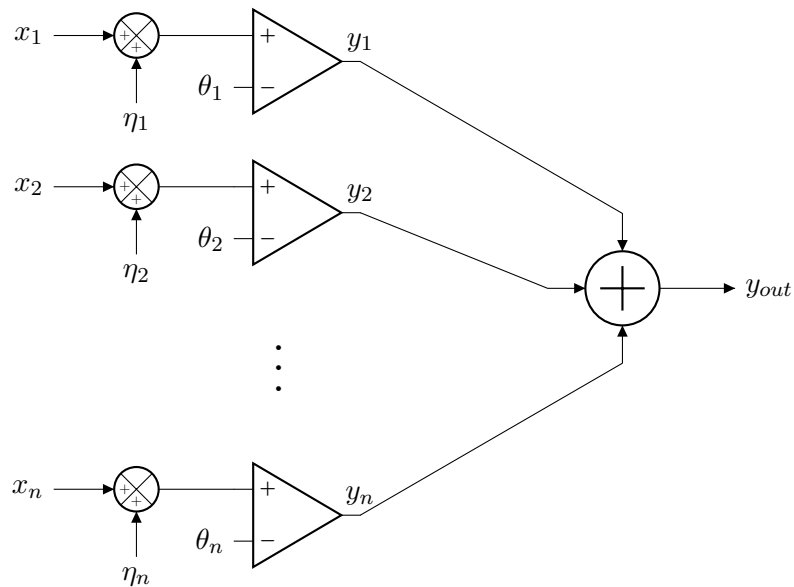
Figure 2-3: Arrays of threshold devices subjected to noise. The parallelization of the threshold systems works to average out the signal outliers, i.e. output noise. This arrangement can also be changed by cascading a filter after a threshold device.
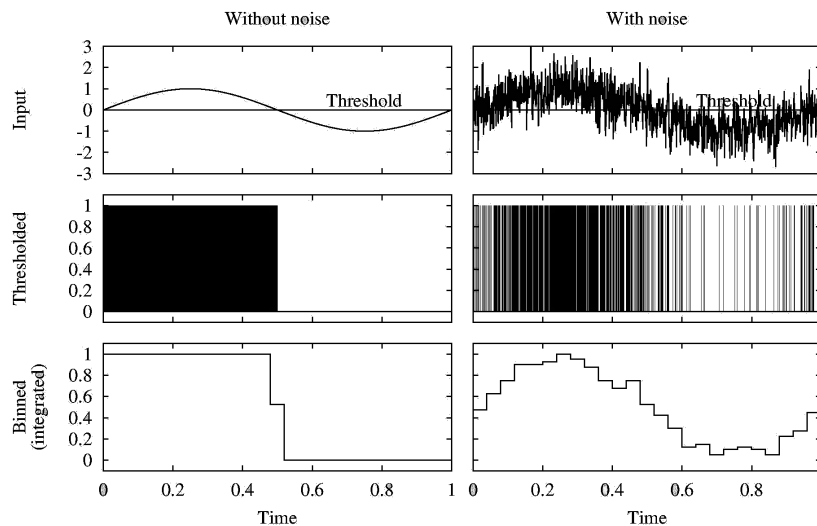
Figure 2-4: Illustration of suprathreshold SR. Without noise, the output is always in high state for positive amplitude and vice versa. By adding noise, changes between states occur more frequently, resulting in an output that, when integrated, more closely resembles the original signal. (Figure taken from [1].)

where $P_{\text{signal, ideal}}$, P_{noise}, and $P_{\text{distortion}}$ are the ideal signal, noise, and distortion power. It is important to distinguish the noise and distortion contribution, and this might be quite difficult to do because this suggests that one needs to be able to distinguish the ideal output signal, assuming the system is ideal, from the ideal "expected" output of the real system. It should also be noted that P_{signal} in (2-2) is different from $P_{\text{signal, ideal}}$ in (2-3). In (2-2), the signal still contains the distortion while the one in (2-3) is only the input signal multiplied by a certain gain or attenuation factor.

Mutual Information

One performance metric that can be used to quantify the similarity between two signals is mutual information. Mutual information is the amount of information from the input that is transmitted to the output, measured in bits. For a stochastic input and output with random variables X and Y, respectively, the mutual information is formulated as

$$I(X,Y) = \int_X \int_Y f_{XY}(x,y) \log_2 \left(\frac{f_{XY}(x,y)}{f_X(x)f_Y(y)} \right) \mathrm{d}x \, \mathrm{d}y \,, \tag{2-4}$$

where f_X, and f_Y are the probability density function (PDF) of X and Y, while f_{XY} is the joint PDF of both random variables.

The mutual information can also be written as

$$I(X,Y) = H(Y) - H(Y \,|\, X), \tag{2-5}$$

where $H(\cdot)$ is an information entropy, which is the average amount of information contained in each signal, mathematically defined by

$$\begin{aligned} H(Y) &\stackrel{\text{def}}{=} \mathbf{E}\left[I(Y)\right] \\ &= -\int_Y f_Y(y) \log_2 f_Y(y) \, \mathrm{d}y \,. \end{aligned} \tag{2-6}$$

Consequently, the conditional entropy can be calculated by substituting the random variable Y in (2-6) with $Y \,|\, X$. The existence of two variables requires double integrals, which results in

$$H(Y \,|\, X) = -\int_X \int_Y f_{XY}(x,y) \log_2 \left(\frac{f_{XY}(x,y)}{f_X(x)} \right) \mathrm{d}x \, \mathrm{d}y \,. \tag{2-7}$$

In the case of X and Y (i.e. the input and output signals) being statistically independent, (2-7) will be equal to (2-6). Hence, $I(X,Y)$ will be equal to zero [16].

In threshold-based systems, a finite and countable number of output states make it similar to a semi-infinite channel [17]. Therefore, (2-5) can be written as

$$I(X,Y) = -\sum_Y \Pr(y) \log_2 \Pr(y) - \left(-\int_X f_X(x) \sum_Y \Pr(y \,|\, x) \log_2 \Pr(y \,|\, x) \, \mathrm{d}x \right). \tag{2-8}$$

The use of mutual information provides an advantage in quantifying the interdependence between the input and output signals. It also gives an opportunity to effectively calculate the performance for non-sinusoidal signals, especially signals with a given PDF. The maximum value of $I(x,y)$ is achieved when all information contained in X is transferred to Y, i.e. $H(Y) = H(X)$. However, this is ineffective in the case of deterministic input signals since, for deterministic signals, $\Pr(y \,|\, x)$ will be either 0 or 1.

Correlation Coefficient

Another way to measure the similarity of input and output signals is by using the correlation coefficient [12]. This is a more general measure of the normalized power norm, which was proposed by Collins et al. in [9] to detect the occurrence of aperiodic SR in the FitzHugh-Nagumo (FHN) neuron model. Instead of comparing the input signal with the mean firing rate as in the normalized power norm, the correlation coefficient compares the input and output signals directly through calculating the covariance. Therefore, it can be used for non-excitable systems. The correlation coefficient is calculated as

$$
\begin{aligned}
\rho_{x,y} &= \frac{\mathrm{cov}[x,y]}{\sqrt{\mathrm{var}[x]\mathrm{var}[y]}} \\
&= \frac{\mathbf{E}[xy] - \mathbf{E}[x]\mathbf{E}[y]}{\sqrt{\mathrm{var}[x]\mathrm{var}[y]}},
\end{aligned}
\tag{2-9}
$$

where x and y are the input and output signals of the system, respectively. This is convenient for signal reconstruction measures, because the correlation coefficient is bounded between -1 and $+1$. Similar to mutual information, for statistically independent input-output pairs, $\rho_{x,y}$ will be equal to zero.

Since the correlation coefficient is initially used to quantify the linear correlation of two data (or, in this case, signals), it might seem strange to use this as a measure for SR, which can only occur in nonlinear systems. However, McDonnell et al. argued that it just means that the $\rho_{x,y}$ can never be equal to one. Moreover, different from linear systems, where high correlation means high information content, high $\rho_{x,y}$ in nonlinear systems cannot be interpreted as high mutual information [12].

2-1-4 Performance Comparison

For a simple threshold-based system with input signal x, threshold level θ, and subjected to noise η, its output y can be formulated as

$$
y = \mathrm{sgn}[x + \eta - \theta],
\tag{2-10}
$$

where $\mathrm{sgn}[\cdot]$, i.e. the signum function, takes value of either $+1$ or -1 depending on whether $x + \eta - \theta \geq 0$ or not. From (2-10), it can be seen that, besides the signal itself, the intensity of noise and the threshold level also determine the performance of the system.

Maximizing the performance of the system can be thought of as ensuring the frequency of the combination of the signal and noise crossing the threshold level. In general, the performance of subthreshold SR systems is lower than that of suprathreshold SR systems. This is due to the fact that the probability of a subthreshold signal crossing the threshold level is much lower than that of a suprathreshold signal. In other words, subthreshold SR systems will preserve less information. When reconstructed, the decoded subthreshold signal might not be able to resemble its input form for the part that is far from the threshold level, resulting in smaller correlation coefficient. However, the performance for subthreshold SR systems can be increased by minimizing the distance between the peak of the signal and the threshold level. For instance, Collins et al. claimed that the normalized power norm, i.e. correlation coefficient, of their FHN model could reach approximately 0.9 [9].

Figure 2-5 illustrates the mutual information for various threshold levels θ and noise intensities σ. The standard deviation of the input signal is set to one. It can be seen that the performance drops as the threshold level increases. Moreover, SR occurs for higher noise intensity for every increase in the threshold level. This is fairly logical since as the distance between the input and threshold increases, more energy provided by the noise is necessary to switch the output states.

Kawaguchi et al. in [3] simulate the change of mutual information in relation to a mixture of subthreshold and suprathreshold stimuli in a population of neuron models, as shown in Figure 2-6. RSL denotes the ratio of neurons that are stimulated by suprathreshold stimuli to the total population of neurons, where RSL = 1.0 means that the entire population of neurons is subjected to suprathreshold stimuli. The result of the research shows that the maximum performance can be achieved by subjecting the entire population of neurons to suprathreshold signals. Based on these findings, it can be concluded that suprathreshold SR is more advantageous than subthreshold SR in achieving the maximum performance of a system.

2-1-5   Choosing the Most Suitable Performance Metric for Mathematical Operators

From the explanations in Section 2-1-3, it can be concluded that there is no absolute best metric to measure the performance of a system. Rather than that, it makes more sense to choose the most suitable metric that can accurately quantify the performance of a system, based on its purpose(s). Therefore, it is important to first examine the purpose of the system of interest.

This thesis will focus on building mathematical operators based on the SR phenomenon as mentioned in Chapter 1. Mathematical operators, such as adders and multipliers, take two or more inputs and produce an output that corresponds to the property of the operation. For example, a multiplier can take two inputs and generate an output that is a multiplication of both inputs. It is not hard to argue that, especially for input signals in time domain, the performance of mathematical operators are defined more in the resemblance of the shape of the output signal rather than the information entropy. Thus, the mutual information is unfit as a performance metric for mathematical operators.

Secondly, this research is conducted with a vision that the proposed designs can be implemented in electronic circuits in the future. In electronics engineering, the terms SNR and SNDR are far more familiar than the correlation coefficient as noises and distortions are well-understood. Therefore, in this thesis, SNR and SNDR will be used as the measure of performance for the next chapters.

2-2   Teager Energy Operator (TEO)

2-2-1   TEO as an Algorithm to Calculate the "Energy" of a Signal

The Teager Energy Operator (TEO) or Nonlinear Energy Operator (NEO) is an algorithm to calculate the energy necessary to generate a signal [18]. It is inspired by the fact that
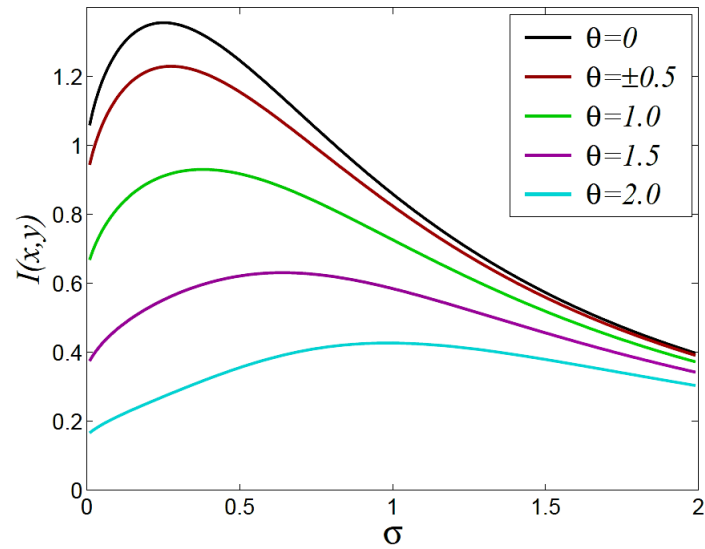
Figure 2-5: Illustration on mutual information $I(x, y)$ as a function of noise intensity σ for various threshold levels θ. Since the signal and noise have even PDFs, $\theta = +0.5$ and $\theta = -0.5$ produce the same performance. The further θ is from 0, the lower $I(x, y)$ is. (Figure taken from [2].)
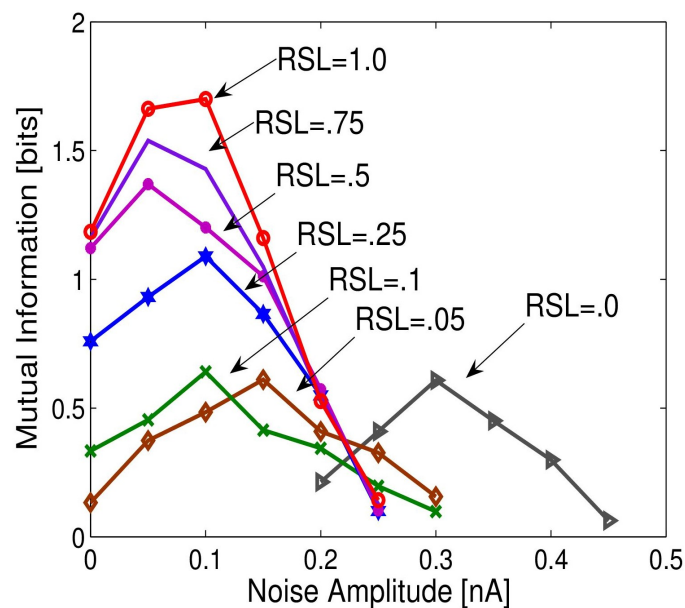
Figure 2-6: Mutual information for different ratios of sub-threshold and suprathreshold stimuli in a population of neuron models. RSL denotes the ratio of neurons that are stimulated by suprathreshold stimuli to the total population of neurons and RSL $= 1.0$ means that the entire population of neurons is subjected to suprathreshold stimuli. The performance of the population of neurons decreases with the decrease of RSL. (Figure taken from [3].)

the energy to generate a sinusoidal signal in a simple harmonic motion is proportional to the square of its amplitude and frequency. The continuous-time TEO is defined by

$$\psi(x) \stackrel{\text{def}}{=} \left(\frac{\mathrm{d}x(t)}{\mathrm{d}t}\right)^2 - x(t)\frac{\mathrm{d}^2x(t)}{\mathrm{d}t^2} \tag{2-11}$$

and its discrete-time equivalent as

$$\psi[x] \stackrel{\text{def}}{=} x^2(n) - x(n-1)x(n+1). \tag{2-12}$$

From (2-11), it can be deduced that TEO does not only take into account the amplitude of the signal, but also its derivatives. This means that the output of TEO for a more "active" signal (e.g. signal with higher frequency) will be larger than a less "active" one.

The discrete-time TEO calculation in (2-12) will result in higher time resolution than the conventional energy calculation since it only needs three samples (i.e. $x(n), x(n-1)$, and $x(n+1)$). However, the use of $x(n+1)$ in the equation implied that the system is noncausal, which is is not possible for real-time calculation. Therefore, in the case of real-time discrete calculation, the logical choice would be to calculate $\psi[x(n-1)]$ instead of $\psi[x(n)]$. This means that the output of the system would be delayed by one sample.

2-2-2   TEO for Well-Known Signals

Table 2-1 shows the TEO outputs for well-known signals. Most of the results are fairly logical since TEO is defined as giving a constant output for sinusoidal signals. The TEO output of multisine is not a constant and this is explained by the addition properties in Table 2-2. It is due to the cross-interaction property that produces the second term as shown in Table 2-1.

2-2-3   Properties of TEO

Due to its nonlinearity, the common additivity property does not hold in the TEO. Therefore, it is important to also define the interaction of two functions $x(t)$ and $y(t)$. The cross-interaction TEO, $\psi_c(x, y)$, has been defined in [19] by

$$\psi_c(x, y) \stackrel{\text{def}}{=} \frac{\mathrm{d}x}{\mathrm{d}t} \cdot \frac{\mathrm{d}y}{\mathrm{d}t} - x\frac{\mathrm{d}^2y}{\mathrm{d}t^2}. \tag{2-13}$$

It is important to notice that ψ_c is noncommutative, i.e. $\psi_c(x, y) \neq \psi_c(y, x)$.
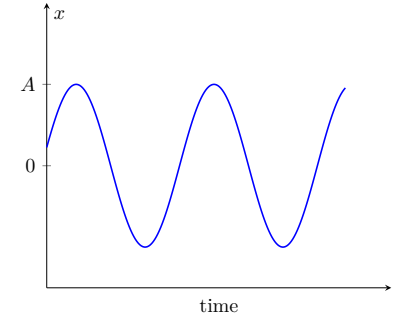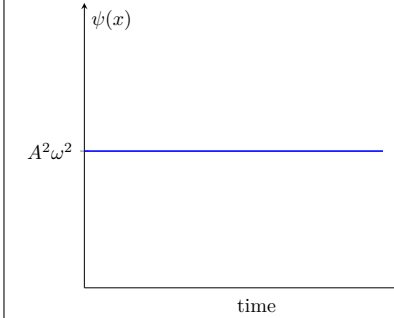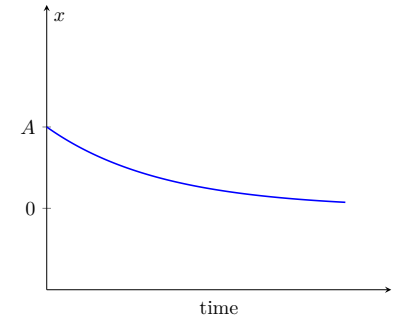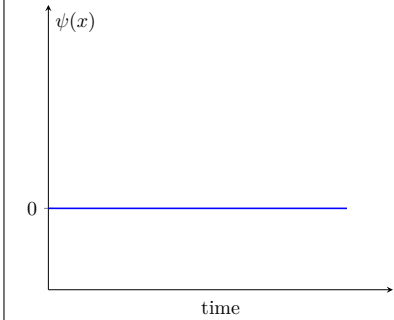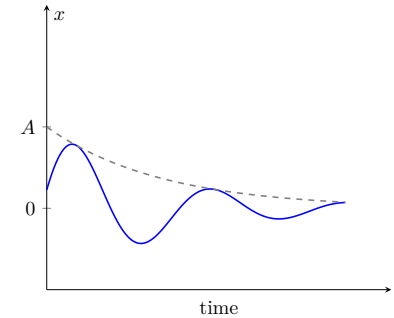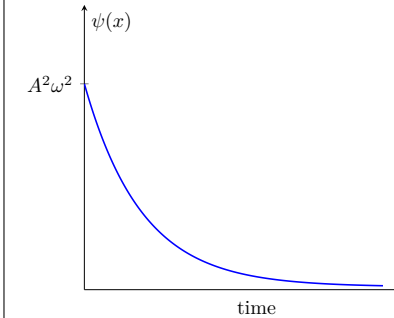
By defining the cross-interaction TEO, several important properties can be analyzed, as extensively explained in [19] and summarized in Table 2-2.

2-2-4   The Effect of Noise on TEO

Consider that noise η is added to signal s at the input of TEO. For $x = s + \eta$,
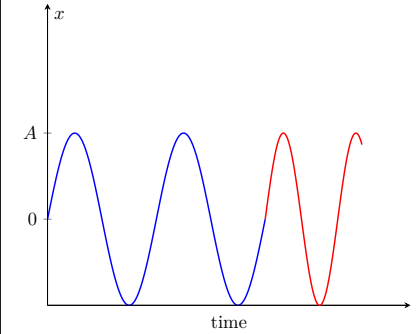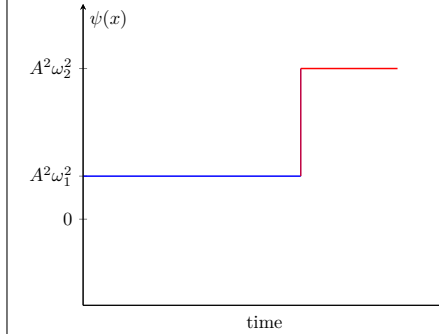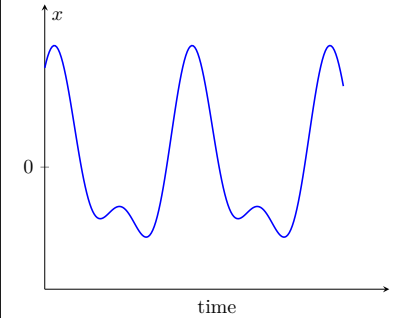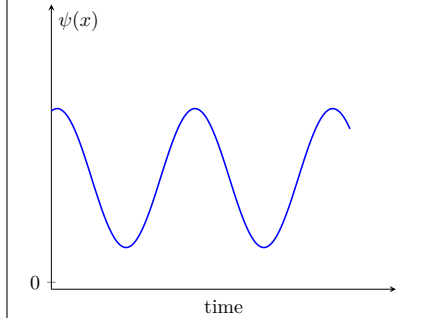
$$\begin{aligned}
\psi(x) &= (\dot{s} + \dot{\eta})^2 - (s + \eta)(\ddot{s} + \ddot{\eta}) \\
&= (\dot{s}^2 - s\ddot{s}) + (\dot{\eta}^2 - \eta\ddot{\eta}) + 2\dot{s}\dot{\eta} - s\ddot{\eta} - \eta\ddot{s} \\
&= \psi(s) + \psi(\eta) + \psi_c(s, \eta) + \psi_c(\eta, s)
\end{aligned} \tag{2-14}$$

Table 2-1: Teager Energy Operator outpus for various well-known signals.

	Input Signal $x(t)$		Output TEO $\psi(x(t))$	
Sinusoid	$A\sin(\omega t + \phi)$		$A^2\omega^2$	
Exponent	$Ae^{-\alpha t}$		0	
Exponentially Damped Sinusoid	$Ae^{-\alpha t}\sin(\omega t + \phi)$		$A^2\omega^2 e^{-2\alpha t}$	

Continued on the next page

Table 2-1: *continued*

	Input Signal $x(t)$		Output TEO $\psi(x(t))$	
Different Frequency Sinusoid	$A\sin(\omega_1 t + \phi_1), t < t_0$ $A\sin(\omega_2 t + \phi_2), t > t_0$		$A^2\omega_1^2, t < t_0$ $A^2\omega_2^2, t > t_0$	
Multisine	$A_1\sin(\omega_1 t + \phi_1)$ $+A_2\sin(\omega_2 t + \phi_2)$		$A_1^2\omega_1^2 + A_2^2\omega_2^2$ $+A_1 A_2\times$ $[1 - \cos(\omega_1 + \omega_2)]$ $\times\cos[(\omega_1 - \omega_2)t$ $+(\phi_1 - \phi_2)]$	

Table 2-2: Properties of TEO

Properties	Formula	Higher Degree Formula
addition	$\psi(x+y) = \psi(g) + \psi(h) + \psi_c(x,y) + \psi_c(y,x)$	$\psi(x+y+z) = \psi(x) + \psi(y) + \psi(z)$ $+\psi_c(x,y) + \psi_c(y,x) + \psi_c(y,z) + \psi_c(z,y)$ $+\psi_c(x,z) + \psi_c(z,x)$
product	$\psi(xy) = x^2\psi(y) + y^2\psi(x)$	$\psi(xyz) = x^2y^2\psi(z) + x^2z^2\psi(y) + y^2z^2\psi(x)$
quotient	$\psi(y/x) = \frac{x^2\psi(y) - y^2\psi(x)}{x^4}$	$\psi(\dot{x}/x) = \frac{1}{x^2}\left[\psi(\dot{x}) - \left(\frac{\dot{x}}{x}\right)^2\psi(x)\right]$
n-th power	$\psi(x^n) = nx^{2n-2}\psi(x)$	
reciprocal	$\psi(1/x) = -\psi(x)/x^4$	
composite	$\psi(y(x(t))) = \dot{x}^2\left[\left(\frac{\mathrm{d}y}{\mathrm{d}x}\right)^2 - y\frac{\mathrm{d}^2y}{\mathrm{d}x^2}\right] - y\frac{\mathrm{d}y}{\mathrm{d}x}\ddot{x}$	
first time derivative	$\psi(\dot{x}) = -\psi_c(\ddot{x}, x) = -\psi_c(x, \ddot{x})$	
integral	$\psi\left(\int\limits_0^t x\,\mathrm{d}t\right) = x^2 - \dot{x}\int\limits_0^t g\,\mathrm{d}t$	
derivative of TEO	$\dot{\psi}(x) = \psi_c(x, \dot{x})$	

It can be seen that the terms $\psi(\eta) + \psi_c(s,\eta) + \psi_c(\eta,s)$ will bias the $\psi(s)$. The expected value of TEO is

$$\begin{aligned}\mathbf{E}[\psi(x)] &= \mathbf{E}[\psi(s) + \psi(\eta) + \psi_c(s,\eta) + \psi_c(\eta,s)] \\ &= \psi(s) + \mathbf{E}[\psi(\eta)]\end{aligned} \tag{2-15}$$

provided that s and η are uncorrelated. In the case of η being a Gaussian noise, $\mathbf{E}[\psi(\eta)]$ is equal to its variance [18].

2-2-5 Implementation of TEO

Figure 2-7 shows the block diagram of the continuous-time TEO. It can be seen that it needs two differentiators, two multipliers, and one subtractor. Because of the use of multipliers that might be expensive in implementation, it is more often implemented in the digital domain using its discrete-time counterpart, i.e. (2-12). This block diagram is not the only way to implement TEO, however. Hiseni et al. in [20] designed a TEO circuit for action potential (AP) detection purposes using the dynamic translinear principle. Due to its low power consumption, compact circuit architecture, and analog implementation, it can be used in a real-time recording system.

2-2-6 TEO as an Action Potential Detection Algorithm

As mentioned in Section 2-2-1, the output of the TEO is determined by both the amplitude and activity of the signal. This becomes an advantage for an action potential (AP) detection
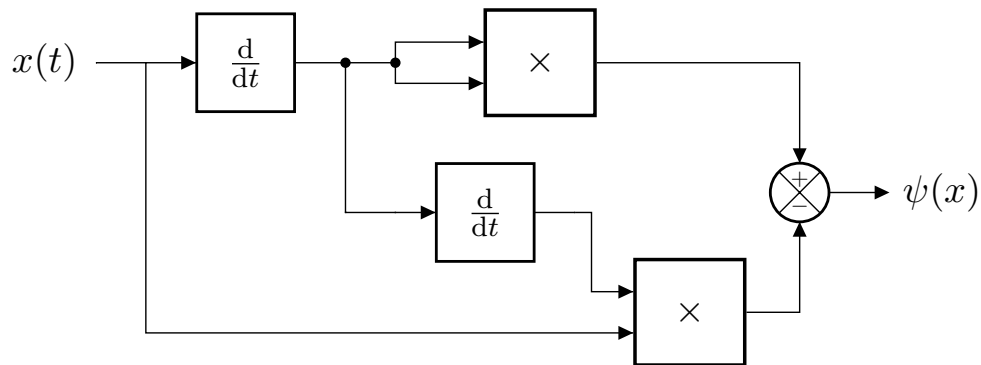
Figure 2-7: Block diagram of a TEO. It can be seen that it needs two differentiators, two multipliers, and one subtractor.

(a)

(b)
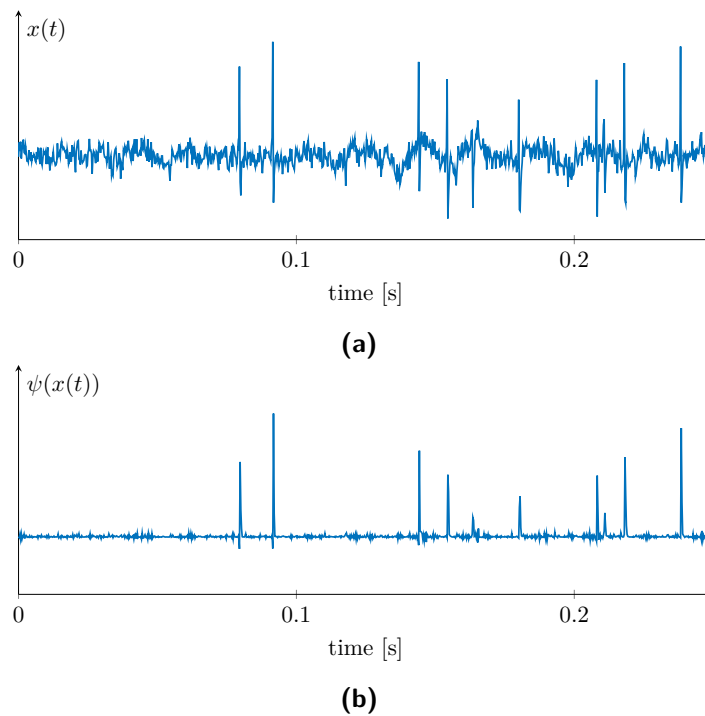
Figure 2-8: An example of an action potential recording subjected to TEO. (a) Action potential recording. (b) The output of TEO. It can be seen that TEO emphasizes the signal when a spike is detected, making it more prominent than the other parts of the signal.

application, since it usually has considerably large amplitude and high activity compared to the rest of the signal (and also the noise) [21]. An example of the output of the TEO for an AP detection is shown in Figure 2-8b. Of course, since they are processed in the same way, the APs that are smaller in amplitude will also have a smaller output. This could pose a problem in the post-processing, especially for an automatic detection where the output of TEO is thresholded with a certain threshold level. The smaller spike could go unnoticed, resulting in a false negative.

2-3   Conclusions

In this chapter, an overview of SR and TEO was given. The definition of SR and how its performance is usually measured was explained. Different types of SR were also introduced and their performance was analyzed, which concludes that the suprathreshold SR has better performance than the subthreshold SR. Due to the properties of mathematical operators and the vision of the research, SNR and SNDR are chosen as the performance metrics.

The definition and properties of the TEO were also given, as well as its sensitivity to noise and how it can be implemented. Finally, in biomedical applications, the TEO can be used to detect APs of a population of neurons.

Chapter 3

Signal Multiplier with Stochastic Resonance-Based Systems

A signal multiplier is used to produce a multiplication of two or more signals. Suppose that $x_1, x_2, \ldots, x_K$ are input signals, the output of an ideal signal multiplier is $x_1 x_2 \cdots x_K$. In this chapter, a signal multiplier with stochastic resonance (SR)-based fundamental building blocks (as shown in Figure 1-1) using XNOR gates will be presented and discussed. The output of the operator is a 1-bit signal that can be averaged to produce the multiplication of the input signals.

3-1 XNOR in SR-Based Systems

An XNOR gate is one possible candidate to implement a signal multiplier. In Boolean logic, the formula of an XNOR is $x_{out} = x_1 \cdot x_2 + \bar{x}_1 \cdot \bar{x}_2$. This fits a multiplier especially for comparators that produce $+V$ as logic 1 and $-V$ as 0. When the signals are either both 1 or both 0, an XNOR will produce output 1. Otherwise, it will produce output 0. The block diagram of an XNOR in combination with SR-based fundamental building blocks is shown in Figure 3-1, where x_1 and x_2 are input signals and η_1 and η_2 are independent white noise.

3-1-1 Output Signal Formula Derivation

As explained before in Chapter 2, SR-based systems use the help of noise to boost their performance. Therefore, the output of the operator in Figure 3-1, while being binary, is not deterministic. The probability of the output of the first comparator $y_1 = 1$ given x_1, as derived in [2], is

$$
\begin{aligned}
\Pr(y_1 = 1 \,|\, x_1) &= \Pr(x_1 + \eta_1 \geq \theta_1 \,|\, x_1) \\
&= \Pr(\eta_1 \geq \theta_1 - x_1 \,|\, x_1) \\
&= 1 - \Pr(\eta_1 < \theta_1 - x_1 \,|\, x_1) \\
&= 1 - F_{\eta_1}(\theta_1 - x_1),
\end{aligned}
\tag{3-1}
$$
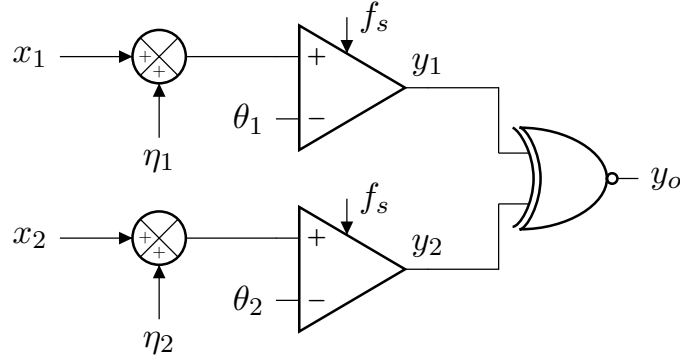
Figure 3-1: XNOR gate in combination with SR-based fundamental building blocks. The output of the operator is a binary signal, and can be averaged to produce the multiplication of both input signals.

where F_{η_1} is the cumulative distribution function (CDF) of η_1. Similarly, the probability of $y_2 = 1$ given x_2 is $\Pr(y_2 = 1|x_2) = 1 - F_{\eta_2}(\theta_2 - x_2)$. Assuming that the inputs are independent, the probability of $y_o = 1$ given x_1 and x_2 is

$$
\begin{aligned}
\Pr(y_o = 1 \,|\, x_1, x_2) &= \Pr(y_1 = 1 \cap y_2 = 1 \,|\, x_1, x_2) + \Pr(y_1 = 0 \cap y_2 = 0 \,|\, x_1, x_2) \\
&= \Pr(y_1 = 1 \,|\, x_1)\Pr(y_2 = 1 \,|\, x_2) + \Pr(y_1 = 0 \,|\, x_1)\Pr(y_2 = 0 \,|\, x_2) \\
&= (1 - F_{\eta_1}(\theta_1 - x_1))(1 - F_{\eta_2}(\theta_2 - x_2)) + F_{\eta_1}(\theta_1 - x_1)F_{\eta_2}(\theta_2 - x_2) \\
&= 1 - \Big(F_{\eta_1}(\theta_1 - x_1) + F_{\eta_2}(\theta_2 - x_2)\Big) + 2F_{\eta_1}(\theta_1 - x_1)F_{\eta_2}(\theta_2 - x_2).
\end{aligned}
\tag{3-2}
$$

Consequently, the probability of $y_o = 0$ given x_1 and x_2 is

$$
\begin{aligned}
\Pr(y_o = 0 \,|\, x_1, x_2) &= 1 - \Pr(y_0 = 1 \,|\, x_1, x_2) \\
&= F_{\eta_1}(\theta_1 - x_1) + F_{\eta_2}(\theta_2 - x_2) - 2F_{\eta_1}(\theta_1 - x_1)F_{\eta_2}(\theta_2 - x_2).
\end{aligned}
\tag{3-3}
$$

The ideal reconstructed output $\hat{y}_{out}$ can be determined by taking the expected value of y_o, as proposed in [22]. Therefore,

$$
\begin{aligned}
\hat{y}_{out} &= \mathbf{E}\left[y_o \,|\, x_1, x_2\right] \\
&= \Pr(y_o = 1 \,|\, x_1, x_2)(+V) + \Pr(y_o = 0 \,|\, x_1, x_2)(-V) \\
&= V - 2V\Big(F_{\eta_1}(\theta_1 - x_1) + F_{\eta_2}(\theta_2 - x_2)\Big) + 4V F_{\eta_1}(\theta_1 - x_1)F_{\eta_2}(\theta_2 - x_2).
\end{aligned}
\tag{3-4}
$$

In Appendix A-2, it is proven that, for independent η_1 and η_2,

$$
\hat{y}_{out} = \frac{\mathbf{E}\left[y_1 \,|\, x_1\right] \mathbf{E}\left[y_2 \,|\, x_2\right]}{V}.
\tag{3-5}
$$

This shows that the SR-based operator indeed behaves as a multiplier. This also means that the performance of the multiplier depends on how good the $\mathbf{E}\left[y_1 \,|\, x_1\right]$ and $\mathbf{E}\left[y_2 \,|\, x_2\right]$ represent x_1 and x_2, respectively.

For a system using Gaussian distributed noise inputs, the CDF of its noise inputs can be approximated as

$$
F(z) \approx \frac{1}{2} + \frac{1}{\sigma\sqrt{2\pi}}(z).
\tag{3-6}
$$

Using (3-6) to approximate F_{η_1} and F_{η_2} in (3-4),

$$
\begin{aligned}
\hat{y}_{out} &\approx V - V \left(1 + \frac{2}{\sqrt{\pi}} \frac{\theta_1 - x_1}{\sigma_1 \sqrt{2}} + 1 + \frac{2}{\sqrt{\pi}} \frac{\theta_2 - x_2}{\sigma_2 \sqrt{2}} \right) \\
&\quad + V \left(1 + \frac{2}{\sqrt{\pi}} \frac{\theta_2 - x_2}{\sigma_2 \sqrt{2}} + \frac{2}{\sqrt{\pi}} \frac{\theta_1 - x_1}{\sigma_1 \sqrt{2}} + \frac{2}{\pi} \frac{(\theta_1 - x_1)(\theta_2 - x_2)}{\sigma_1 \sigma_2} \right) \\
&= \frac{2V}{\pi \sigma_1 \sigma_2} (\theta_1 - x_1)(\theta_2 - x_2).
\end{aligned}
\tag{3-7}
$$

To produce a "clean" multiplication, θ_1 and θ_2 should be set to 0. Assuming that $\sigma_1 = \sigma_2 = \sigma$, the final formula is

$$
\hat{y}_{out} \approx \frac{2V}{\pi \sigma^2} x_1 x_2.
\tag{3-8}
$$

In the following sections, it will be assumed that the noise signals used have Gaussian distribution and the same power.

3-1-2   Output Noise

In practice, the output signal will never be as noiseless as $\hat{y}_{out}$ since the averaging is done either by filtering or finite parallelization. The real final output will be

$$
y_{out} = \hat{y}_{out} + \eta_{out},
\tag{3-9}
$$

where $\hat{y}_{out}$ is the expected output formulated by (3-4) and η_{out} is the output noise.

The nature of η_{out} comes from the fact that the probability of the output y_o is determined by inputs x_1 and x_2 as well as the noise. The noise contributes in bringing the value of the inputs across the threshold, such that the state of y_o changes. By rising the intensity of the noise, the state of y_o will be solely determined by the noise itself rather than the combination of the inputs and noise and therefore it will lead to the generation of the output noise. In other words, the smaller $\left| \frac{\theta - \max |x|}{\sigma} \right|$ is, the larger the output noise will be. Beside filtering, the amount of noise can be decreased by finite parallelization. For N parallel systems, the noise intensity σ_{out} will decrease by a factor of $\frac{1}{\sqrt{N}}$, as shown in Figure 3-2.

The conditional expected value of the squared distance is

$$
\begin{aligned}
\mathbf{E}\left[(y_o - \hat{y}_{out})^2 \,\middle|\, x_1, x_2 \right] &= (V - \hat{y}_{out})^2 \Pr(y_0 = 1 \,|\, x_1, x_2) + (V + \hat{y}_{out})^2 \Pr(y_o = 0 \,|\, x_1, x_2) \\
&= V^2 - \hat{y}_{out}^2.
\end{aligned}
\tag{3-10}
$$

The output noise power, denoted by P_{noise}, is the expected value of (3-10) over x_1 and x_2. It should be noted that, since the mean of the output noise is zero, the output noise power will be equal to the output noise variance. Suppose that $\hat{y}_{out}(n)$ has length M, the output noise power can be written as

$$
\begin{aligned}
P_{\text{noise}} = \sigma_{out}^2 &= \mathbf{E}\left[\mathbf{E}\left[(y_o - \hat{y}_{out})^2 \,\middle|\, x_1, x_2 \right] \right] \\
&= \frac{1}{M} \sum_{n=0}^{M-1} \left(V^2 - \hat{y}_{out}^2(n) \right).
\end{aligned}
\tag{3-11}
$$
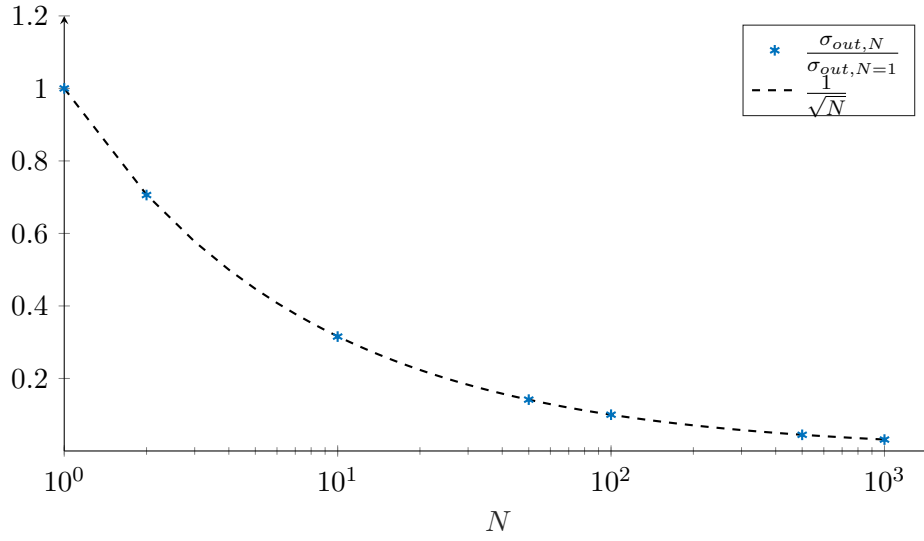
Figure 3-2: Standard deviation of output noise based on the number of parallelization N. The standard deviation is normalized to $\sigma_{out,N=1}$. It follows the pattern of $\frac{1}{\sqrt{N}}$.

The overall noise power is

$$P_{\text{noise},N} = \sigma_{out,N}^2 = \frac{\mathbf{E}\left[\mathbf{E}\left[(y_o - \hat{y}_{out})^2 \,|\, x_1, x_2\right]\right]}{N}$$

$$= \frac{1}{MN} \sum_{n=0}^{M-1} \left(V^2 - \hat{y}_{out}^2(n)\right). \tag{3-12}$$

The simulated and predicted standard deviation and noise power in the case of two sinusoidal inputs with a unity amplitude is presented in Figure 3-3. V is set to 1 and their phase differences were arranged such that the correlation coefficients, ρ, vary from -1 to $+1$. The first noise behavior that should be noted from this operator is: it saturates at $\sigma_{out,N=1} = V^2$ for large σ. This behavior can be explained by looking at the distribution of the output noise. As σ increases, the output of the multiplier decreases by a factor of $\frac{2V}{\pi\sigma^2}$. For large σ, this will become very small and η_{out} wil be approximately close to y_o. Since y_o only has a value of either $-V$ or $+V$ and zero mean, it will have a standard deviation of V^2. The second noise behavior that can be inferred is: input signals with $\rho = \pm 1$ generate smaller output noise. This is because, for the same σ, they produce the largest, albeit distorted, max $|\hat{y}_{out}|$. Based on (3-10), this will lead to smaller σ_{out}.

For white input noise sources with a large number of samples, the output noise is white and bandlimited with a maximum frequency of half the sampling frequency [22]. Therefore, for the averaging done by filtering, the noise power is determined by

$$P_{\text{noise, filtered}} = \sigma_{out,\text{filtered}}^2 = \frac{2\sigma_{out,N=1}^2}{f_s} \cdot \Delta f_{ENBW}, \tag{3-13}$$

where f_s is the sampling frequency and Δf_{ENBW} is the equivalent noise bandwidth (ENBW). Figure 3-4 shows the result of the same case as the previous one, sampled with a sampling
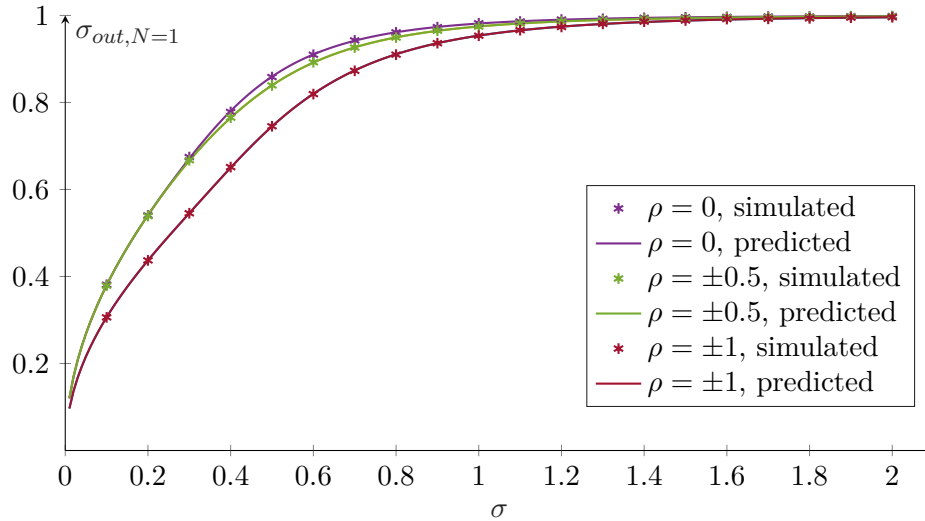
(a)
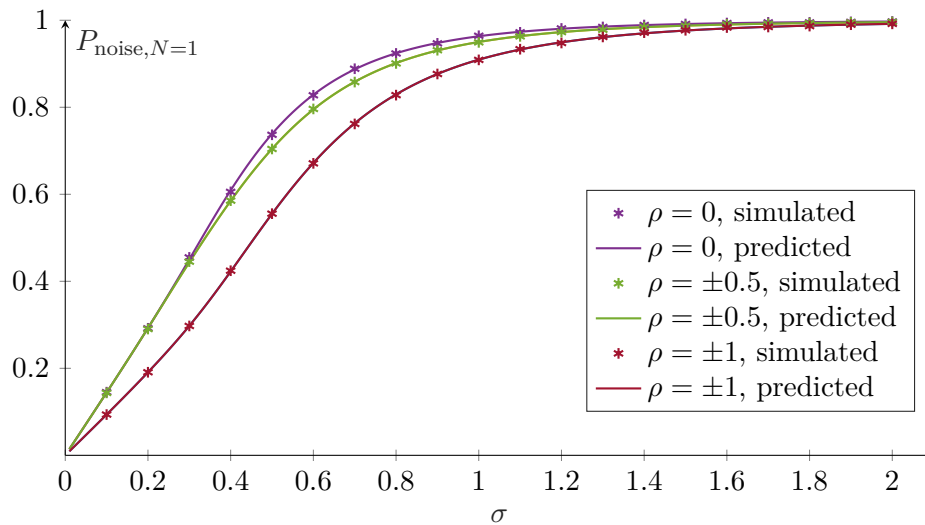
(b)

Figure 3-3: The output noise for two sinusoidal inputs with a unity amplitude and frequency, sampled with a sampling frequency of 1 kHz and subjected to a second order Butterworth LPF with cut-off frequency of 20 Hz. V is set to 1. The asterisks mark the simulated results and the solid lines are the predicted results based on the formula. (a) Standard deviation for $N = 1$. (b) The noise power for $N = 1$. As σ goes up, the output noise becomes larger and its power becomes closer to V^2.

frequency of 1 kHz and subjected to a second order Butterworth LPF with a cut-off frequency of 20 Hz. It can be seen that the simulated data falls within a reasonable range when compared to the predicted value computed with (3-13). In the end, the noise power is

$$
P_{\text{noise,out}} =
\begin{cases}
\dfrac{1}{MN} \displaystyle\sum_{n=0}^{M-1} \left(V^2 - \hat{y}_{out}^2(n) \right) & \text{for parallelization} \\[2em]
\dfrac{2\Delta f_{ENBW}}{M f_s} \displaystyle\sum_{n=0}^{M-1} \left(V^2 - \hat{y}_{out}^2(n) \right) & \text{for filtering}
\end{cases}
. \tag{3-14}
$$

The signal-to-noise ratio (SNR) for the multiplier can then be calculated. Figure 3-5 shows the SNR of the previous case. It can be seen that the operator reaches its maximum performance when not subjected to noise. Therefore, in this particular case, the stochastic resonance phenomenon does not happen for SNR.

3-1-3   Distortion

The approximation done in Section 3-1-1 is true for $\left| \dfrac{\theta_1 - x_1}{\sigma_1 \sqrt{2}} \right| \approx 0$ and $\left| \dfrac{\theta_2 - x_2}{\sigma_2 \sqrt{2}} \right| \approx 0$. The higher order approximation is

$$
y_{out} \approx \frac{2V}{\pi\sigma^2}(x_1 x_2) - \frac{V}{3\pi\sigma^4}(x_1 x_2^3 + x_1^3 x_2) + \frac{V}{18\pi\sigma^6} x_1^3 x_2^3 \tag{3-15}
$$

which contains fourth and sixth order harmonics. To decrease the harmonics influence (the second and third terms), it is necessary to ensure that the second term is small enough, i.e.

$$
\frac{V}{3\pi\sigma^4} << 1 \implies \sigma >> \sqrt[4]{\frac{V}{3\pi}}. \tag{3-16}
$$

Unfortunately, this is only feasible to implement for systems with an incredibly good averaging technique since, as explained in Section 3-1-2, the larger the input noise sources are, the higher the output noise will be.

The second and third terms (and possibly other higher-order terms) in (3-15) also influence the gain of $x_1 x_2$. Therefore, in general, it does not make sense to expect $\dfrac{2V}{\pi\sigma^2}$ as the output gain of the multiplier, and calculating the distortion only by referring to those two terms can be misleading. The better alternative is to introduce an ideal output signal with a certain gain $\hat{G}$ that produces the least-square distortion value. Suppose that $\hat{\mathbf{Y}}_{\mathbf{out}} = [\hat{y}_{out}(0) \quad \hat{y}_{out}(1) \quad \cdots \quad \hat{y}_{out}(M-1)]^{\mathrm{T}}$ and $\mathbf{X} = [x_1(0)x_2(0) \quad x_1(1)x_2(1) \quad \cdots \quad x_1(M-1)x_2(M-1)]^{\mathrm{T}}$, using the least-square error (LSE) method, the linear gain $\hat{G}$ can be determined as

$$
\hat{G} = \left(\mathbf{X}^{\mathrm{T}} \mathbf{X} \right)^{-1} \mathbf{X}^{\mathrm{T}} \hat{\mathbf{Y}}_{\mathbf{out}} \tag{3-17}
$$

The distortion power then can be calculated as

$$
\begin{aligned}
P_{\text{distortion}} &= \frac{1}{M} \sum_{n=0}^{M-1} \left| \hat{y}_{out}(n) - \hat{G} x_1(n) x_2(n) \right|^2 \\
&= \frac{1}{M} \sum_{n=0}^{M-1} \left| \hat{y}_{out}(n) - \left(\mathbf{X}^{\mathrm{T}} \mathbf{X} \right)^{-1} \mathbf{X}^{\mathrm{T}} \hat{\mathbf{Y}}_{\mathbf{out}} x_1(n) x_2(n) \right|^2 .
\end{aligned} \tag{3-18}
$$
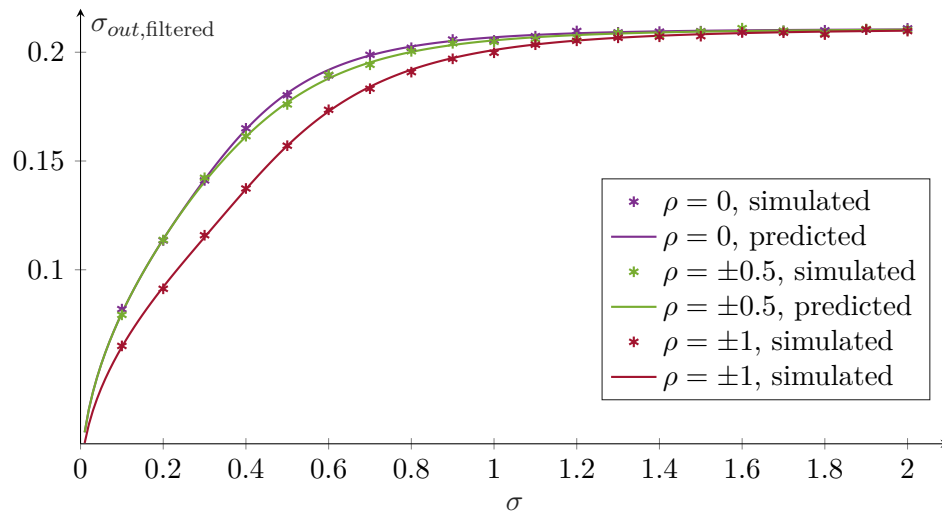
(a)
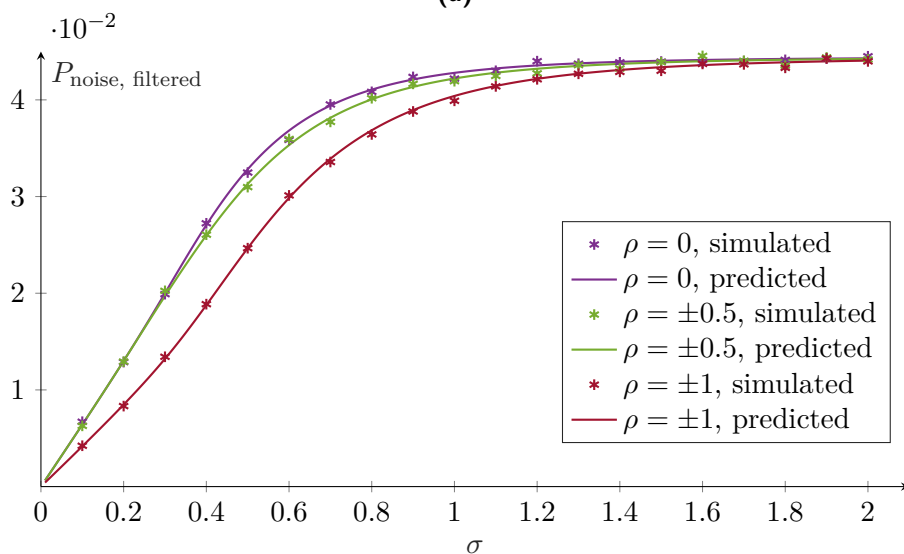
(b)

Figure 3-4: The output noise for two sinusoidal inputs with a unity amplitude and frequency, sampled with a sampling frequency of 1 kHz and subjected to a second order Butterworth LPF with cut-off frequency of 20 Hz. V is set to 1. The asterisks mark the simulated results and the solid lines are the predicted results based on the formula. (a) The standard deviation. (b) The noise power.

Figure 3-5: Signal-to-noise ratio for two sinusoidal inputs with a unity amplitude and frequency, sampled with a sampling frequency of 1 kHz and subjected to a second order Butterworth LPF with cut-off frequency of 20 Hz. V is set to 1. The asterisks mark the simulated results and the solid lines are the predicted results based on the formula. The stochastic resonance does not happen since the performance is at maximum when $\sigma = 0$.

The plot of $\hat{G}$ in the same case as the previous one is shown in Figure 3-6a. As a reference, the predicted linear gain is also presented. There are two things that can be derived from this figure. Firstly, as σ goes up, the two values become closer and the difference becomes approximately zero, which implies a decrease in distortion power as shown in Figure 3-6b. This means that, as predicted, by increasing the noise intensity, the operator can operate in the region that gives the best representation of an ideal multiplier. Secondly, the amount of distortion varies by the correlation coefficient (ρ) of the input signals. Since XNOR multiplies y_1 and y_2, the position of 1's and 0's in each signals determine the number of 1's and 0's produced at y_o. For $\rho = +1$, the signals tend to behave in a similar way, i.e. when y_1 produces 1, it is most probable that y_2 also produces 1, and vice versa. This raises the chance of y_o produces more 1 than 0. This results in the averaged output $\hat{y}_{out}$ to have a high rate near zero and then saturate near the maximum value. A similar thing happens for inputs with $\rho = -1$. However, it will saturate near the minimum value instead. The minimum distortion is achieved when the number of 1 and 0 are approximately the same, and this happens for $\rho = 0$. In this case, $\hat{y}_{out}$ will have zero mean and therefore the distortion near the extreme values can be minimized.

The signal-to-noise-and-distortion ratio (SNDR) is calculated and shown in Figure 3-7. First of all, an SNDR peak can be observed in the multiplier. Secondly, as expected, the best performance is achieved for input signals with $\rho = 0$ since they produce the largest LSE gain while having the smallest distortion power.

(a)

(b)
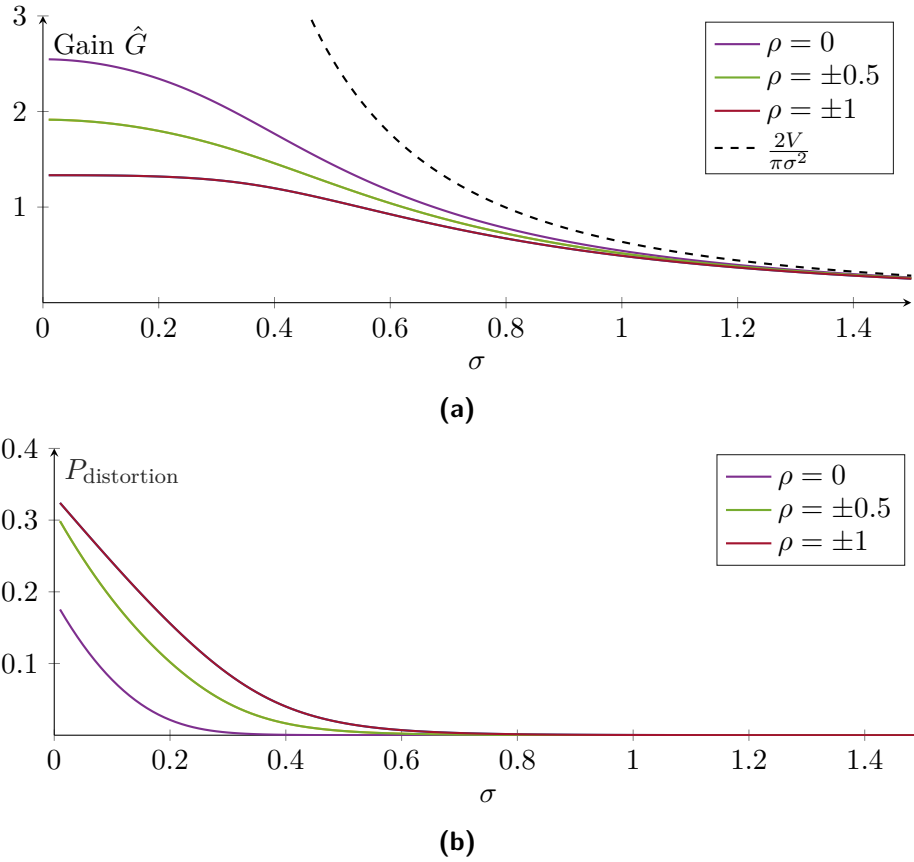
Figure 3-6: The distortion for two sinusoidal inputs with a unity amplitude and frequency. V is set to 1. (a) The LSE gain and the predicted linear gain. The gain depends on the correlation coefficient of the input signals. (b) The distortion power. As σ goes up, the output becomes more linear and the distortion power gets closer to zero.

3-2   Ternary Logic XNOR

As discussed in Section 3-1-3, the distortion is the worst for input signals with $\rho = \pm 1$. To compensate for this, one proposed solution is to use ternary logic. In ternary logic, instead of 1 and 0, the output of the system is divided into three states: $+1$ for HIGH, -1 for LOW, and 0 for UNKNOWN. The existence of 0 is the key to help distribute the distortion of the output signal. Figure 3-8 shows the block diagram of the multiplier, and based on Kleene's strong three-valued logics [23], the output is determined by

$$y_o = \max(\min(x_1, x_2), \min(-x_1, -x_2)). \tag{3-19}$$

3-2-1   Output Signal Formula Derivation

Different from the binary comparator, a ternary comparator has two thresholds, denoted by θ_L for the low threshold and θ_H for the high threshold. The comparator outputs $+V$ or logic
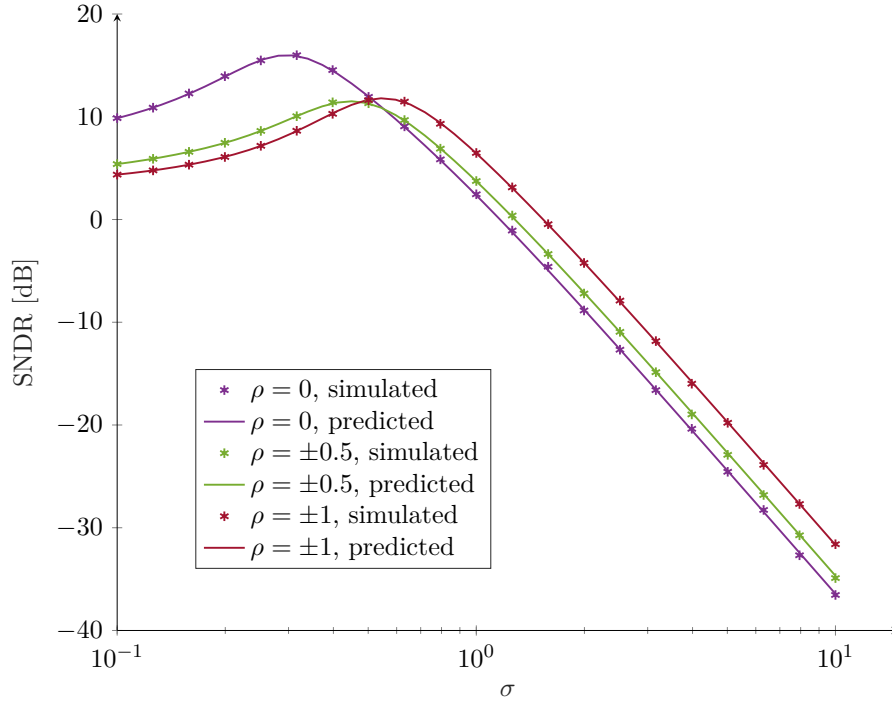
Figure 3-7: Signal-to-noise-and-distortion ratio for two sinusoidal inputs with a unity amplitude and frequency, sampled with a sampling frequency of 1 kHz and subjected to a second order Butterworth LPF with cut-off frequency of 20 Hz. V is set to 1. The asterisks mark the simulated results and the solid lines are the predicted results based on the formula. The SNDR peaks can be found at different σ's for different ρ's.

+1 if the input is larger than θ_H, $-V$ or logic -1 if the input is smaller than θ_L, and 0 if it is in-between the two thresholds. The probabilities of y_1 given x_1 are

$$\begin{aligned} \Pr(y_1 = +1 \,|\, x_1) &= \Pr(x_1 + \eta_1 \geq \theta_{H1} \,|\, x_1) \\ &= 1 - F_{\eta_1}(\theta_{H1} - x_1), \end{aligned} \tag{3-20}$$

and

$$\begin{aligned} \Pr(y_1 = -1 \,|\, x_1) &= \Pr(x_1 + \eta_1 \leq \theta_{L1} \,|\, x_1) \\ &= F_{\eta_1}(\theta_{L1} - x_1), \end{aligned} \tag{3-21}$$

$$\begin{aligned} \Pr(y_1 = 0 \,|\, x_1) &= \Pr(\theta_{L1} \leq x_1 + \eta_1 < \theta_{H1} \,|\, x_1) \\ &= F_{\eta_1}(\theta_{H1} - x_1) - F_{\eta_1}(\theta_{L1} - x_1). \end{aligned} \tag{3-22}$$
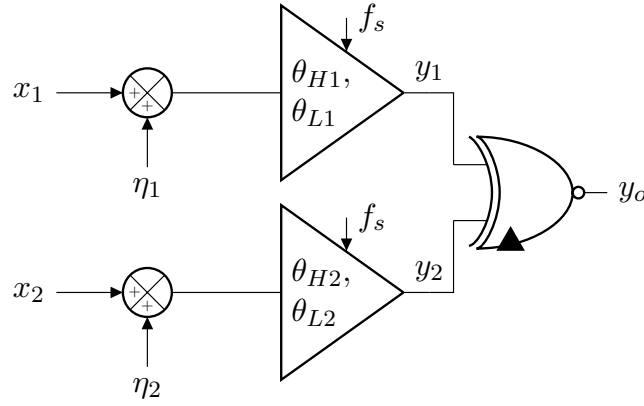
Figure 3-8: Ternary XNOR gate in combination with SR-based fundamental building blocks. The output of the operator is a ternary signal. The black $\triangle$ is used to mark a ternary gate.

Following the same procedure as in Section 3-1-1,

$$
\Pr(y_o \,|\, x_1, x_2) = \begin{cases}
\begin{aligned}
& \left(1 - F_{\eta_1}(\theta_{H1} - x_1)\right)\left(1 - F_{\eta_2}(\theta_{H2} - x_2)\right) \\
& + \left(F_{\eta_1}(\theta_{L1} - x_1)\right)\left(F_{\eta_2}(\theta_{L2} - x_2)\right)
\end{aligned} & y_o = +1 \\[2em]
\begin{aligned}
& \left(F_{\eta_1}(\theta_{H1} - x_1) - F_{\eta_1}(\theta_{L1} - x_1)\right) \\
& + \left(F_{\eta_2}(\theta_{H2} - x_2) - F_{\eta_2}(\theta_{L2} - x_2)\right) \\
& - \left(F_{\eta_1}(\theta_{H1} - x_1) - F_{\eta_1}(\theta_{L1} - x_1)\right) \\
& \times \left(F_{\eta_2}(\theta_{H2} - x_2) - F_{\eta_2}(\theta_{L2} - x_2)\right)
\end{aligned} & y_o = 0 \\[2em]
\begin{aligned}
& \left(1 - F_{\eta_1}(\theta_{H1} - x_1)\right)\left(F_{\eta_2}(\theta_{L2} - x_2)\right) \\
& + \left(F_{\eta_1}(\theta_{L1} - x_1)\right)\left(1 - F_{\eta_2}(\theta_{H2} - x_2)\right)
\end{aligned} & y_o = -1
\end{cases}, \tag{3-23}
$$

and thus

$$
\begin{aligned}
\hat{y}_{out} &= \mathbf{E}[y_o \,|\, x_1, x_2] \\
&= V + V\left[F_{\eta_1}(\theta_{L1} - x_1) + F_{\eta_1}(\theta_{H1} - x_1)\right]\left[F_{\eta_2}(\theta_{L2} - x_2) + F_{\eta_2}(\theta_{H2} - x_2)\right] \\
&\quad - V\left[F_{\eta_1}(\theta_{L1} - x_1) + F_{\eta_1}(\theta_{H1} - x_1) + F_{\eta_2}(\theta_{L2} - x_2) + F_{\eta_2}(\theta_{H2} - x_2)\right].
\end{aligned} \tag{3-24}
$$

By setting the $\theta_{L1} = \theta_{L2} = -\delta$, $\theta_{H1} = \theta_{H2} = +\delta$, and $\sigma_1 = \sigma_2 = \sigma$, the higher degree Taylor approximation for the Gaussian noises-induced system is

$$
\hat{y}_{out} \approx \frac{2V}{\pi\sigma^2}x_1 x_2 - \frac{V}{3\pi\sigma^4}x_1 x_2\left(6\delta^2 + x_1^2 + x_2^2\right) + \frac{V}{18\pi\sigma^6}x_1 x_2\left(3\delta^2 + x_1^2\right)\left(3\delta^2 + x_2^2\right). \tag{3-25}
$$

It should be noticed that if $\delta = 0$, (3-25) will be identical to (3-15), meaning that it becomes a binary operator.

3-2-2   Output Noise

The noise power of this multiplier can also be calculated with the same method as (3-14). However, instead of $(V^2 - \hat{y}_{out})$, $\mathbf{E}\left[(y_o - \hat{y}_{out})^2 \mid x_1, x_2\right]$ is formulated as

$$
\begin{aligned}
\mathbf{E}\left[(y_o - \hat{y}_{out})^2 \mid x_1, x_2\right] &= (V - \hat{y}_{out})^2 \Pr(y_o = +1 \mid x_1, x_2) + (-\hat{y}_{out})^2 \Pr(y_o = 0 \mid x_1, x_2) \\
&\quad + (-V - \hat{y}_{out})^2 \Pr(y_o = -1 \mid x_1, x_2) \\
&= 2V^2 \Pr\left(y_o = -1 \mid x_1, x_2\right) + V\hat{y}_{out} - \hat{y}_{out}^2.
\end{aligned}
\tag{3-26}
$$

The behavior of the noise standard deviation and power for two sinusoidal inputs with various ρ is shown in Figure 3-9. In this case, V is set to 1 and δ is set to 0.5. The ternary multiplier produces smaller output noise compared to the binary multiplier due to the state 0.

The SNR of the ternary multiplier for the same case as Figure 3-5 is presented in Figure 3-10. δ is also set to 0.5. Again, SR does not occur in this particular case.

3-2-3   Distortion

The LSE method is also used to measure the distortion in this operator. Figure 3-11 presents the LSE gain and the distortion power when V and δ is set to 1 and 0.5, respectively. Although the LSE gain is smaller than it is in the binary multiplier, the distortion power is also smaller.

The SNDR for the same case is shown in Figure 3-12. Compared to the performance in Figure 3-7, the SNDR for signals with $\rho = \pm 1$ and $\rho = \pm 0.5$ are better. These findings are expected since the distortion power is smaller. However, contrary to what is displayed in the binary multiplier, the SNDR of signals with $\rho = 0$ is the smallest in the ternary multiplier. This is due to the value of δ that does not match well in ensuring the maximum performance for signals with $\rho = 0$. The effect of the value of δ is discussed in Section 3-2-4.

3-2-4   The Effect of δ

The performance of the ternary muliplier is not only determined by ρ, but the combination of both ρ and δ. This is because the value of δ influences the probability of the output signal of the comparators and the optimum probability depends on ρ. For example, for signals with $\rho = +1$, the optimum probability is achieved when δ is set to half of the signal's amplitude. This is to make sure that the probability of the output of the comparators are equal for every states and this leads to the probability of $+1$, 0, and -1 at the output of the XNOR being $\frac{1}{2}$, $\frac{1}{2}$, and 0. For signals with $\rho = 0$, the ratio of the probability of the states at the output of the XNOR needs to be the same, i.e. $\Pr(+1) : \Pr(0) : \Pr(-1) = \frac{1}{3} : \frac{1}{3} : \frac{1}{3}$. This corresponds to a ratio of around $0.4 : 0.2 : 0.4$ for the probability of each states at the output of the comparators. This gives the indication of what the optimum value of δ will be. Figure 3-13 shows the various SNDR depending on the value of δ for input signals with $\rho = 0$. As expected, the maximum performance is achieved when δ is set to be lower than 0.5, in this case 0.2.
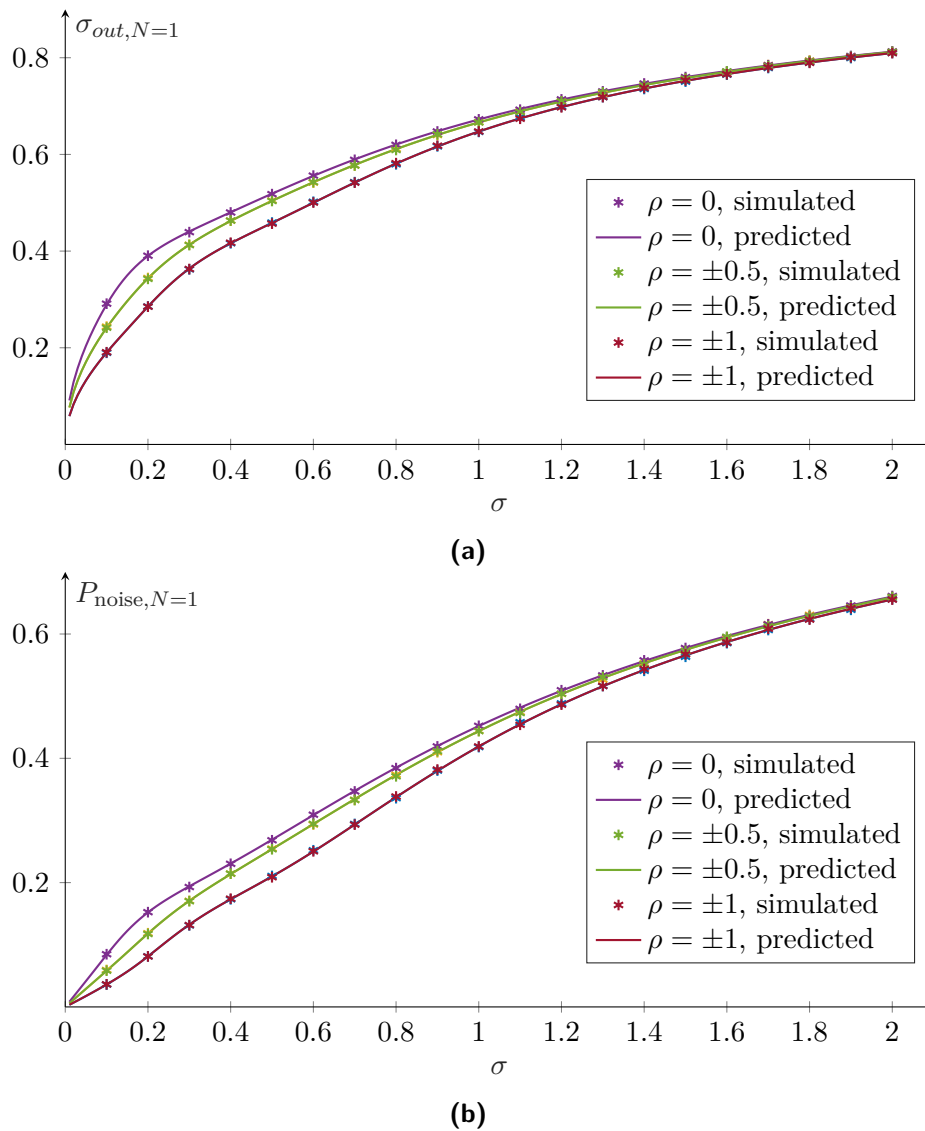
Figure 3-9: The output noise of the ternary SR-based multiplier for two sinusoidal inputs with a unity amplitude. V is set to 1 and δ is set to 0.5. The asterisks mark the simulated results and the solid lines are the predicted results based on the formula. (a) Standard deviation for $N = 1$. (b) The noise power for $N = 1$. The output noise is smaller than the output noise of the binary multiplier.
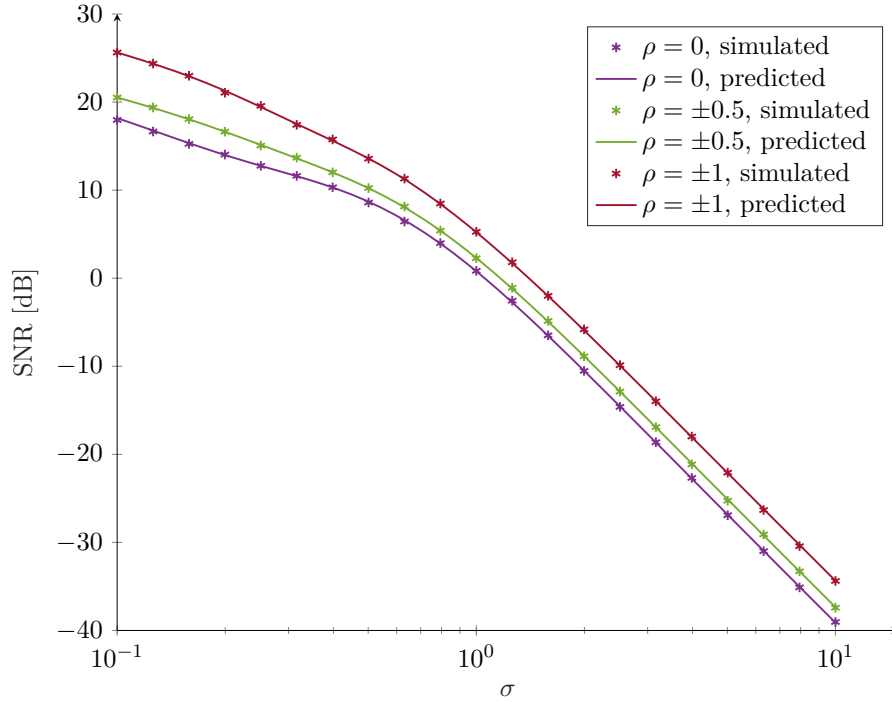
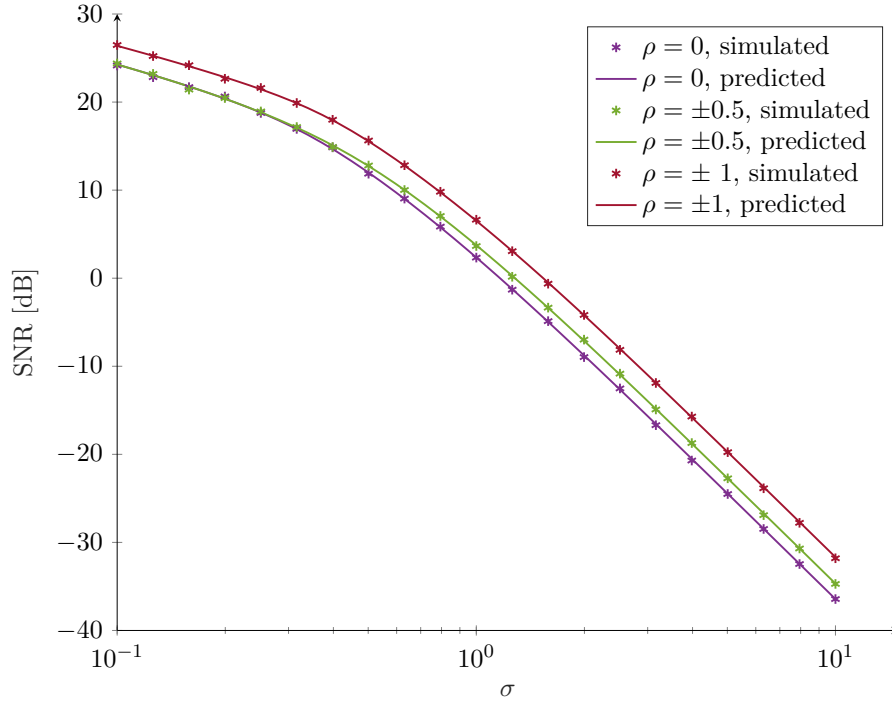**Figure 3-10:** Signal-to-noise ratio of the ternary SR-based multiplier for two sinusoidal inputs with a unity amplitude and frequency, sampled with a sampling frequency of 1 kHz and subjected to a second order Butterworth LPF with cut-off frequency of 20 Hz. V is set to 1 and δ is set to 0.5. The asterisks mark the simulated results and the solid lines are the predicted result based on the formula. The stochastic resonance does not happen since the performance is at maximum when $\eta = 0$.

3-3 Multiple Inputs Multiplier with XNOR

3-3-1 3 Inputs Multiplier

The diagram for three inputs SR-based multiplier is shown in Figure 3-14. It is basically a cascade of two SR-based multipliers. Using the same procedure, the expected output is derived as

$$
\begin{aligned}
\hat{y}_{out} = V - 2V \Big(& F_{\eta_1}(\theta_1 - x_1) + F_{\eta_2}(\theta_2 - x_2) + F_{\eta_3}(\theta_3 - x_3) \Big) \\
+ 4V \Big(& F_{\eta_1}(\theta_1 - x_1)F_{\eta_2}(\theta_2 - x_2) + F_{\eta_1}(\theta_1 - x_1)F_{\eta_3}(\theta_3 - x_3) + F_{\eta_2}(\theta_2 - x_2)F_{\eta_3}(\theta_3 - x_3) \Big) \\
- 8V & F_{\eta_1}(\theta_1 - x_1)F_{\eta_2}(\theta_2 - x_2)F_{\eta_3}(\theta_3 - x_3).
\end{aligned}
\tag{3-27}
$$

When linearized using a Taylor approximation, (3-27) becomes

$$
\hat{y}_{out} \approx \left(\frac{4V}{\pi\sqrt{2\pi}} \right) \frac{x_1 x_2 x_3}{\sigma^3},
\tag{3-28}
$$

provided that $\theta_1 = \theta_2 = \theta_3 = 0$ and $\sigma_1 = \sigma_2 = \sigma_3 = \sigma$.

(a)

(b)
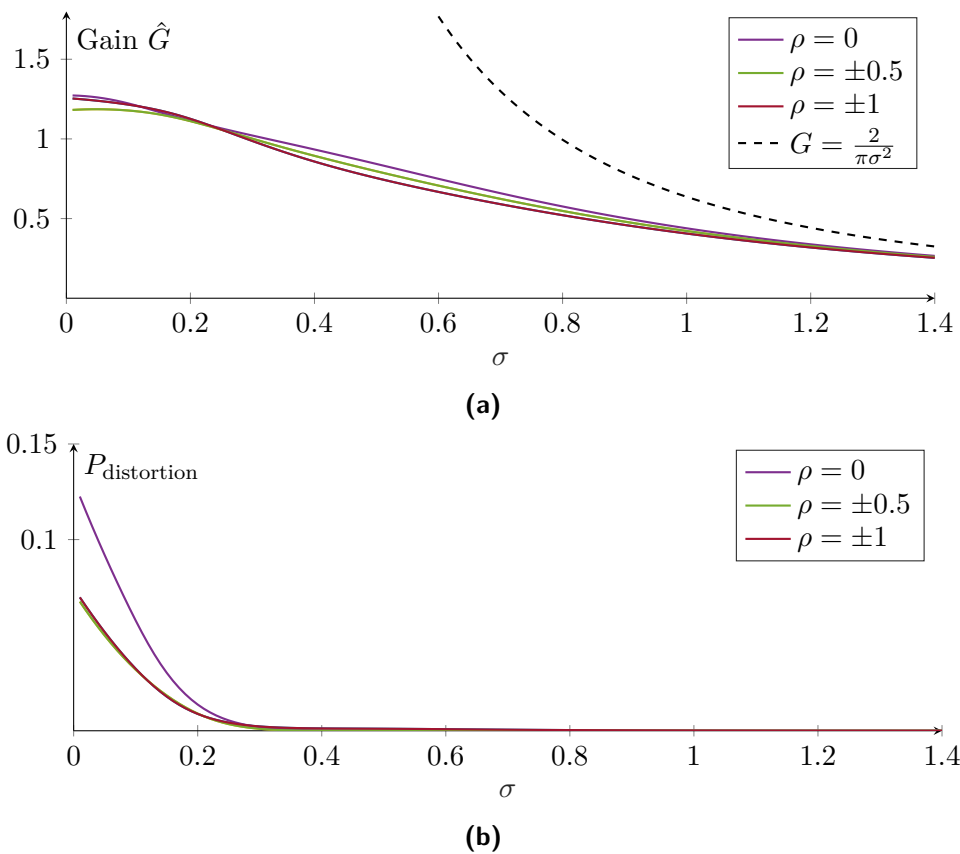
Figure 3-11: The distortion of the ternary SR-based multiplier for two sinusoidal inputs with a unity amplitude. V is set to 1 and δ is set to 0.5. (a) The LSE gain and the predicted linear gain. The gain depends on the correlation coefficient of the input signals. (b) The distortion power. As σ goes up, the output becomes more linear and the distortion power gets closer to zero.
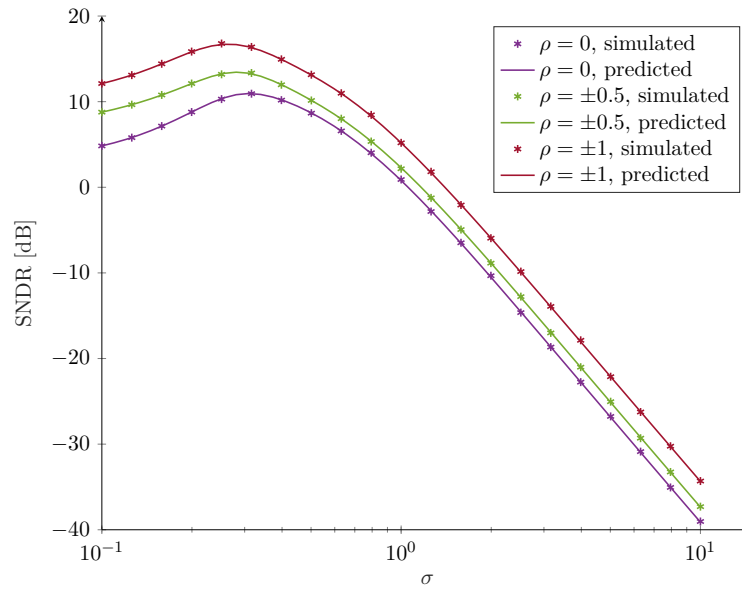
Figure 3-12: Signal-to-noise-and-distortion ratio of the ternary SR-based multiplier for two sinusoidal inputs with a unity amplitude and frequency, sampled with a sampling frequency of 1 kHz and subjected to a second order Butterworth LPF with cut-off frequency of 20 Hz. V is set to 1 and δ is set to 0.5. The asterisks mark the simulated results and the solid lines are the predicted results based on the formula. The stochastic resonance occur around the same σ.
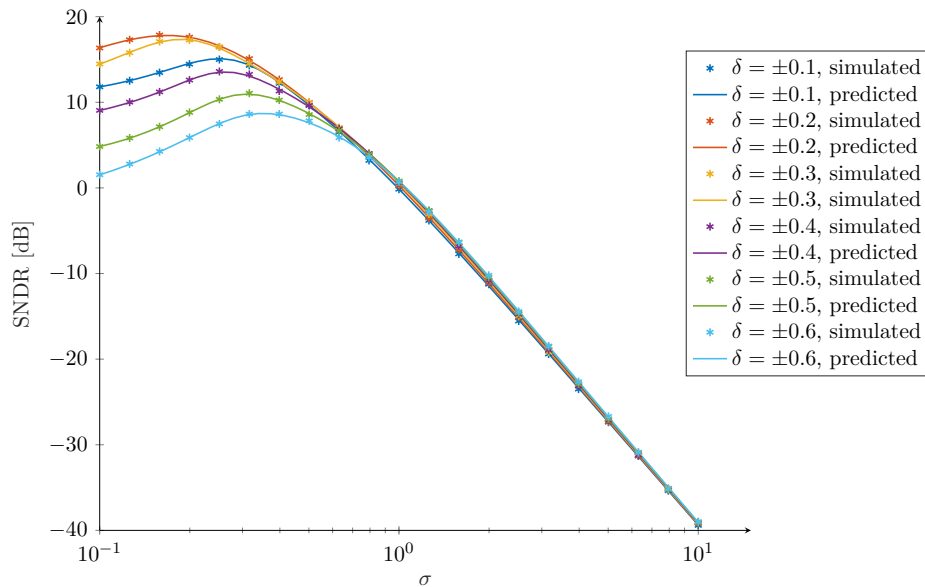
Figure 3-13: Signal-to-noise-and-distortion ratio of the ternary SR-based multiplier for two sinusoidal inputs with a unity amplitude and frequency, sampled with a sampling frequency of 1 kHz and subjected to a second order Butterworth LPF with cut-off frequency of 20 Hz for different values of δ. V is set to 1. The asterisks mark the simulated results and the solid lines are the predicted results based on the formula. The input signals are arranged such that $\rho = 0$.

3-3-2 K Inputs Multiplier

The SR-based multipliers can be cascaded further, to accomodate K input signals as shown in Figure 3-15. The expected value of its output is formulated as

$$\hat{y}_{out,K} = V + V \sum_{k=1}^{K} (-2)^k \sum_{1 \le i_1 < \cdots < i_k \le K} F_{\eta_{i_1}}(\theta_{i_1} - x_{i_1}) \ldots F_{\eta_{i_k}}(\theta_{i_k} - x_{i_k}), \qquad (3\text{-}29)$$

where the second term denotes the sum of all possible subproduct of $F_\eta(\theta - x)$. The Taylor approximation is given by

$$\hat{y}_{out,K} \approx V \left(-\sqrt{\frac{2}{\pi}} \right)^K \prod_{k=1}^{K} \frac{\theta_k - x_k}{\sigma_k}. \qquad (3\text{-}30)$$

The derivations of (3-29) and (3-30) are provided in Appendix A-3 and A-4, respectively. Based on (3-30), it can be said that each stage of the multiplier will either amplify or attenuate the input signals by a factor that is proportional to $\frac{1}{\sigma}$. This means that at the same σ, the output noise will be higher the larger K is. This is also demonstrated in Figure 3-16. In general, the noise behavior can be predicted with (3-14). Moreover, going through the pattern, the conditional expected value can also be calculated with (3-10).

The distortion behavior can be calculated with (3-18), where $\hat{\mathbf{Y}}_{\mathbf{out}}$ and $\mathbf{X}$ are given by

$$\hat{\mathbf{Y}}_{\mathbf{out}} = [\hat{y}_{out,K}(0) \quad \hat{y}_{out,K}(1) \quad \cdots \quad \hat{y}_{out,K}(M-1)]^{\mathrm{T}}$$
$$\text{and}$$
$$\mathbf{X} = \left[\prod_{k=1}^{K} x_k(0) \quad \prod_{k=1}^{K} x_k(1) \quad \cdots \quad \prod_{k=1}^{K} x_k(M-1) \right]^{\mathrm{T}}. \qquad (3\text{-}31)$$

The plot of the distortion behavior is presented in Figure 3-17. Since the LSE gain will eventually be proportional to $\frac{1}{\sigma^K}$, after a certain point, $\hat{G}$ will roll off steeper the larger K is. The distortion power also becomes higher the larger K is. This makes sense, since the distortion that is contained in the output of the previous XNOR is transferred to the next XNOR.
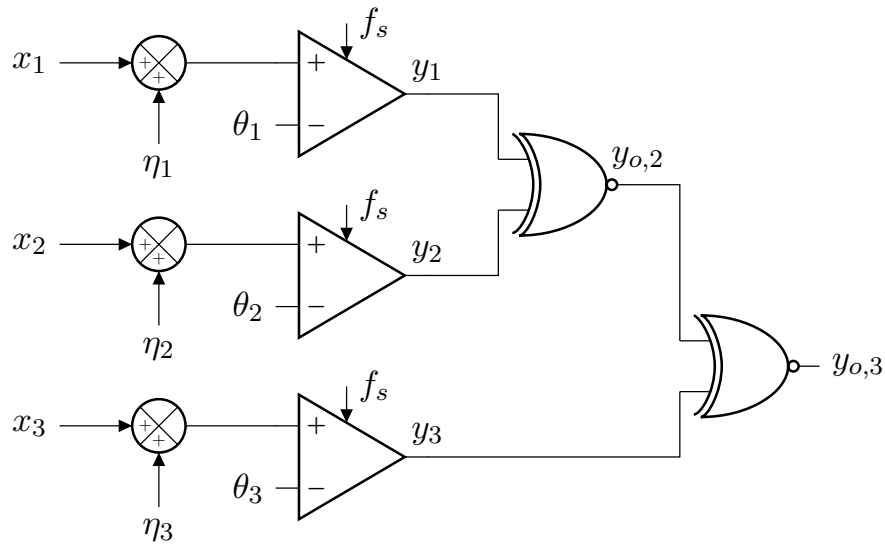
Figure 3-14: Three inputs SR-based multiplier.
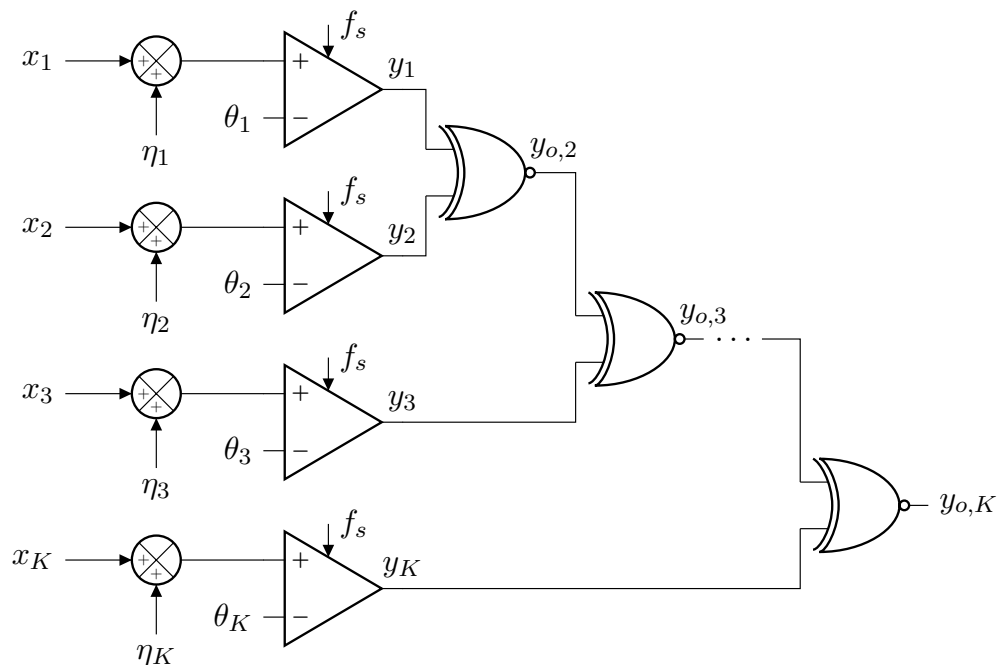
Figure 3-15: SR-based multiplier for K inputs.
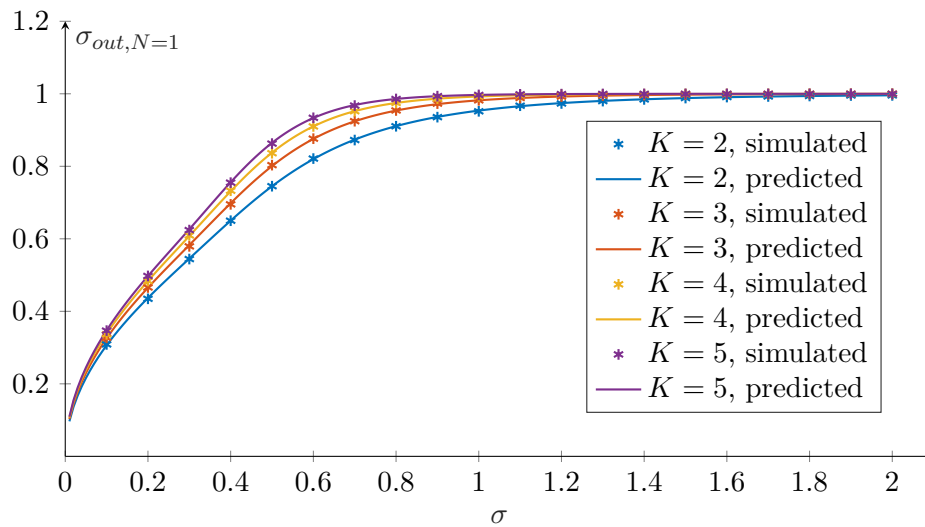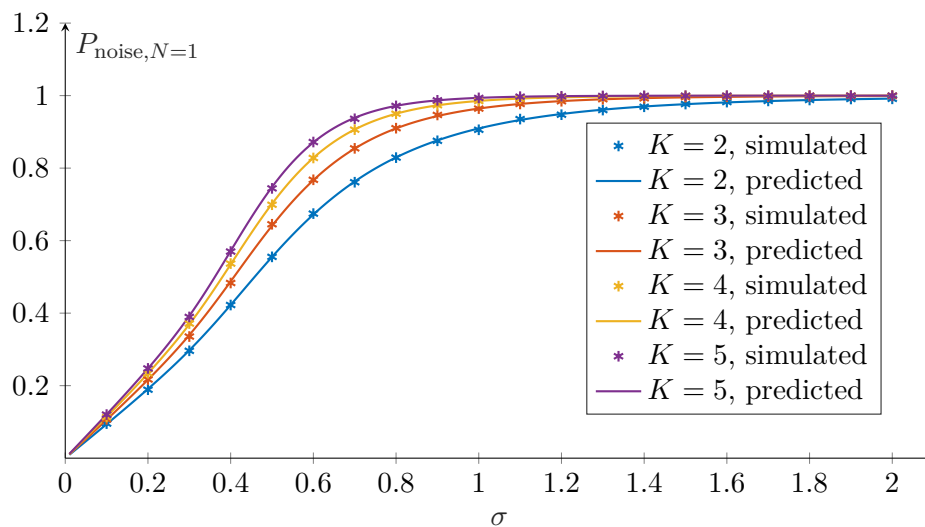
Figure 3-16: The output noise for K identical sinusoidal inputs with a unity amplitude. V is set to 1. The asterisks mark the simulated results and the solid lines are the predicted results based on the formula. (a) Standard deviation for $N = 1$. (b) The noise power for $N = 1$.
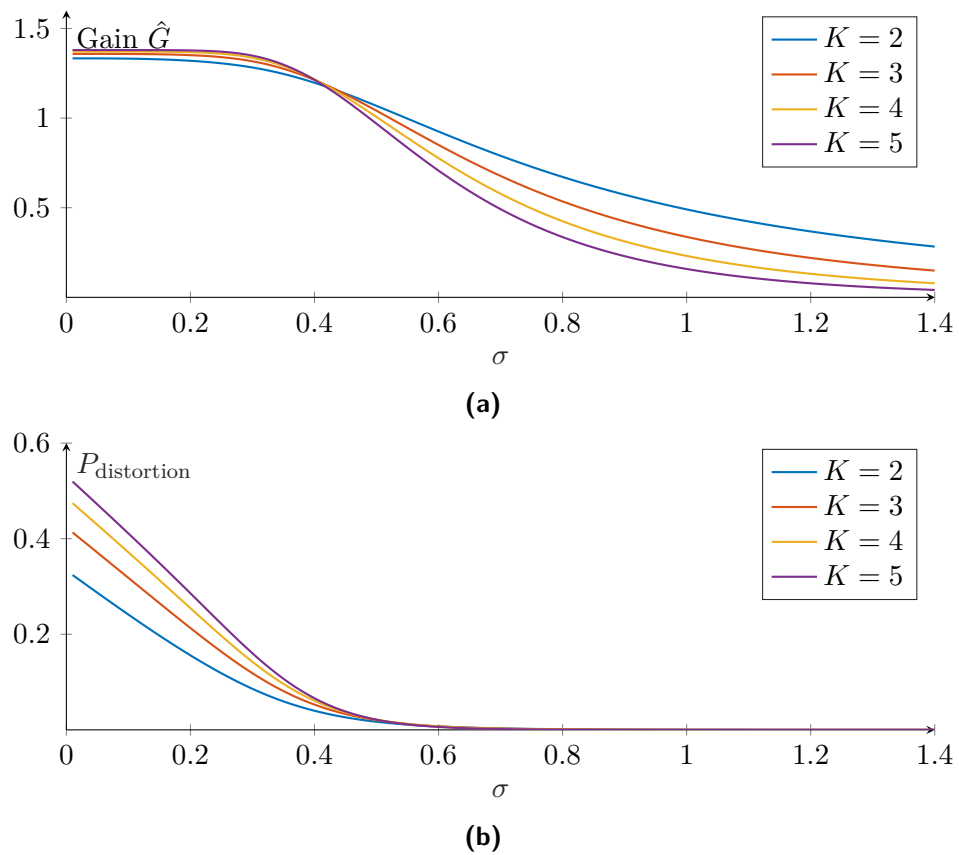
Figure 3-17: The distortion for K identical sinusoidal inputs with a unity amplitude. V is set to 1. (a) The LSE gain. (b) The distortion power. For larger K, the distortion power is higher.

3-4 Conclusions

In this chapter, the combination of an XNOR gate and SR-based fundamental building blocks is proposed to produce a signal multiplier. From the theoretical approach, the expected value of the output signal, the noise power, and the distortion power are formulated. The formulas are proven by comparing them to the simulation results. Using SNDR as the performance metric, a performance peak can be observed when the operator is subjected to noise.

Chapter 4

Signal Adder with Stochastic Resonance-Based Systems

Generating a binary signal that contains the information of the sum of two input signals can be done just by adding the input signals in analog domain, e.g. using a summing amplifier, and convert it using a 1-bit analog-to-digital converter (ADC). However, it can also be realized by converting both inputs to binary signals and do a binary addition. This way, it will generate an output that, when averaged, produces the sum of these inputs. The purpose of this chapter is to explain the design and properties of a signal adder with stochastic resonance (SR)-based systems.

4-1 SR-Based Adder in Binary Domain

The obvious choice for an SR-based adder is to use a binary half adder, shown in Figure 4-1. The operator generates two binary outputs b_0 and b_1 that, when converted to decimal and then averaged, represent the sum of both inputs.
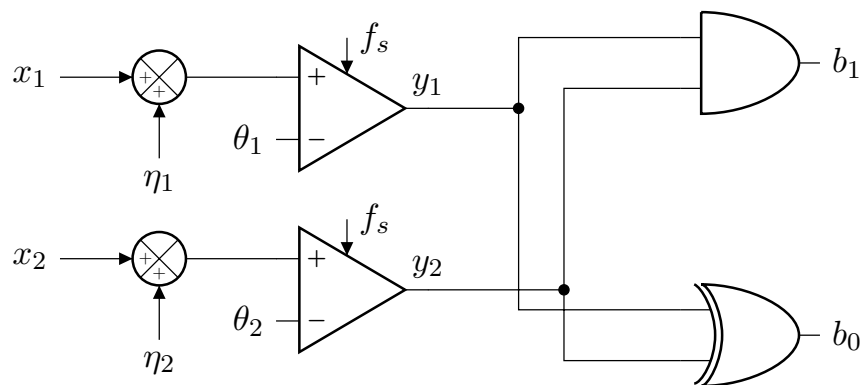
Figure 4-1: The proposed SR-based adder using binary half adder.

4-1-1   Output Signal Formula Derivation

For comparators producing outputs $\pm V$, the total sum will have a maximum value of $2V$. The output y_o can be determined by

$$y_o = 2V(2b_1 + b_0) - 2V. \tag{4-1}$$

The probabilities of y_o given x_1 and x_2 are

$$
\begin{aligned}
\Pr\left(y_o = +2V \mid x_1, x_2\right) &= \Pr\left(b_1 = 1 \cap b_0 = 0 \mid x_1, x_2\right) \\
&= \Pr\left(y_1 = 1 \cap y_2 = 1 \mid x_1, x_2\right) \\
&= \Pr\left(y_1 = 1 \mid x_1, x_2\right)\Pr\left(y_2 = 1 \mid x_1, x_2\right) \\
&= \left(1 - F_{\eta_1}\left(\theta_1 - x_1\right)\right)\left(1 - F_{\eta_2}\left(\theta_2 - x_2\right)\right) \\
&= 1 - \left(F_{\eta_1}\left(\theta_1 - x_1\right) + F_{\eta_2}\left(\theta_2 - x_2\right)\right) \\
&\quad + F_{\eta_1}\left(\theta_1 - x_1\right)F_{\eta_2}\left(\theta_2 - x_2\right),
\end{aligned} \tag{4-2}
$$

$$
\begin{aligned}
\Pr\left(y_o = 0 \mid x_1, x_2\right) &= \Pr\left(b_1 = 0 \cap b_0 = 1 \mid x_1, x_2\right) \\
&= \Pr\left(y_1 = 1 \cap y_2 = 0 \cup y_1 = 0 \cap y_2 = 1 \mid x_1, x_2\right) \\
&= \Pr\left(y_1 = 1 \mid x_1, x_2\right)\Pr\left(y_2 = 0 \mid x_1, x_2\right) \\
&\quad + \Pr\left(y_1 = 0 \mid x_1, x_2\right)\Pr\left(y_2 = 1 \mid x_1, x_2\right) \\
&= \left(1 - F_{\eta_1}\left(\theta_1 - x_1\right)\right)F_{\eta_2}\left(\theta_2 - x_2\right) \\
&\quad + F_{\eta_1}\left(\theta_1 - x_1\right)\left(1 - F_{\eta_2}\left(\theta_2 - x_2\right)\right) \\
&= \left(F_{\eta_1}\left(\theta_1 - x_1\right) + F_{\eta_2}\left(\theta_2 - x_2\right)\right) \\
&\quad - 2F_{\eta_1}\left(\theta_1 - x_1\right)F_{\eta_2}\left(\theta_2 - x_2\right),
\end{aligned} \tag{4-3}
$$

and

$$
\begin{aligned}
\Pr\left(y_o = -2V \mid x_1, x_2\right) &= \Pr\left(b_1 = 0 \cap b_0 = 0 \mid x_1, x_2\right) \\
&= \Pr\left(y_1 = 0 \cap y_2 = 0 \mid x_1, x_2\right) \\
&= \Pr\left(y_1 = 0 \mid x_1, x_2\right)\Pr\left(y_2 = 0 \mid x_1, x_2\right) \\
&= F_{\eta_1}\left(\theta_1 - x_1\right)F_{\eta_2}\left(\theta_2 - x_2\right).
\end{aligned} \tag{4-4}
$$

Using (4-2), (4-3), and (4-4), the expected value of y_o is

$$
\begin{aligned}
\hat{y}_{out} = \mathbf{E}\left[y_o \mid x_1, x_2\right] &= \Pr\left(y_o = 2V \mid x_1, x_2\right)(+2V) + \Pr\left(y_o = 0 \mid x_1, x_2\right)(0) \\
&\quad + \Pr\left(y_o = -2V \mid x_1, x_2\right)(-2V) \\
&= 2V\left(1 - \left(F_{\eta_1}\left(\theta_1 - x_1\right) + F_{\eta_2}\left(\theta_2 - x_2\right)\right)\right),
\end{aligned} \tag{4-5}
$$

which is the sum of $\mathbf{E}\left[y_1 \mid x_1\right]$ and $\mathbf{E}\left[y_2 \mid x_2\right]$. Using (3-6), the approximation of (4-5) for Gaussian noise inputs is

$$
\begin{aligned}
\hat{y}_{out} &\approx 2V\left(1 - \left(\frac{1}{2} + \frac{\theta_1 - x_1}{\sigma_1\sqrt{2\pi}} + \frac{1}{2} + \frac{\theta_2 - x_2}{\sigma_2\sqrt{2\pi}}\right)\right) \\
&= 2V\left(-\left(\frac{\theta_1 - x_1}{\sigma_1\sqrt{2\pi}} + \frac{\theta_2 - x_2}{\sigma_2\sqrt{2\pi}}\right)\right),
\end{aligned} \tag{4-6}
$$

which, for $\theta_1 = \theta_2 = 0$ and $\sigma_1 = \sigma_2 = \sigma$, becomes

$$\hat{y}_{out} \approx \frac{2V}{\sigma\sqrt{2\pi}}\left(x_1 + x_2\right). \tag{4-7}$$

Due to generating a 2-bit output, it is difficult to place this operator at the beginning of an SR-based system. For example, it is not possible to do an operation $f(x) = x_1(x_2 + x_3)$ only by adding x_2 and x_3, then multiplying it by x_1, because the SR-based multiplier cannot take 2-bit inputs. It is, however, easier to use the adder at the end of the system by rearranging $f = x_1 x_2 + x_1 x_3$. In this case, the system operates $x_1 \times x_2$ and $x_1 \times x_3$ first, and then adds the outputs of these multipliers, as shown in Figure 4-2. For this case, two multipliers are required as opposed to the first case that only needs one multiplier.
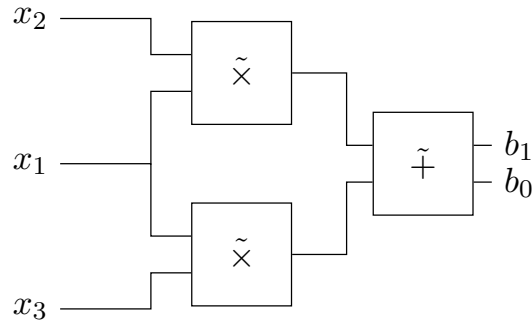
Figure 4-2: Block diagram of a system that produces $f = x_1(x_2 + x_3)$. The $\tilde{\times}$'s and $\tilde{+}$ represent SR-based operators.

4-1-2   Output Noise

The process of finding the output noise power is the same as in Section 3-1-2. The expected value of the square of the difference between y_o and $\hat{y}_{out}$ given x_1 and x_2 is

$$
\begin{aligned}
\mathbf{E}\left[\left(y_o - \hat{y}_{out}\right)^2 \mid x_1, x_2\right] &= \Pr\left(y_o = +2V \mid x_1, x_2\right)\left(2V - \hat{y}_{out}\right)^2 + \Pr\left(y_o = 0 \mid x_1, x_2\right)\left(-\hat{y}_{out}\right)^2 \\
&\quad + \Pr\left(y_o = -2V \mid x_1, x_2\right)\left(-2V - \hat{y}_{out}\right)^2 \\
&= \left(\frac{\hat{y}_{out}}{2V} + \Pr\left(y_o = -2V \mid x_1, x_2\right)\right)\left(4V^2 - 4V\hat{y}_{out} + \hat{y}_{out}^2\right) \\
&\quad + \left(1 - \frac{\hat{y}_{out}}{2V} - 2\Pr\left(y_o = -2V \mid x_1, x_2\right)\right)\left(\hat{y}_{out}^2\right) \\
&\quad + \Pr\left(y_o = -2V \mid x_1, x_2\right)\left(4V^2 + 4V\hat{y}_{out} + \hat{y}_{out}^2\right) \\
&= 8V^2 F_{\eta_1}\left(\theta_1 - x_1\right) F_{\eta_2}\left(\theta_2 - x_2\right) + 2V\hat{y}_{out} - \hat{y}_{out}^2.
\end{aligned}
\tag{4-8}
$$

The output noise is still white, hence the overall noise power is

$$
P_{\text{noise,out}} = \begin{cases} \dfrac{1}{MN} \displaystyle\sum_{n=0}^{M-1} \left(\mathbf{E}\left[(y_o(n) - \hat{y}_{out}(n))^2 \,\middle|\, x_1(n), x_2(n) \right] \right) & \text{for parallelization} \\[4mm] \dfrac{2\Delta f_{ENBW}}{Mf_s} \displaystyle\sum_{n=0}^{M-1} \left(\mathbf{E}\left[(y_o(n) - \hat{y}_{out}(n))^2 \,\middle|\, x_1(n), x_2(n) \right] \right) & \text{for filtering} \end{cases}.
$$

$$(4\text{-}9)$$

Figures 4-3a and 4-3b show the output noise power for an SR-based adder without any averaging and with filtering, respectively. The inputs are three sets of two sinusoidal signals that are arranged such that their correlation coefficients are $\rho = \{0, +0.5, +1\}$. From both figures, it can be seen that the output noise power for every case is the same. This makes sense because, in the end, y_o is equal to $y_1 + y_2$. Since the output noise for y_1 and y_2 is the same for every sinusoidal input with the same amplitude and frequency regardless of their phase differences, the output noise of the total system will be the same for every ρ.

With the reasoning stated above, it should be possible to derive (4-8) by calculating the output noise power for each comparator's output. Since the comparator generates a binary output, (3-10) holds. $\hat{y}_{1,out}$ and $\hat{y}_{2,out}$, derived in Appendix A-1, are formulated by (A-1). The expected value of the square of the difference between y_o and $\hat{y}_{out}$ given x_1 and x_2 is

$$
\begin{aligned}
\mathbf{E}\left[(y_o - \hat{y}_{out})^2 \,\middle|\, x_1, x_2 \right] &= \mathbf{E}\left[(y_1 - \hat{y}_{1,out})^2 \,\middle|\, x_1 \right] + \mathbf{E}\left[(y_2 - \hat{y}_{2,out})^2 \,\middle|\, x_2 \right] \\
&= \left(V^2 - \hat{y}_{1,out}^2 \right) + \left(V^2 - \hat{y}_{2,out}^2 \right) \\
&= 4V^2 F_{\eta_1}(\theta_1 - x_1) - 4V^2 F_{\eta_1}^2(\theta_1 - x_1) \\
&\quad + 4V^2 F_{\eta_2}(\theta_2 - x_2) - 4V^2 F_{\eta_2}^2(\theta_2 - x_2) \\
&= 4V^2 \Big(F_{\eta_1}(\theta_1 - x_1) - F_{\eta_1}^2(\theta_1 - x_1) + F_{\eta_2}(\theta_2 - x_2) - F_{\eta_2}^2(\theta_2 - x_2) \Big).
\end{aligned}
$$

$$(4\text{-}10)$$

In Appendix A-5, it is proven that (4-8) and (4-10) are equivalent.

The plots of simulated and predicted signal-to-noise ratio (SNR) are shown in Figure 4-4. The maximum SNR is achieved when the adder is noiseless.

4-1-3   Distortion

Similar to an SR-based multiplier, the distortion behavior of an SR-based adder can be calculated with (3-18), where $\hat{\mathbf{Y}}_{\mathbf{out}}$ and $\mathbf{X}$ are given by

$$
\begin{aligned}
\hat{\mathbf{Y}}_{\mathbf{out}} &= [\hat{y}_{out}(0) \quad \hat{y}_{out}(1) \quad \cdots \quad \hat{y}_{out}(M-1)]^{\mathrm{T}} \\
&\text{and} \\
\mathbf{X} &= [x_1(0) + x_2(0) \quad x_1(1) + x_2(1) \quad \cdots \quad x_1(M-1) + x_2(M-1)]^{\mathrm{T}}.
\end{aligned}
$$

$$(4\text{-}11)$$

Since $\mathbf{X}$ consists of an addition of two input matrices, $\hat{G}$ will always be the same for inputs that only differ in phases (e.g. different correlation coefficients for sinusoidal inputs), as shown in Figure 4-5a. As σ goes up, the adder becomes more linear and the gain approaches the
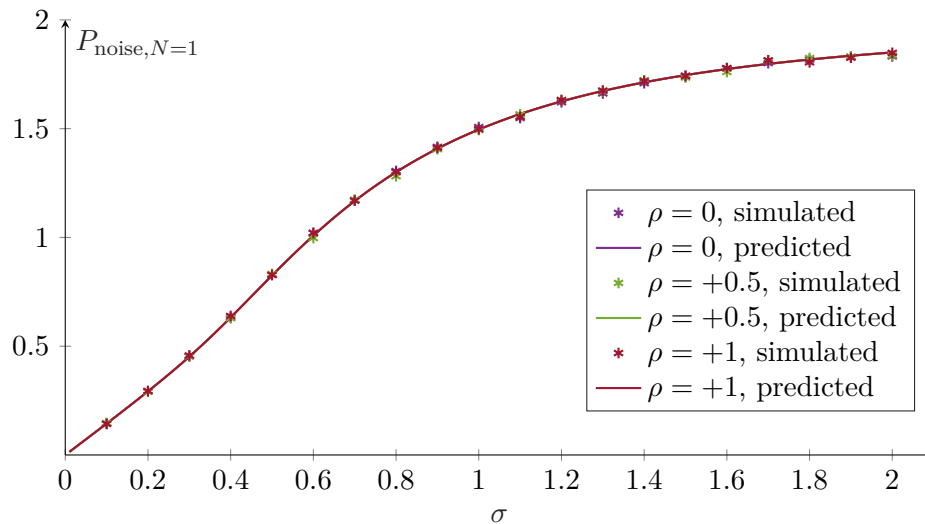
(a)
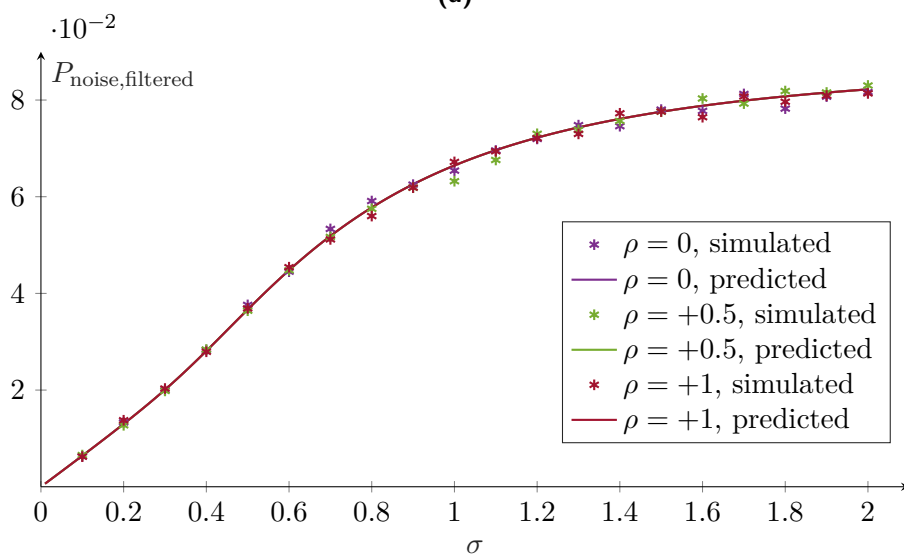
(b)

Figure 4-3: The output noise for two sinusoidal inputs with a unity amplitude, sampled with a sampling frequency of 1 kHz. V is set to 1. The asterisks mark the simulated results and the solid lines are the predicted results based on the formula. (a) The noise power without any averaging. (b) The noise power for the output signal filtered with a second order Butterworth LPF with a cut-off frequency of 20 Hz. As σ goes up, the output noise becomes larger.
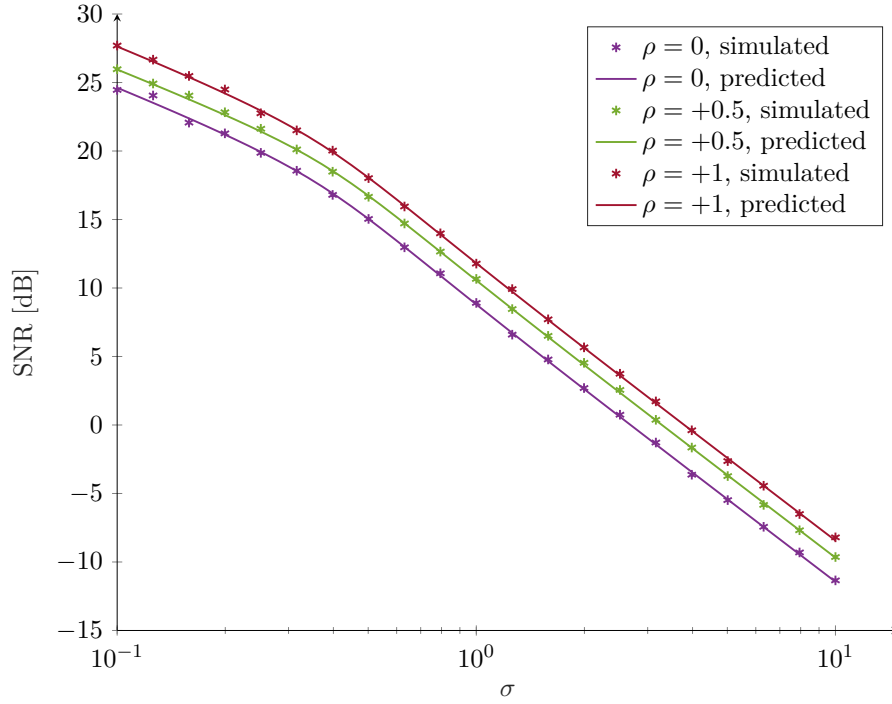
Figure 4-4: Signal-to-noise ratio for two sinusoidal inputs with a unity amplitude and frequency, sampled with a sampling frequency of 1 kHz and subjected to a second order Butterworth LPF with cut-off frequency of 20 Hz. V is set to 1. The asterisks mark the simulated results and the solid lines are the predicted results based on the formula. The stochastic resonance does not happen since the performance is at maximum when $\sigma = 0$.

linear gain $\dfrac{2V}{\sigma \sqrt{2\pi}}$. Although the gains are the same for every case, the distortion powers are different. Going through the definition of distortion power,

$$
\begin{aligned}
P_{\text{distortion}} &= \mathbf{E}\left[\left(\hat{y}_{out} - \hat{G}(x_1 + x_2)\right)^2\right] \\
&= \mathbf{E}\left[\left((\hat{y}_{1,out} - \hat{G}x_1) + (\hat{y}_{2,out} - \hat{G}x_2))\right)^2\right] \\
&= \mathbf{E}\left[\left(\hat{y}_{1,out} - \hat{G}x_1\right)^2\right] + \mathbf{E}\left[\left(\hat{y}_{2,out} - \hat{G}x_2\right)^2\right] + 2\mathbf{E}\left[(\hat{y}_{1,out} - \hat{G}x_1)(\hat{y}_{2,out} - \hat{G}x_2)\right].
\end{aligned}
$$

$$(4\text{-}12)$$

For the case shown in Figure 4-5, the first and second terms are always the same. The third term, however, changes depending on the phase difference of the input.

Figure 4-6 presents the SNDR for three sets of two sinusoidal inputs with a unity amplitude and frequency that differ in phase, sampled with a sampling frequency of 1 kHz and subjected to a second order Butterworth LPF with a cut-off frequency of 20 Hz. As in the case with the SR-based multiplier in Chapter 3, SNDR peaks can be found for $\sigma \neq 0$.

(a)

(b)
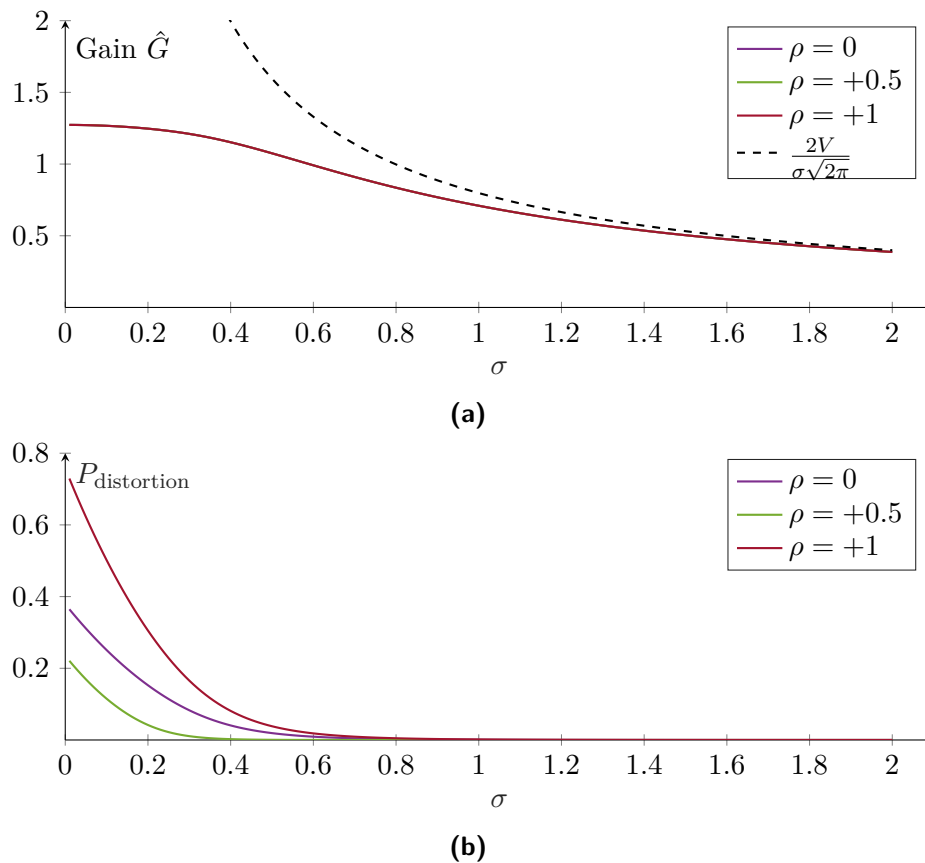
Figure 4-5: The distortion for two sinusoidal inputs with a unity amplitude, sampled with a sampling frequency of 1 kHz. V is set to 1. (a) The LSE gain and the predicted linear gain. The gains are the same for sinusoidal inputs regardless of their correlation coefficients. (b) The distortion power. As σ goes up, the output becomes more linear and the distortion power gets closer to zero.
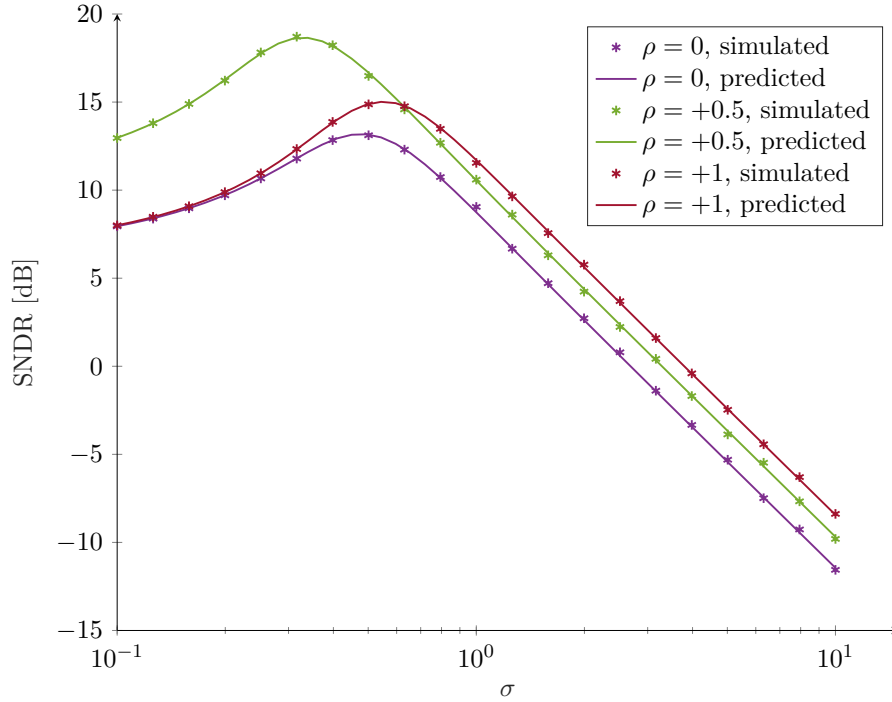
Figure 4-6: Signal-to-noise-and-distortion ratio for two sinusoidal inputs with a unity amplitude and frequency, sampled with a sampling frequency of 1 kHz and subjected to a second order Butterworth LPF with a cut-off frequency of 20 Hz. V is set to 1. The asterisks mark the simulated results and the solid lines are the predicted results based on the formula. The SNDR peaks can be found at different σ's for different ρ's.

4-2   SR-Based Subtractor

Subtracting y_2 from y_1 is the same as adding y_1 to $-y_2$. This means that a subtractor can be constructed from an adder that takes two inputs: y_1 and $-y_2$. Since y_2 has a value of $\pm V$, getting the inverse of y_2 can be achieved by putting an inverter in front of y_2 or inverting the input of the second comparator. The proposed SR-based subtractor is shown in Figure 4-7. The expected value of y_o, as derived in Appendix A-6, is

$$
\begin{aligned}
\hat{y}_{out} &= 2V\Big(-\big(F_{\eta_1}\left(\theta_1 - x_1\right) - F_{\eta_2}\left(\theta_2 - x_2\right)\big)\Big) \\
&= \mathbf{E}\left[y_1 \mid x_1\right] - \mathbf{E}\left[y_2 \mid x_2\right].
\end{aligned}
\tag{4-13}
$$

Using (3-6), the approximation of (4-13) for Gaussian noise inputs with $\theta_1 = \theta_2 = 0$ and $\sigma_1 = \sigma_2 = \sigma$ is

$$
\hat{y}_{out} \approx \frac{2V}{\sigma\sqrt{2\pi}}\left(x_1 - x_2\right).
\tag{4-14}
$$
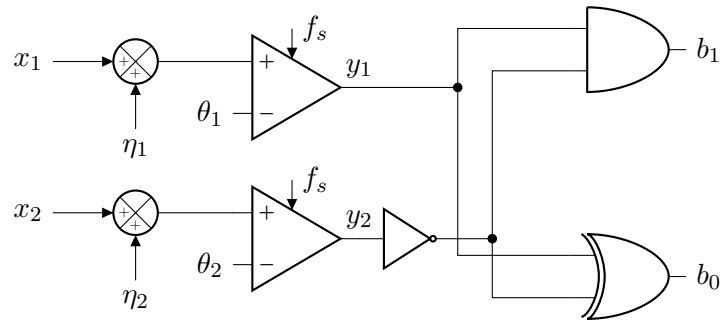
Figure 4-7: An SR-based subtractor using an SR-based adder with inverted y_2.

4-2-1 Output Noise and Distortion

Due to the SR-based subtractor fundamentally being an SR-based adder, the output noise of the subtractor will behave the same as that of the adder, i.e. (4-10). Thus, for the same case, the output noise power of the SR-based subtractor is also shown in Figure 4-3. It also should be noted that for the SR-based subtractor, (4-8) and (4-10) are not equivalent since the $\hat{y}_{out}$'s are different. The distortion power of two sets of two sinusoidal inputs with a unity amplitude are presented in Figure 4-8. The case of $\rho = +1$ will have zero distortion power, thus it is not included.
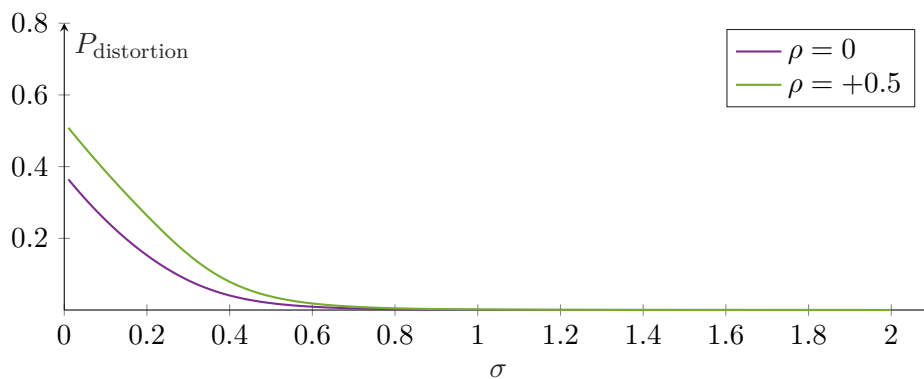
Figure 4-8: The distortion power of the SR-based subtractor for two sinusoidal inputs with a unity amplitude, sampled with a sampling frequency of 1 kHz. V is set to ± 1. As σ goes up, the output becomes more linear and the distortion power gets closer to zero.

4-3 Multiple Inputs Adder

4-3-1 3 Inputs Adder

Since the outputs of a two inputs SR-based adder are 2-bit signals, a 3 inputs SR-based adder cannot be constructed by cascading two 2 inputs SR-based adders. The only option is to construct an adder that produces the outputs based on a truth table. Table 4-1 shows the
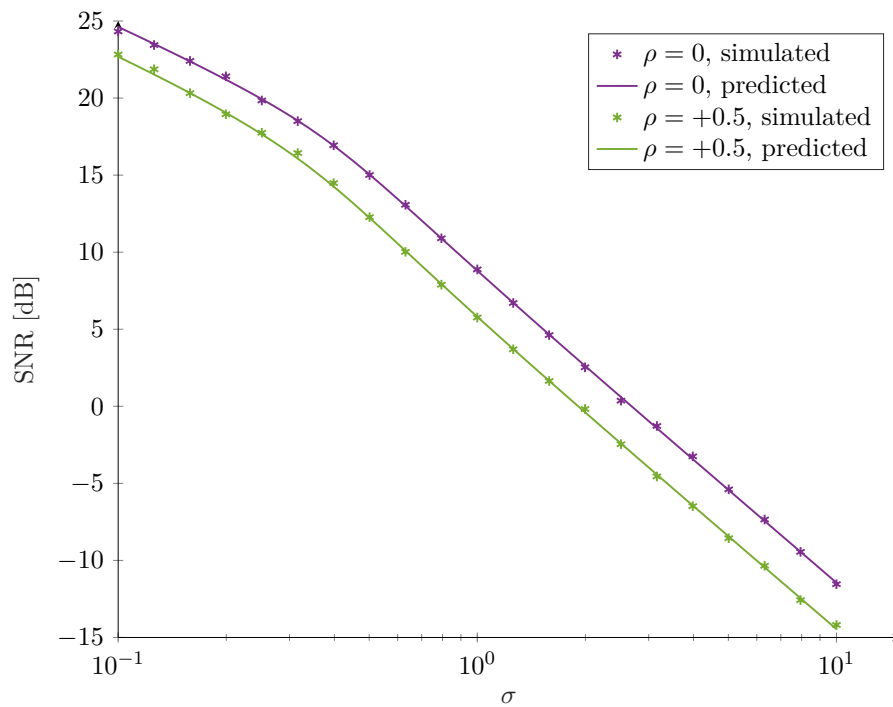
(a)
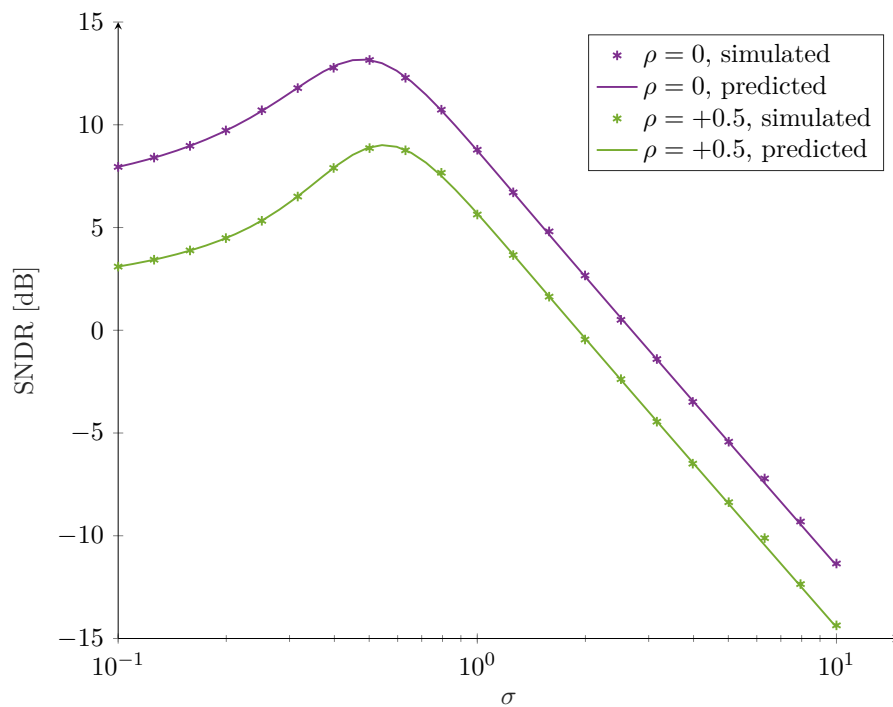
(b)

Figure 4-9: (a) Signal-to-noise ratio and (b) signal-to-noise-and-distortion ratio for two sinusoidal inputs with a unity amplitude and frequency, sampled with a sampling frequency of 1 kHz and subjected to a second order Butterworth LPF with a cut-off frequency of 20 Hz. V is set to 1. The asterisks mark the simulated results and the solid lines are the predicted results based on the formula. The stochastic resonance occurs in SNDR at different σ for different ρ.

truth table of a 3 inputs adder and it can be formulated as boolean function

$$b_0 = y_1 \oplus y_2 \oplus y_3,$$
$$b_1 = y_1 \cdot y_2 \oplus y_2 \cdot y_3 \oplus y_1 \cdot y_3. \tag{4-15}$$

The 2-bit output can be converted to a decimal value with formula

$$y_o = 2V(2b_1 + b_0) - 3V. \tag{4-16}$$

since the maximum value of the output is $+3V$, its expected value is formulated as

$$\hat{y}_{out} = 3V - 2V\left(F_{\eta_1}(\theta_1 - x_1) + F_{\eta_2}(\theta_2 - x_2) + F_{\eta_3}(\theta_3 - x_3)\right), \tag{4-17}$$

which can be approximated as

$$\hat{y}_{out} \approx \frac{2V}{\sigma\sqrt{2\pi}}(x_1 + x_2 + x_3) \tag{4-18}$$

for Gaussian noise sources, $\theta_1 = \theta_2 = 0$, and $\sigma_1 = \sigma_2 = \sigma$.

Table 4-1: Truth table of a 3 inputs adder.

y_1	y_2	y_3	b_1	b_0
0	0	0	0	0
0	0	1	0	1
0	1	0	0	1
0	1	1	1	0
1	0	0	0	1
1	0	1	1	0
1	1	0	1	0
1	1	1	1	1

The block diagram of a 3 inputs SR-based adder that satisfies (4-15) is shown in Figure 4-10. It can be seen that the 3 inputs SR-based adder is way more complex than the 2 inputs SR-based adder. Although still producing a 2-bit output, the 3 input adder requires 5 more logic circuits compared to the 2 input adder that only needs 2 logic circuits. Fortunately, (4-15) is not the only formula that satisfies Table 4-1. b_1 is also equal to $(y_1 \oplus y_2) \cdot y_3 + y_1 \cdot y_2$, therefore the 3 inputs SR-based adder can also be realized with the circuit in Figure 4-11. This alternative is less costly since it only needs 5 logic circuits.

4-3-2 K Inputs Adder

As discussed previously, cascading SR-based adders does not work in constructing a K inputs SR-based adder due to the increasing number of output bits. In fact, the number of bits produced by the operator is equal to $\lfloor \log_2 K \rfloor + 1$, where $\lfloor x \rfloor$, the floor function, gives the closest integer that is less than or equal to x. Therefore, it is more beneficial to hold onto
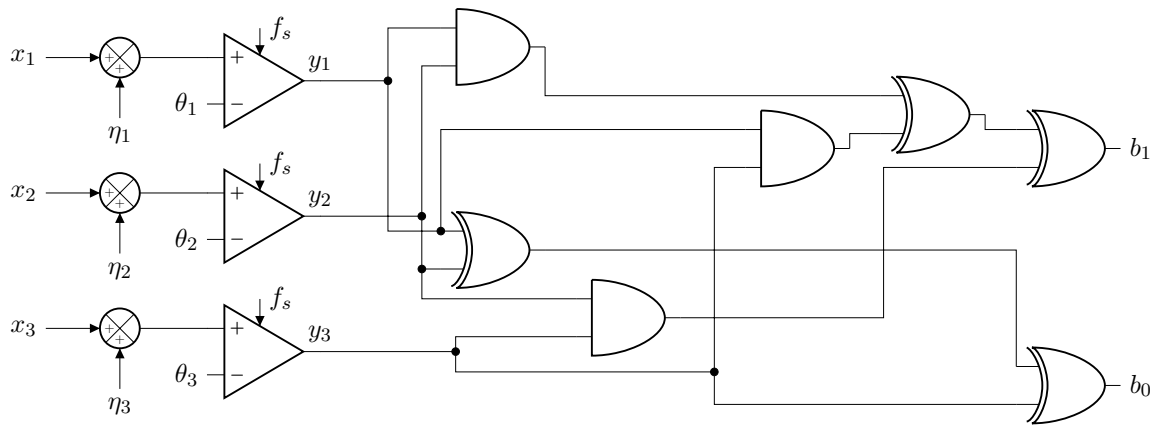
Figure 4-10: Three inputs SR-based adder.
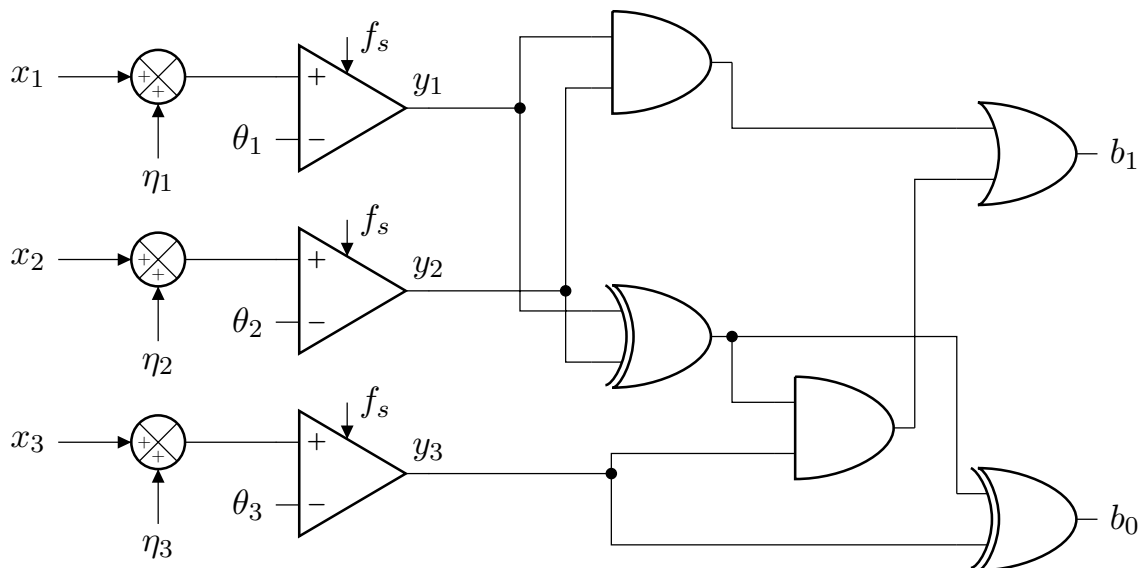
Figure 4-11: Alternative of three inputs SR-based adder.

the boolean function of the output bits rather than the strict block diagrams of the operator. The boolean outputs are formulated as

$$b_0 = \bigoplus_{k=1}^{K} y_k,$$

$$b_1 = \bigoplus_{1 \le i_1 < i_2 \le K} y_{i_1} \cdot y_{i_2},$$

$$b_2 = \bigoplus_{1 \le i_1 < i_2 < i_3 < i_4 \le K} y_{i_1} \cdot y_{i_2} \cdot y_{i_3} \cdot y_{i_4},$$

$$\cdot$$
$$\cdot$$
$$\cdot$$

$$b_{\lfloor \log_2 K \rfloor} = \bigoplus_{1 \le i_1 < \cdots < i_{2\lfloor \log_2 K \rfloor} \le K} y_{i_1} \cdot \cdots \cdot y_{i_{2\lfloor \log_2 K \rfloor}}.$$

$(4\text{-}19)$

$\bigoplus$ denotes the big operator for XOR and $\displaystyle\bigoplus_{k=1}^{K} y_k$ simply means $y_1 \oplus y_2 \oplus \cdots \oplus y_K$. Regardless of the complexity of the circuits, implementing K inputs adders can reduce the number of required input channels of the digital signal processor from K to $\lfloor \log_2 K \rfloor + 1$.

Setting the output $y_{o,K}$ equal to $2V \left(\displaystyle\sum_{k=0}^{\lfloor \log_2 K \rfloor} 2^k b_k \right) - KV$, the expected value of $y_{o,K}$ is

$$\hat{y}_{out,K} = KV - 2V \sum_{k=1}^{K} F_{\eta_k} \left(\theta_k - x_k \right), \tag{4-20}$$

which can be approximated as

$$\hat{y}_{out,K} \approx \frac{-2V}{\sqrt{2\pi}} \sum_{k=1}^{K} \left(\frac{\theta_k - x_k}{\sigma_k} \right). \tag{4-21}$$

Equation (4-20) and (4-21) are proven in Appendix A-7.

It has been explained in Section 4-1-2 that the output noise of the SR-based adder is the sum of output noise produced by the individual comparators. Therefore, the output noise power for a K inputs SR-based adder can be calculated with (4-9), where

$$\mathbf{E}\left[\left(y_o - \hat{y}_{out,K} \right)^2 \Big| x_1, \cdots, x_K \right] = 4V^2 \sum_{k=1}^{K} \left(F_{\eta_k} \left(\theta_k - x_k \right) - F_{\eta_k}^2 \left(\theta_k - x_k \right) \right). \tag{4-22}$$

The standard deviation and output noise power for K identical sinusoidal inputs with a unity amplitude are presented in Figure 4-12. Since the maximum output is proportional to K and V^2, so is the noise power.

The distortion power is calculated with (3-18), where

$$\hat{\mathbf{Y}}_{\mathbf{out}} = [\hat{y}_{out,K}(0) \quad \hat{y}_{out,K}(1) \quad \cdots \quad \hat{y}_{out,K}(M-1)]^{\mathrm{T}}$$

and

$$\mathbf{X} = \left[\sum_{k=1}^{K} x_k(0) \quad \sum_{k=1}^{K} x_k(1) \quad \cdots \quad \sum_{k=1}^{K} x_k(M-1)\right]^{\mathrm{T}}. \tag{4-23}$$

The LSE gain and distortion power for the same case as Figure 4-12 is shown in Figure 4-13. Although the LSE gains are the same for every case, the distortion power increases because the ideal output power itself increases.
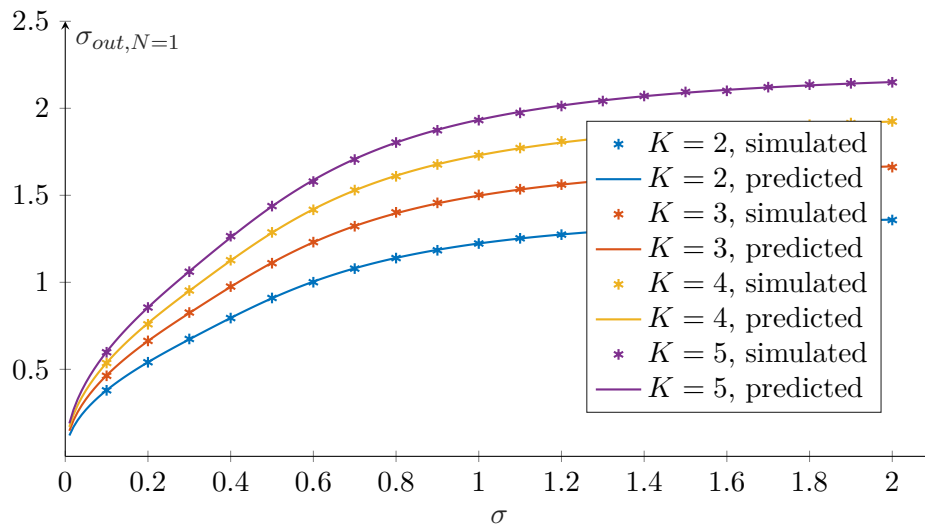
(a)
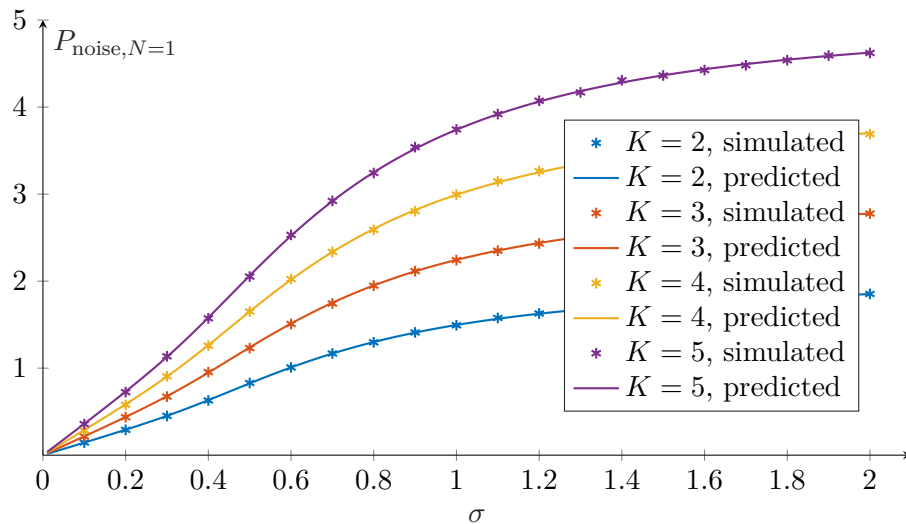
(b)

Figure 4-12: The output noise for K identical sinusoidal inputs with a unity amplitude. V is set to 1. The asterisks mark the simulated results and the solid lines are the predicted results based on the formula. (a) Standard deviation for $N = 1$. (b) The noise power for $N = 1$.

(a)

(b)
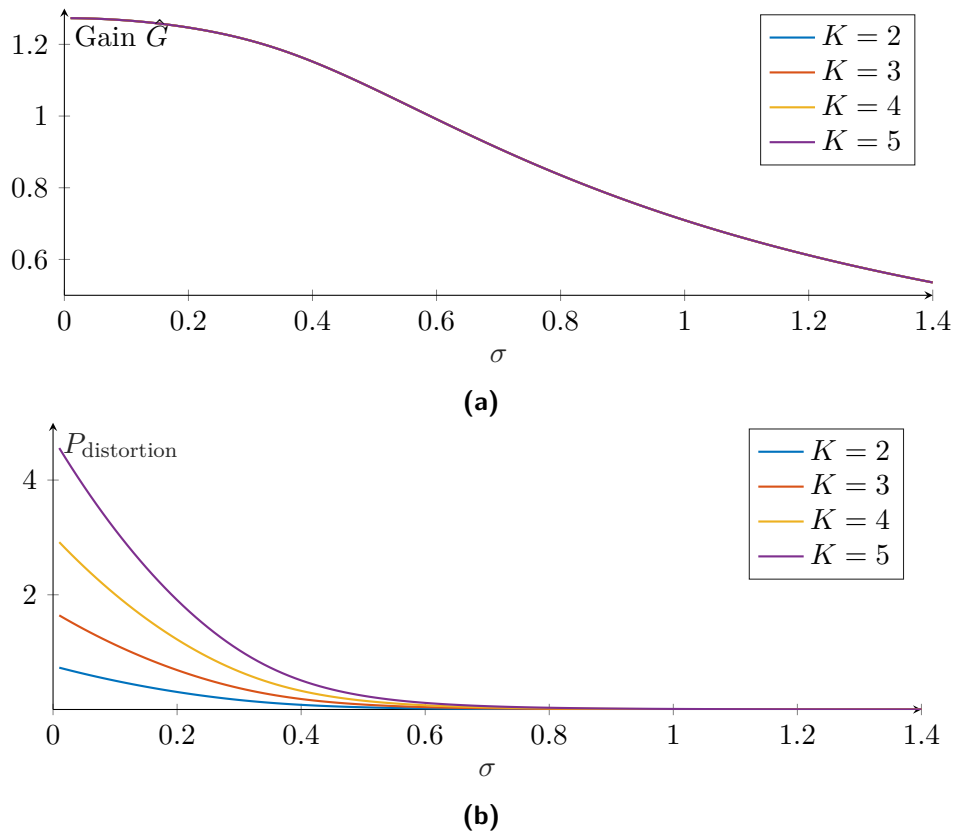
Figure 4-13: The distortion for K identical sinusoidal inputs with a unity amplitude. V is set to 1. (a) The LSE gain. (b) The distortion power. For larger K, the distortion power is higher.

4-4   Conclusions

In this chapter, a binary half-adder is used in combination with SR-based fundamental building blocks to produce an SR-based adder. The properties of the operator consisting of the expected value of the output, the output noise power, and the distortion power are formulated and compared with the simulation results. An SR-based subtractor can be constructed by inserting an inverter after one of the SR-based blocks. Using SNDR as the performance measure, a performance peak can be observed when the operator is subjected to noise.

Chapter 5

Implementing Stochastic Resonance-based Operators in Mathematical Functions

As mathematical operator building blocks, an adder, subtractor, and multiplier should also function in building a system. This chapter discusses the feasibility of using stochastic resonance (SR)-based mathematical operators that have been proposed in the previous chapters to construct several systems. Ultimately, the SR-based mathematical operators are used to construct a Teager Energy Operator (TEO) as an action potential (AP) detection system.

5-1 Implementation of $f = x_1(x_2 + x_3)$

As explained in Chapter 4, it is easier to implement the SR-based adder at the end of the system. In this case, the system can be written as $f = x_1 x_2 + x_1 x_3$. The implementation of f by SR-based operators is presented in Figure 5-1. The important thing that should be noted here is that two comparators are necessary to accomodate x_1. Moreover, each noise must be independent of each other. These are done such that y_1, y_2, y_3, and y_4 are conditionally independent of each other, given the input signals. Otherwise, there is no guarantee that the SR-based operators will work as desired. To simplify the analysis, Gaussian white noise sources with identical powers are used.

As a test case, three sinusoidal signals with a unity amplitude and frequency are used, as shown in Figure 5-2a. The three signals are: $x_1 = \sin(2\pi t), x_2 = \sin\left(2\pi t - \frac{\pi}{3}\right)$, and $x_3 = \sin\left(2\pi t - \frac{2\pi}{3}\right)$. The system is sampled with a sampling frequency of 100 kHz and filtered by a second-order Butterworth LPF with a cut-off frequency of 20 Hz. The output value V and input noise power σ^2 are set as 1 and 0.64, respectively. This input noise power is set such that the SNDR of the output is near its maximum.
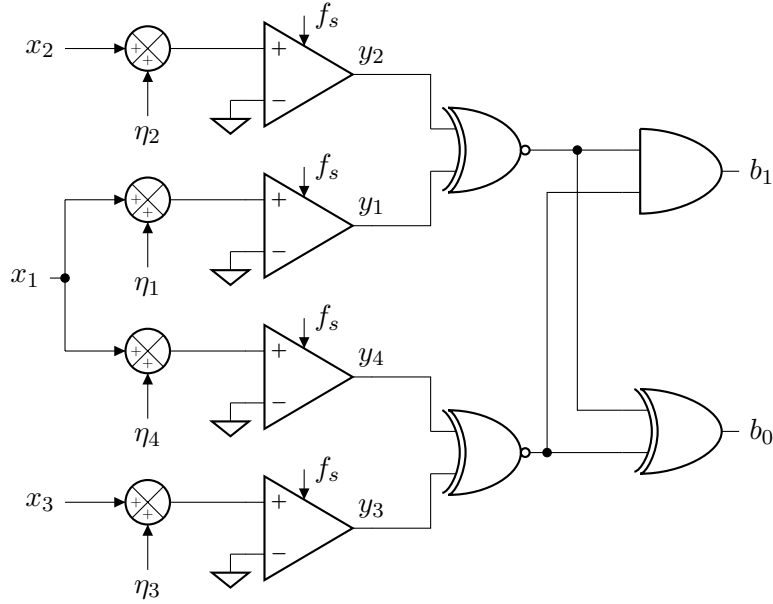
Figure 5-1: The proposed SR-based implementation of $f = x_1(x_2 + x_3)$.

While the calculation of the least-square error (LSE) gain and distortion power are trivial, the output noise power is formulated as

$$P_{\text{noise,out}} = \frac{2\Delta f_{ENBW}}{f_s}\left(\mathbf{E}\left[V^2 - \left(\frac{\mathbf{E}[y_1 \mid x_1]\mathbf{E}[y_2 \mid x_2]}{V}\right)^2\right] + \mathbf{E}\left[V^2 - \left(\frac{\mathbf{E}[y_4 \mid x_1]\mathbf{E}[y_3 \mid x_3]}{V}\right)^2\right]\right).$$
$$\tag{5-1}$$

The averaged, expected, and amplified ideal outputs are shown in Figure 5-2b. The LSE gain and SNDR are 0.74 and 21 dB, respectively. Comparing the averaged output with the ideal output both qualitatively and quantitatively, it can be said that, in this case, the SR-based system manages to produce the desired output.

5-2 Implementation of TEO

In this thesis, an SR-based derivative is not designed. Thus, the TEO cannot be implemented purely by SR-based operators. By substituting the multipliers and subtractor in Figure 2-7, an SR-based TEO can be constructed. However, the amplitude of a derivative and second derivative of an input x in most cases will be larger than the amplitude of x itself. For example, a sinusoidal input with an amplitude and frequency of A_1 and f_0 will have a second derivative of a sine with an amplitude of $(2\pi f_0)^2 A_1$. This big difference in amplitude will pose problems since, for achieving an optimum performance, the amount of noise that should be added to the system has to follow the largest input. This will result in an enormous amount of output noise and thus a high performance averaging technique will be needed. To avoid this, each differentiator is set to have a time constant τ of $\left(\frac{1}{2\pi f_0}\right)$ so that the derivative of the input will be comparable in amplitude with the original input. The final block diagram
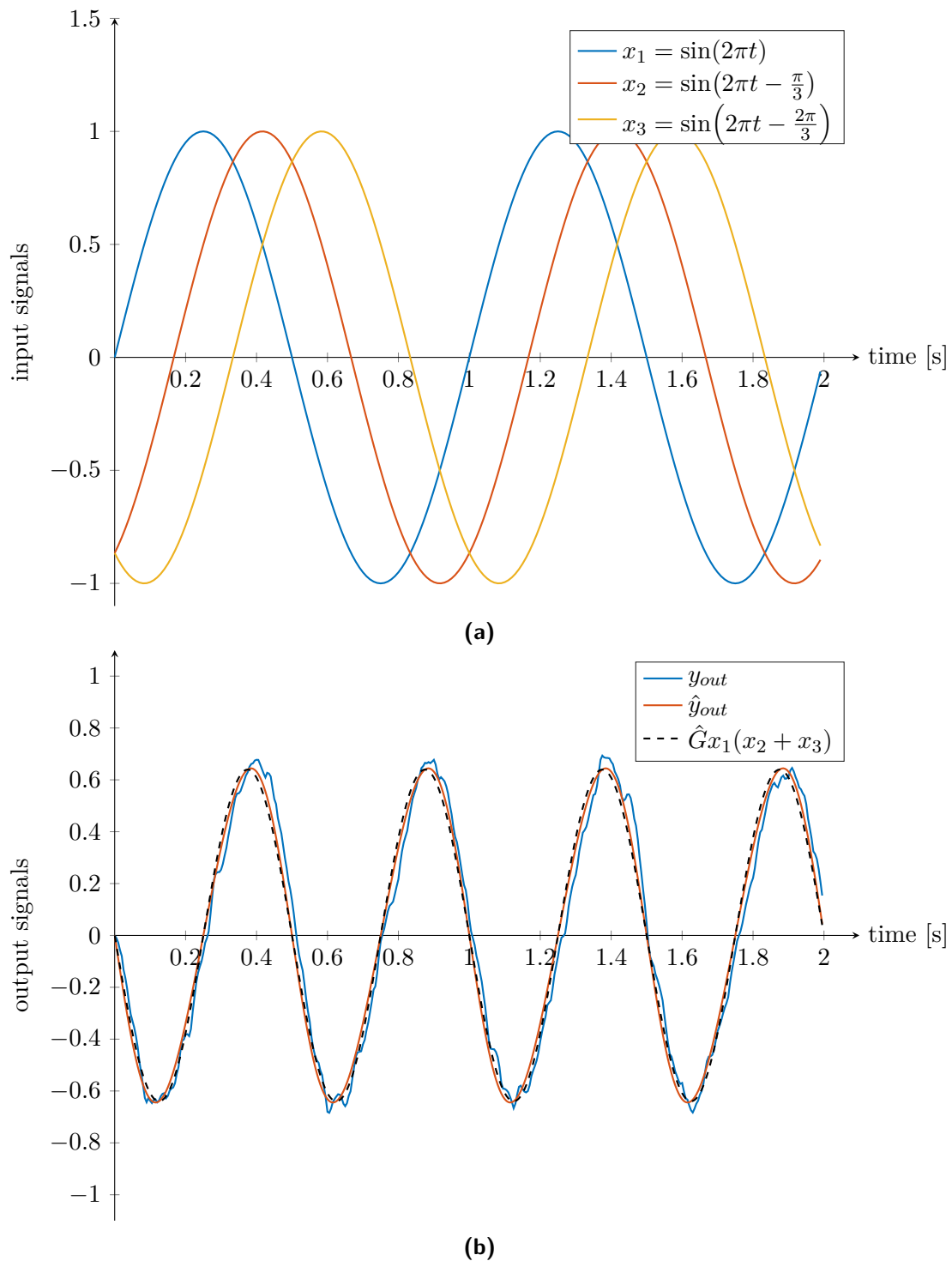
Figure 5-2: Inputs and outputs of $f = x_1(x_2 + x_3)$ using the proposed SR-based system. The sampling frequency, V, input noise power, and cut-off frequency of the second-order Butterworth LPF are 100 kHz, 1, 0.64, and 20 Hz, respectively. (a) Input signals. (b) The averaged, expected, and amplified ideal outputs.

of the SR-based TEO is shown in Figure 5-3. This system will produce a TEO output that is attenuated by a factor of $\left(\frac{1}{2\pi f_0}\right)^2$. In the following cases, the following parameters are set: $V = 1$, the sampling frequency is 100 kHz, the averaging technique used is a second-order Butterworth filter with a cut-off frequency of 10 Hz, and the simulation time is 2.5 s.
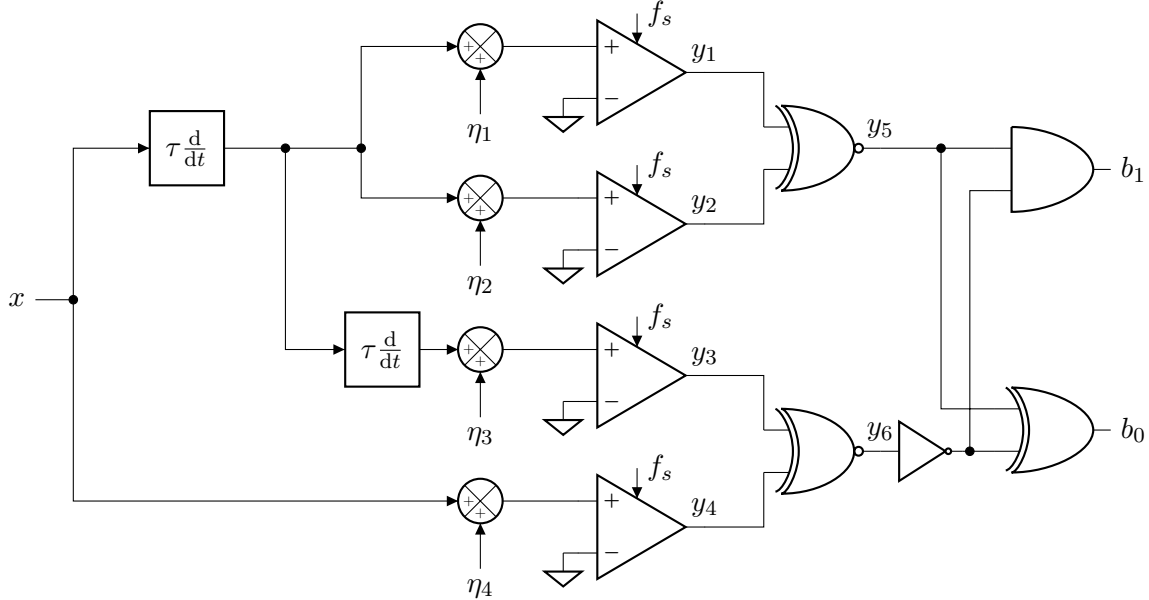
Figure 5-3: The proposed SR-based implementation of the continuous-time TEO.

5-2-1   Case Study: Sinusoidal Signal

As a test case, input $x = 0.1\sin(2\pi t)$ is used. This input is supposed to make the SR-based TEO generates output $\psi(x) = 0.01$. $\sigma = 0.1$ is chosen as it results in a near-optimum SNDR. The output of the TEO is presented in Figure 5-4, with $\hat{G} = 50$, SNR$= 28$ dB, and SNDR$= 24$ dB.

Comparing the amplified ideal output with the expected output in Figure 5-4, it can be seen that, instead of a constant, a sinusoidal ripple is present at the output. This is due to the distortion at the output of each comparator. To decrease this distortion, uniformly distributed white noise sources can be used instead of Gaussian distributed white noise sources, which is discussed extensively in Appendix D.

To remove the distortion completely and produce a near-optimum SNDR, the noise power should be chosen as the square of the maximum of the absolute value of the inputs over three, i.e.

$$\sigma_0 = \frac{1}{\sqrt{3}} \max \left\{ |x|, \frac{1}{2\pi f_0}\left|\frac{\mathrm{d}x}{\mathrm{d}t}\right|, \frac{1}{(2\pi f_0)^2}\left|\frac{\mathrm{d}^2 x}{\mathrm{d}t^2}\right| \right\}. \tag{5-2}$$
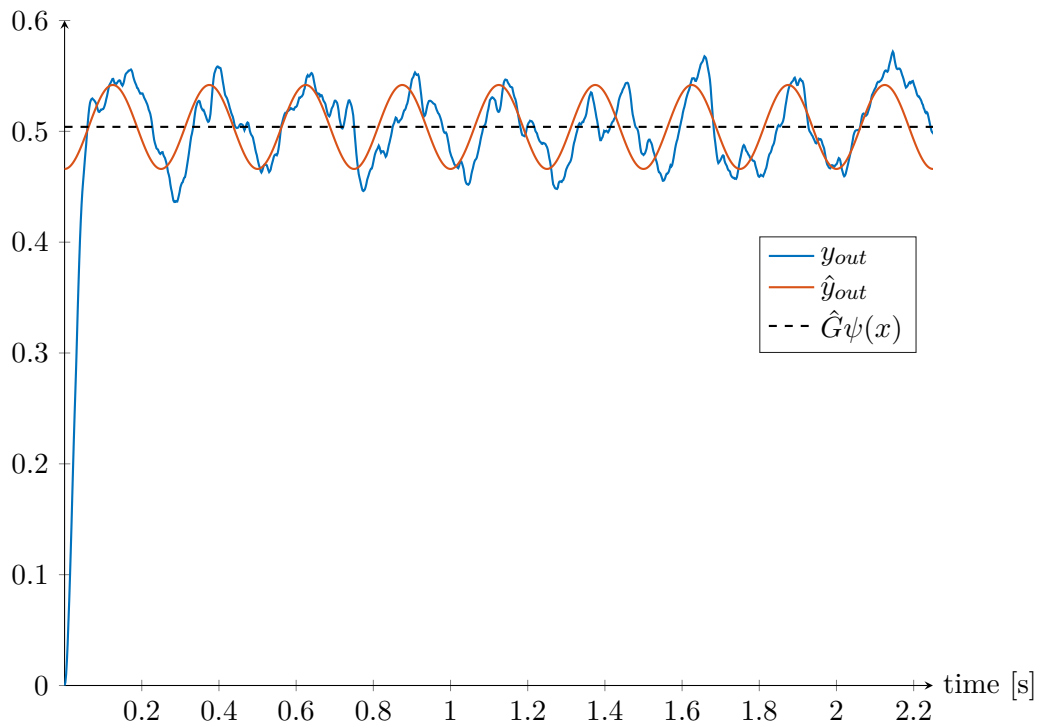
Figure 5-4: The averaged, expected, and amplified ideal outputs of the TEO of input $x = 0.1\sin(2\pi t)$ subjected to Gaussian distributed white noise sources.
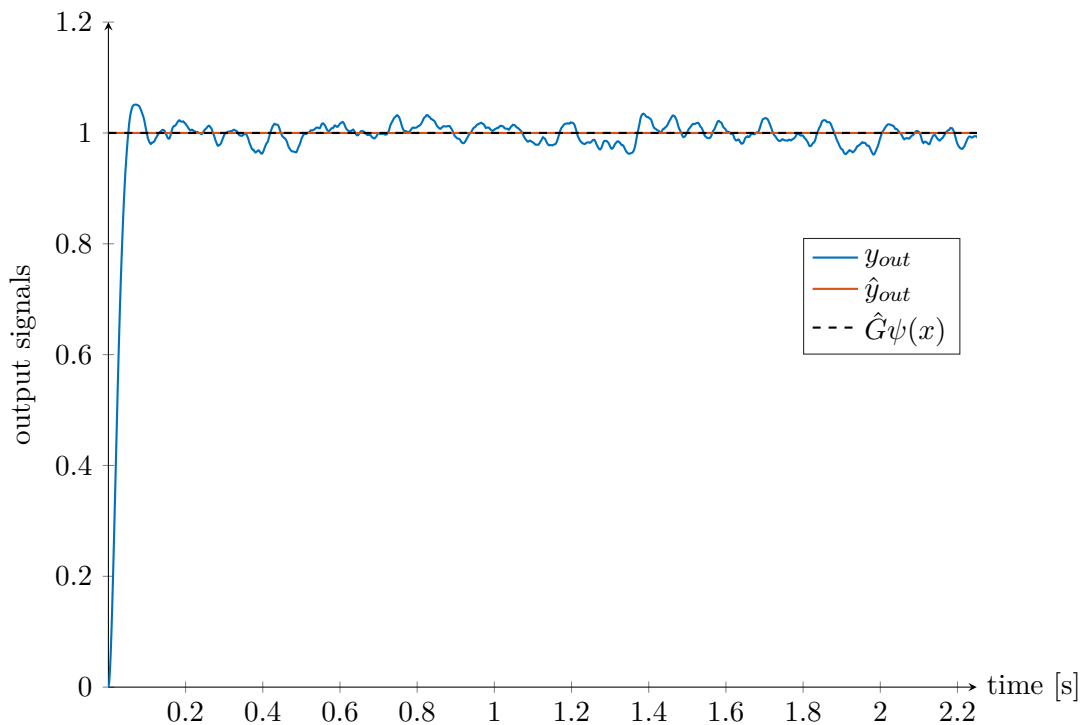
Figure 5-5: The averaged, expected, and amplified ideal outputs of the TEO of input $x = 0.1\sin(2\pi t)$ subjected to uniformly distributed white noise sources.

In this case, $\sigma_0 = \frac{0.1}{\sqrt{3}}$. The output of the TEO is presented in Figure 5-5. This output has $\hat{G} = 100$ and SNR=SNDR= 35 dB. As theorized, there is no distortion at the output, which qualitatively can be seen by comparing the ideal with the expected output in Figure 5-5 and quantitatively by comparing the SNR and SNDR.

5-2-2 Case Study: Exponentially Damped Sinusoidal Signal

In this case, input $x = 0.1 \exp(-t) \sin(2\pi t)$ is used. This input corresponds to $\psi = 0.01 \exp(-2t)$. Uniform white noise sources are used and σ_0 is set as $\frac{0.1}{\sqrt{3}}$ which makes $\hat{G} = 100$. The output of the TEO is presented in Figure 5-6. For this case, SNR and SNDR are not suitable to measure the performance since a negative exponential signal (e.g. $\exp(-2t)$) has zero average power over infinite time. However, for a simulation time of 2.5 s, SNR=SNDR= 23 dB.

5-2-3 Case Study: Multisine Signal

For the last case study, a multisine input $x = 0.1 \sin(2\pi t) + 0.05 \sin(4\pi t)$ is used. The optimum noise RMS value is

$$\sigma_0 = 0.1 \sin(2\pi t_0) + 0.2 \sin(4\pi t_0), \tag{5-3}$$

where $t_0 = \frac{1}{2\pi} \arccos\left(\frac{-1+\sqrt{129}}{16}\right)$. The averaged, expected, and ideal outputs are presented in Figure 5-7 where $\hat{G} = 13.4$, SNR=SNDR= 24 dB.

From the three cases, it can be concluded that the proposed SR-based TEO can generate outputs that resemble the outputs of the ideal TEO. The differences lie in the output noise part, which can be minimized by using better averaging techniques.

5-3 SR-Based TEO as an Action Potential Detection System

The nature of an AP signal is different from that of the well-known signals that are used as test cases in Section 5-2. Figure 5-8 shows an example of an AP, its first, and second derivatives that are already amplified and sampled with a sampling frequency f_s of 20 kHz. As can be seen, there are huge differences in their maximum values such that τ in the SR-based TEO has to be in the range of 5×10^{-5} to 1×10^{-4}.

Since the required value of τ is close to $1/f_s$, it is possible to use the discrete-time version of the TEO, as formulated by (2-12). In this formula, there is no need of differentiators and the output is attenuated by $\left(\frac{1}{f_s}\right)^2$, thus an SR-based TEO can be constructed using delay blocks in addition to two SR-based multipliers and a subtractor. However, as discussed in Section 2-2-1, the system is impossible to be constructed since it is noncausal. This problem can be solved by shifting the output of the system by one sample, and thus a discrete-time SR-based TEO is proposed in Figure 5-9.

As the AP signal has a large bandwidth already, the output of its TEO will also have a large bandwidth. In fact, the output signal power is distributed from zero Hz to $f_s/2$. This fact makes averaging using a filter impossible, and therefore the parallelization technique is
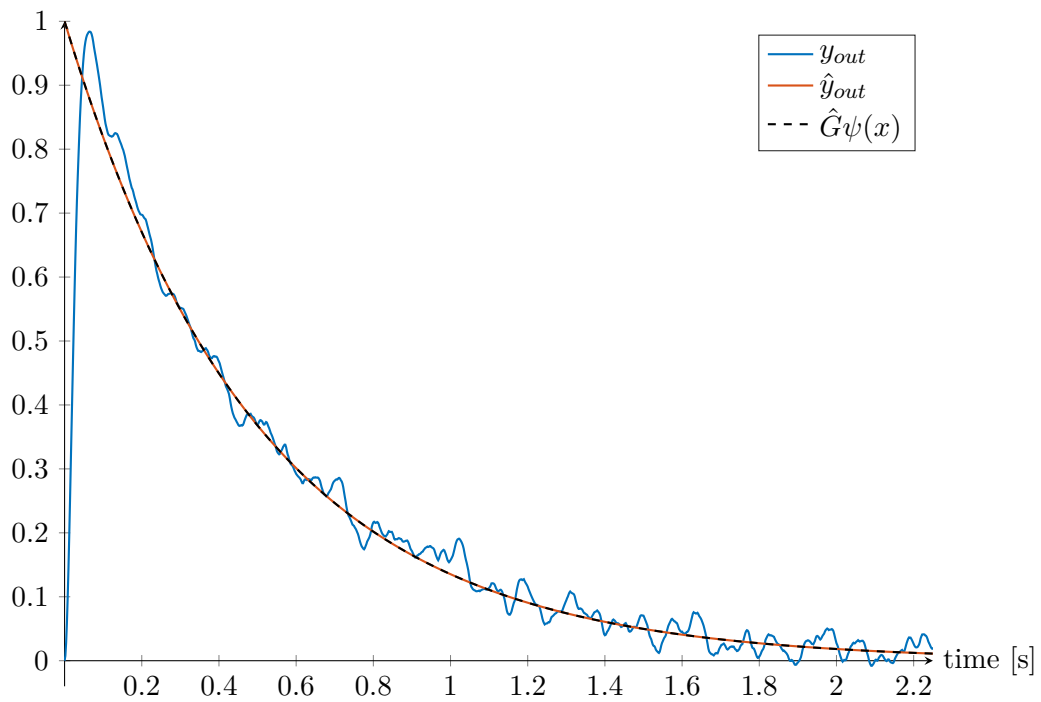
Figure 5-6: The averaged, expected, and amplified ideal outputs of the TEO of input $x = 0.1\exp(-t)\sin(2\pi t)$ subjected to uniformly distributed white noise sources.
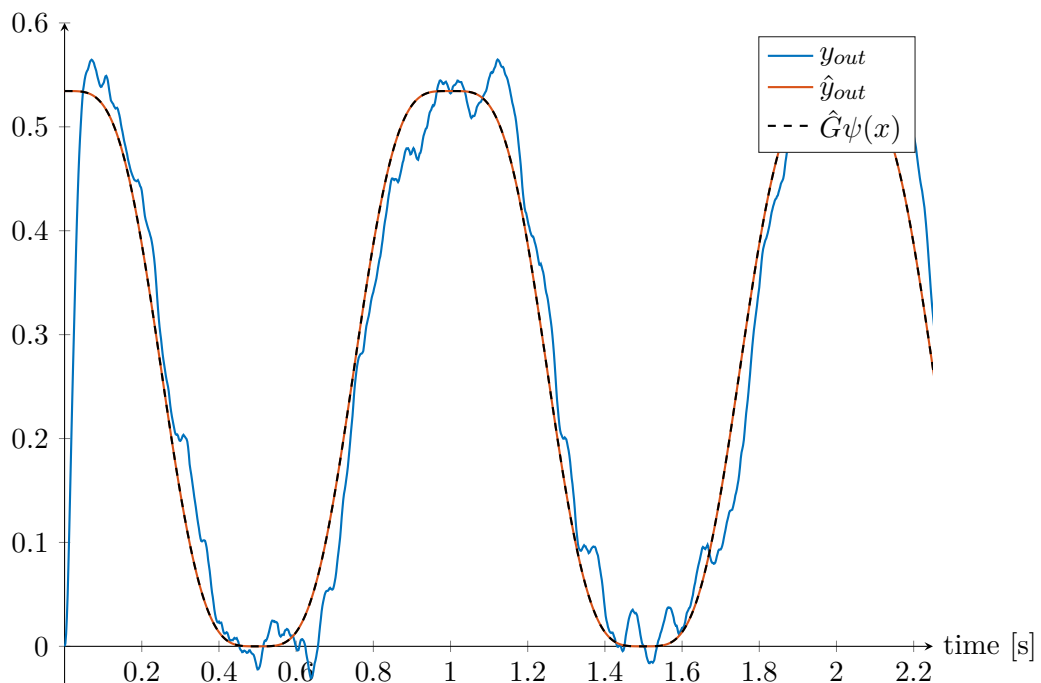
Figure 5-7: The averaged, expected, and amplified ideal outputs of the TEO of input $x = 0.1\sin(2\pi t) + 0.05\sin(4\pi t)$ subjected to uniformly distributed white noise sources.
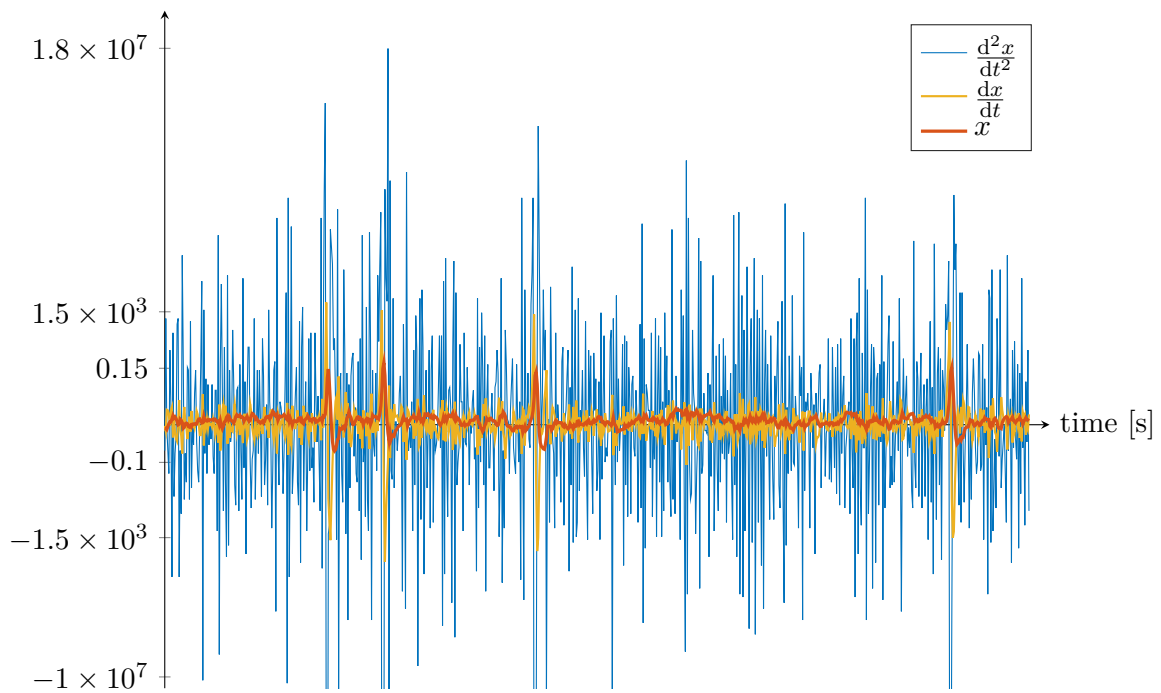
Figure 5-8: The difference in range of an AP signal and its derivatives.
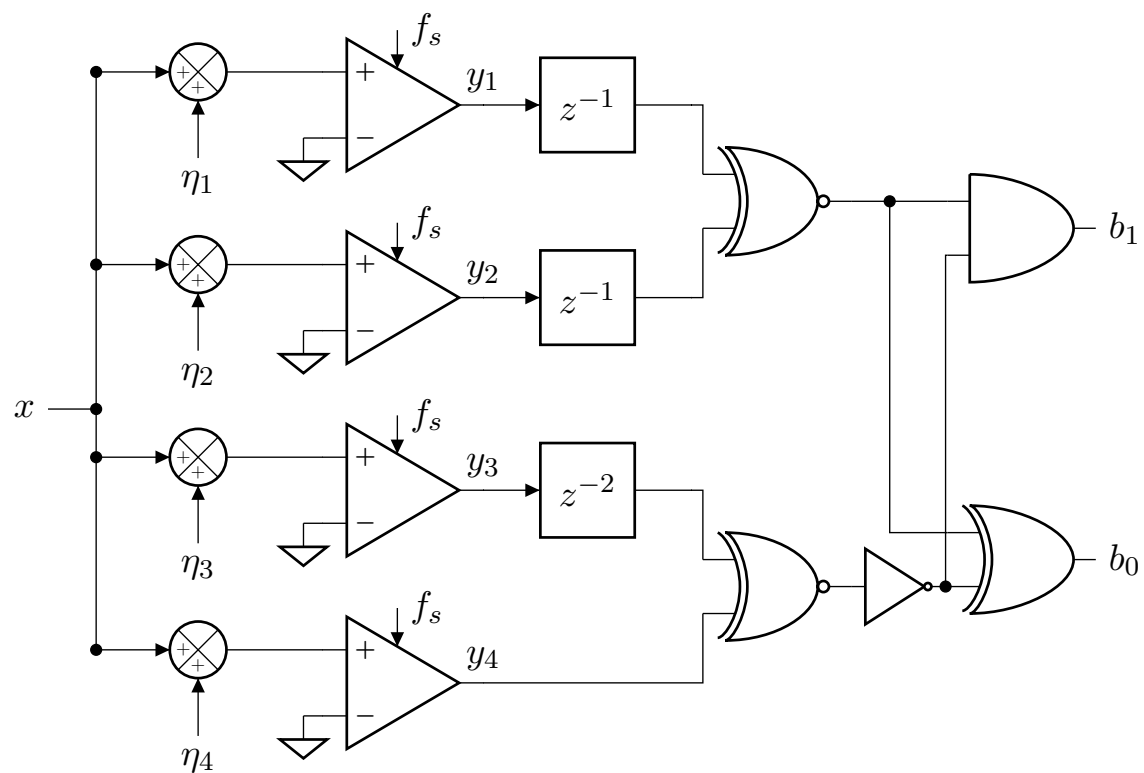
Figure 5-9: The proposed SR-based implementation of the discrete-time TEO.

used. Figure 5-10a and Figure 5-10b present the output of the proposed SR-based TEO with parallelizations of $10,000$ and $100,000$, respectively. There is no distortion present in either output since a uniformly distributed white noise with $\sigma = \dfrac{\max |x|}{\sqrt{3}}$ is used.

5-4   Quantifying the Performance of AP SR-Based TEO

Up to this point, signal-to-noise ratio (SNR) and signal-to-noise-and-distortion ratio (SNDR) have been used to measure the performance of SR-based systems. However, in the case of the SR-based TEO for AP detection applications, this proves to be misleading. Firstly, the SNDRs for the proposed SR-based TEO with $10,000$ and $100,000$ are -7.5 and 2.5 decibel (dB), respectively. This is very low, although not very surprising considering the average signal power of an AP signal is fundamentally low. Despite that, looking at Figure 5-10, the spikes can be distinguished rather easily from the noise. Therefore, a more practical performance measure has to be used.

As an action potential detection system, the most important thing for this system is to inform the user(s) whenever an AP occurs. Thus, the performance can be quantified by counting how many APs are accurately detected by the system, or conversely: how many APs are **inaccurately** detected by the system. The second approach is easier to interpret since the better the system is, the closer to zero its inaccuracy is. In this section, two types of inaccuracies are used. The first type of inaccuracy is a false positive (FP). In this type, the system detects an AP when no AP is present. The second type is a false negative (FN). Contrary to the first type, in this type, the system does not detect any AP when in reality an AP activity occurs. Figure 5-11 illustrates the FP and FN in an AP detection system. From these two quantities, the False Positive Value and sensitivity of the system can be calculated [24]. These two metrics are formulated as

$$\text{False Positive Value} = \frac{\text{FP}}{\text{TP} + \text{FP}} \times 100\% \tag{5-4}$$

and

$$\text{Sensitivity} = \frac{\text{TP}}{\text{TP} + \text{FN}} \times 100\%, \tag{5-5}$$

where TP, the true positive, is how many APs that are supposed to be detected by the system. The lower the False Positive Value and the higher the sensitivity, the better the system.

As a test case, an AP signal of an epileptic mouse from the Department of Neuroscience, Erasmus Medical Center, Rotterdam, the Netherlands, is used. This signal is sampled with a sampling frequency of 20 kHz for 5 s. At the time of the recording, 211 APs are detected by the ideal TEO, and this is considered as the TP and the reference for the SR-based TEO. The detection level for an AP occurence is set to be $\hat{G} \cdot 4 \times 10^{-3}$, where $\hat{G}$ is the LSE gain of the system. The performance of the proposed system for different numbers of parallelizations is presented in Table 5-1. From these two results, it can be concluded that, disregarding the detection level contribution, increasing the parallelizations by ten times produces a far more accurate system.
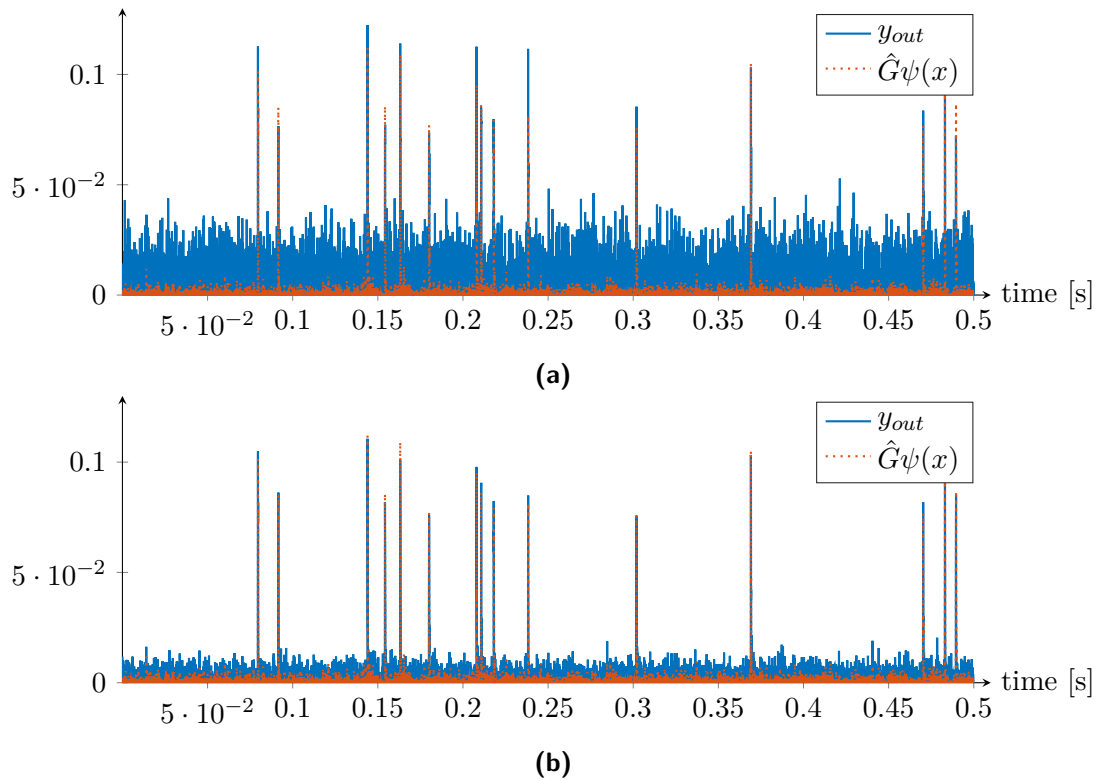
Figure 5-10: The averaged and amplified ideal outputs of the TEO with an AP signal as the input. (a) Parallelization of $N = 10,000$. (b) Parallelization of $N = 100,000$.
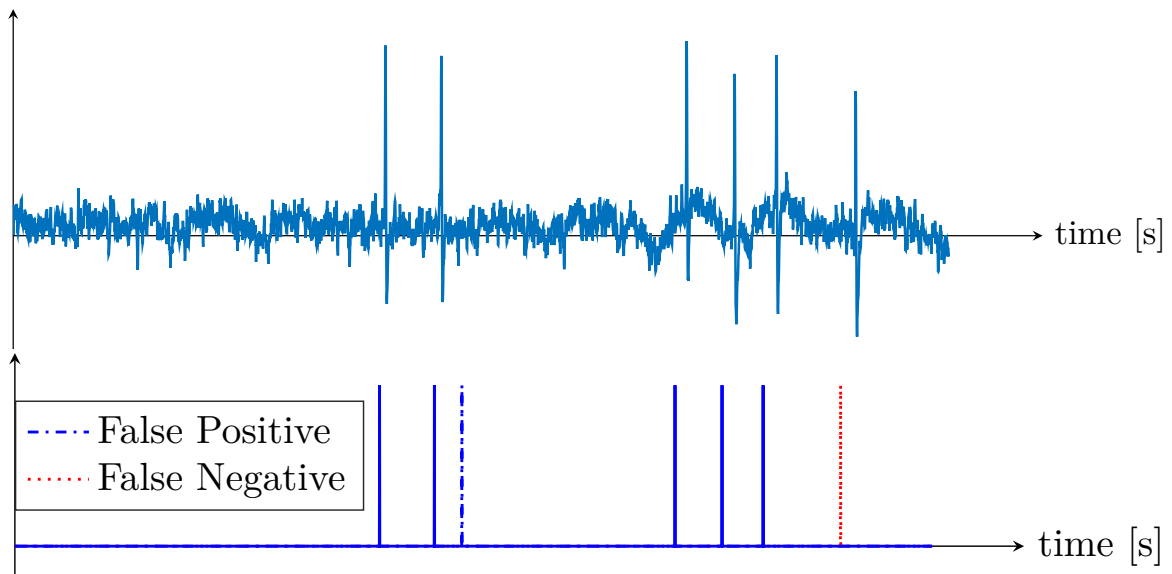
Figure 5-11: The inaccuracies of AP detections systems. A false positive occurs when the system detects an AP when there is no spike and a false negative occurs when the system does not detect any AP when it is actually there.

Table 5-1: Performance of the Proposed SR-based TEO as an AP detection system

	FP	FN	False Positive Value (%)	Sensitivity (%)
N=10,000	451	23	68.13	90.17
	483	39	69.60	84.40
	482	24	69.55	89.79
	433	28	67.24	88.28
	465	37	68.79	85.08
average	462.8	30.2	68.68	87.48
N=100,000	11	7	4.95	96.79
	11	7	4.95	96.79
	11	7	4.95	96.79
	10	9	4.52	95.90
	10	6	4.52	97.26
average	10.6	7.2	4.78	96.70

5-5   Conclusions

In this chapter, the SR-based multiplier, adder, and subtractor are used to implement several functions. From the test cases, it can be concluded that the SR-based operators can be used to build systems. By using uniformly distributed white noise sources, the distortion contribution of a system can be removed and its performance is determined by how good the averaging technique used is. As an AP detection system, a parallelization of 100,000 is necessary to get a good performance.

Chapter 6

Conclusions and Recommendations for Future Work

6-1 Conclusions

The stochastic resonance (SR) phenomenon is able to boost the performance of a nonlinear system, especially in threshold-based systems. Using a simple comparator subjected to noise, a 1-bit analog-to-digital converter (ADC) can be built. In this thesis, the possibility of manipulating the information that is preserved by the stochastic resonance (SR)-based systems are examined. The research subquestions are answered as follows:

1. **Is it possible to implement mathematical operators using SR?**
   It is possible to implement SR-based multipliers and adders, as extensively discussed in Chapters 3 and 4. The performance of the operators depends on how good the information that is preserved by the SR-based fundamental building blocks is.

2. **How can one define and predict the performance of the operators?**
   Based on the purpose of the operators and how the content of this thesis can be developed further in the electronics field, signal-to-noise ratio (SNR) and signal-to-noise-and-distortion ratio (SNDR) are used as the performance metrics as discussed in Chapter 2. The performance can be predicted by defining the output noise and distortion, which is discussed in Chapters 3 and 4.

3. **Is it possible to build a system out of the SR-based math operators?**
   It is possible to build a system from the SR-based operators, as demonstrated in Chapter 5. Moreover, using the appropriate noise type and power, SR-based systems are not only able to handle arbitrary input signals, but also physiological signals such as action potentials (APs).

Therefore, the answer to the main research question **"Is it possible to use the SR phenomenon to manipulate information that is contained in the output signal?"** is

"Yes, it is possible. The performance of the information manipulators, namely the mathematical operators, depend on the performance of the SR-based building blocks themselves.".

6-2 Contributions

In this thesis, the following contributions are made:

1. In Chapter 3, a new design of a system-level signal multiplier is proposed. This design makes use of an independent randomness that is introduced in SR-based fundamental blocks such that it only takes an XNOR gate to act as a multiplication operator. It is shown mathematically that, as long as the noise sources are independent, the XNOR itself will act as an ideal multiplier and thus, the performance of the total multiplier is determined by the performance of the individual SR-based fundamental blocks;

2. In Chapter 4, a half-adder is used in combination with SR-based fundamental blocks to produced an SR-based adder. With this configuration, an SR-based subtractor can be designed. An observation is made that, compared to adding and subtracting them digitally, processing the signals in the mixed-signal domain can decrease the number of necessary input ports in the digital signal processor from K to $\lfloor \log_2 K \rfloor + 1$, where K is the number of input signals. In Appendix B, a design of a 1-bit output SR-based adder is proposed. It can approximate the properties of an adder, but the behaviors of the operator are not sucessfully characterized;

3. In Chapter 5, the proposed SR-based operators in the previous chapters are used to build several systems, specifically the Teager Energy Operator (TEO). Due to the 2-bit output of the SR-based adder and subtractor, the configuration of a system might have to be changed. However, it is shown that it is possible to build a system or mathematical functions out of these SR-based operators as they produced the expected outputs. It is also shown that, by applying uniformly distributed noise signals as observed in Appendix D, a nondistorted output can be acquired. In an AP detection application, a large number of parallelization is necessary to get a system with a good performance.

6-3 Recommendations for Future Work

There are at least three directions that can be taken to continue the research in this thesis.

1. **Going broad: investigate the possibility of other SR-based math operators at the system level.**
   In this thesis, only the SR-based adder, subtractor, and multiplier have been successfully designed. There are still the divider, differentiator, integrator, modulo operator, etc. that can be investigated. Is it possible to build these operators? If so, how well do they perform compared to the ideal operators? If not, why?

2. **Going deep: implement the SR-based operators and systems at the circuit level.**
   As discussed in the previous chapters, this research is done with the vision that it can provide alternative designs for mathematical operators in the electronics field. Therefore, it is interesting to implement the proposed operators and systems at the circuit level and investigate how well they perform. Is it possible to use the noise that is omnipresent in electronic circuits, or should one build noise generators for this?

3. **Going perfect: investigate how to improve the performance of the SR-based block.**
   It has been repeatedly discussed that the performance of the math operators depends on the performance of their SR-based blocks. Although it's been pointed out that the output noise can be reduced by the averaging technique while the distortion can be reduced by either increasing the input noise power or using uniformly distributed noise, these options are actually trade-offs of noise and distortion since input noise power will also increase the output noise power. Then, to filter out the increased output noise, a very good averaging technique is necessary, and it can be quite costly from an engineering point of view. Is there a mechanism, such as a negative feedback, to filter out the output noise using only a minimum-performance averaging technique? Also, can the input noise be controlled such that it always gives the optimum power to ensure the occurence of SR?

Appendix A

Derivations and Proofs

A-1 Derivation of the Expected Value of a Fundamental SR-Based Building Block

As described in (3-1), $\Pr\left(y = 1 \,|\, x\right) = 1 - F_\eta(\theta - x)$. Therefore, the expected value of y is

$$
\begin{aligned}
\hat{y}_{out} &= 2V \Pr\left(y = 1 \,|\, x\right) - V \\
&= V\left(1 - 2F_\eta(\theta - x)\right).
\end{aligned}
\tag{A-1}
$$

A-2 Proof of $(3\text{-}5)$

For η_1 and η_2 independent of each other, the left-hand side (LHS) is

$$
\begin{aligned}
\hat{y}_{out} &= \mathbf{E}\left[y_1 \odot y_2 \,|\, x_1, x_2\right] \\
&= 2V\left(\Pr\left(y_1 \odot y_2 = 1 \,|\, x_1, x_2\right)\right) - V \\
&= 2V\Big(\Pr\left(y_1 = 1 \,|\, x_1\right)\Pr\left(y_2 = 1 \,|\, x_2\right) \\
&\quad + (1 - \Pr\left(y_1 = 1 \,|\, x_1\right))(1 - \Pr\left(y_2 = 1 \,|\, x_2\right))\Big) - V \\
&= V\Big(1 - 2\left(\Pr\left(y_1 = 1 \,|\, x_1\right) + \Pr\left(y_2 = 1 \,|\, x_2\right)\right) \\
&\quad + 4\Pr\left(y_1 = 1 \,|\, x_1\right) + \Pr\left(y_2 = 1 \,|\, x_2\right)\Big),
\end{aligned}
\tag{A-2}
$$

and the right-hand side (RHS) is

$$
\begin{aligned}
\frac{\hat{y}_{1,out} \times \hat{y}_{2,out}}{V} &= \frac{\mathbf{E}\left[y_1 \mid x_1\right] \mathbf{E}\left[y_2 \mid x_2\right]}{V} \\
&= \frac{\left(2V\Big(\Pr\left(y_1 = 1 \mid x_1\right)\Big) - V\right)\left(2V\Big(\Pr\left(y_2 = 1 \mid x_2\right)\Big) - V\right)}{V} \\
&= \left(2V\Big(\Pr\left(y_1 = 1 \mid x_1\right)\Big) - V\right)\left(2\Big(\Pr\left(y_2 = 1 \mid x_2\right)\Big) - 1\right) \\
&= V\Big(1 - 2\left(\Pr\left(y_1 = 1 \mid x_1\right) + \Pr\left(y_2 = 1 \mid x_2\right)\right) \\
&\quad + 4\Pr\left(y_1 = 1 \mid x_1\right) + \Pr\left(y_2 = 1 \mid x_2\right)\Big).
\end{aligned}
\tag{A-3}
$$

The LHS and RHS are equivalent, therefore $\hat{y}_{out} = \dfrac{\mathbf{E}\left[y_1 \mid x_1\right] \mathbf{E}\left[y_2 \mid x_2\right]}{V}$.

A-3 Derivation of (3-29)

The probability of output $y_{o,K} = 1$ given $x_1, x_2, \ldots, x_K$ is

$$
\begin{aligned}
\Pr(y_{o,K} = 1 | x_1, \ldots, x_K) &= \Pr(y_{o,K-1} = 1 | x_1, \ldots, x_K)\Pr(y_K = 1 | x_1, \ldots, x_K) \\
&\quad + \Pr(y_{o,K-1} = 0 | x_1, \ldots, x_K)\Pr(y_K = 0 | x_1, \ldots, x_K) \\
&= \Pr(y_{o,K-1} = 1 | x_1, \ldots, x_K)\Pr(y_K = 1 | x_1, \ldots, x_K) \\
&\quad + \Big(1 - \Pr(y_{o,K-1} = 1 | x_1, \ldots, x_K)\Big)\Big(1 - \Pr(y_K = 1 | x_1, \ldots, x_K)\Big) \\
&= 2\Pr(y_{o,K-1} = 1 | x_1, \ldots, x_K)\Pr(y_K = 1 | x_1, \ldots, x_K) \\
&\quad - \Big(\Pr(y_{o,K-1} = 1 | x_1, \ldots, x_K) + \Pr(y_K = 1 | x_1, \ldots, x_K)\Big) + 1 \\
&= 2\Pr(y_{o,K-1} = 1 | x_1, \ldots, x_K)\Big(1 - F_{\eta_K}\left(\theta_K - x_K\right)\Big) \\
&\quad - \Big(\Pr(y_{o,K-1} = 1 | x_1, \ldots, x_K) + 1 - F_{\eta_K}\left(\theta_K - x_K\right)\Big) + 1.
\end{aligned}
\tag{A-4}
$$

To make the writing more concise, $\Pr(y_{o,K} = 1 \,|\, x_1, x_2, \cdots, x_K)$ and $F_{\eta_K}(\theta_K - x_K)$ will be denoted as $\Pr(K)$ and F_{η_K}, respectively, starting from now. Then, (A-4) can be written as

$$
\begin{aligned}
\Pr(K) &= 2\Pr(K-1)(1 - F_{\eta_K}) - (\Pr(K-1) + 1 - F_{\eta_K}) + 1 \\
&= \Pr(K-1)(1 - 2F_{\eta_K}) + F_{\eta_K} \\
&= \big(\Pr(K-2)(1 - 2F_{\eta_{K-1}}) + F_{\eta_{K-1}}\big)(1 - 2F_{\eta_K}) + F_{\eta_K} \\
&= \Pr(K-2)(1 - 2F_{\eta_{K-1}})(1 - 2F_{\eta_K}) + F_{\eta_{K-1}}(1 - 2F_{\eta_K}) + F_{\eta_K} \\
&= \big(\Pr(K-3)(1 - 2F_{\eta_{K-2}}) + F_{\eta_{K-2}}\big)(1 - 2F_{\eta_{K-1}})(1 - 2F_{\eta_K}) + F_{\eta_{K-1}}(1 - 2F_{\eta_K}) + F_{\eta_K} \\
&= \big(\Pr(K-3)(1 - 2F_{\eta_{K-2}})(1 - 2F_{\eta_{K-1}})(1 - 2F_{\eta_K}) + F_{\eta_{K-2}}(1 - 2F_{\eta_{K-1}})(1 - 2F_{\eta_K}) \\
&\quad + F_{\eta_{K-1}}(1 - 2F_{\eta_K}) + F_{\eta_K} \\
&= (1 - F_{\eta_1})\prod_{k=2}^{K}(1 - 2F_{\eta_k}) + F_{\eta_2}\prod_{k=3}^{K}(1 - 2F_{\eta_k}) + F_{\eta_3}\prod_{k=4}^{K}(1 - 2F_{\eta_k}) + \cdots \\
&\quad + F_{\eta_{K-3}}\prod_{k=K-2}^{K}(1 - 2F_{\eta_k}) + F_{\eta_{K-2}}(1 - 2F_{\eta_{K-1}})(1 - 2F_{\eta_{K-2}}) \\
&\quad + F_{\eta_{K-1}}(1 - 2F_{\eta_K}) + F_{\eta_K} \\
&= \left(1 + \sum_{k=2}^{K}(-2)^{k-1}\sum_{2 \le i_1 < \cdots < i_{k-1} \le K} F_{\eta_{i_1}} \cdots F_{\eta_{i_{k-1}}}\right) \\
&\quad - F_{\eta_1}\left(1 + \sum_{k=2}^{K}(-2)^{k-1}\sum_{2 \le i_1 < \cdots < i_{k-1} \le K} F_{\eta_{i_1}} \cdots F_{\eta_{i_{k-1}}}\right) \\
&\quad + F_{\eta_2}\left(1 + \sum_{k=3}^{K}(-2)^{k-2}\sum_{3 \le i_1 < \cdots < i_{k-2} \le K} F_{\eta_{i_1}} \cdots F_{\eta_{i_{k-2}}}\right) \\
&\quad + F_{\eta_3}\left(1 + \sum_{k=4}^{K}(-2)^{k-3}\sum_{4 \le i_1 < \cdots < i_{k-3} \le K} F_{\eta_{i_1}} \cdots F_{\eta_{i_{k-3}}}\right) + \cdots \\
&\quad + F_{\eta_{K-3}}\left(1 + \sum_{k=K-2}^{K}(-2)^{k-(K-2)+1}\sum_{K-2 \le i_1 < \cdots < i_{k-(K-2)+1} \le K} F_{\eta_{i_1}} \cdots F_{\eta_{i_{k-(K-2)+1}}}\right) \\
&\quad + F_{\eta_{K-2}}\left(1 - 2(F_{\eta_{K-1}} + F_{\eta_K}) + 4F_{\eta_{K-1}}F_{\eta_K}\right) + F_{\eta_{K-1}}(1 - 2F_{\eta_K}) + F_{\eta_K}.
\end{aligned}
$$
$$\tag{A-5}$$

The term $\displaystyle\sum_{n\leq i_1<\cdots<i_{k-n}\leq K}$ denotes the possible subproduct of $F_{\eta_{i_{k-n}}}$. The summation from the third until the last terms will result in every possible subproduct of $F_{\eta_{i_k}}$ except for F_{η_1}, but with coefficient of $(-2)^{k-2}$. Therefore, the (A-5) can be simplified as

$$
\begin{aligned}
\Pr(K) = {} & 1 + \sum_{k=2}^{K}(-2)^{k-1}\sum_{2\leq i_1<\cdots<i_{k-1}\leq K}F_{\eta_{i_1}}\cdots F_{\eta_{i_{k-1}}} \\
& - F_{\eta_1}\left(1 + \sum_{k=2}^{K}(-2)^{k-1}\sum_{2\leq i_1<\cdots<i_{k-1}\leq K}F_{\eta_{i_1}}\cdots F_{\eta_{i_{k-1}}}\right) \\
& + \sum_{k=2}^{K}(-2)^{k-2}\sum_{2\leq i_1<\cdots<i_{k-1}\leq K}F_{\eta_{i_1}}\cdots F_{\eta_{i_{k-1}}} \\
= {} & 1 + \sum_{k=2}^{K}\left[(-2)^{k-1}+(-2)^{k-2}\right]\sum_{2\leq i_1<\cdots<i_{k-1}\leq K}F_{\eta_{i_1}}\cdots F_{\eta_{i_{k-1}}} \\
& - F_{\eta_1}\left(1 + \sum_{k=2}^{K}(-2)^{k-1}\sum_{2\leq i_1<\cdots<i_{k-1}\leq K}F_{\eta_{i_1}}\cdots F_{\eta_{i_{k-1}}}\right) \\
= {} & 1 - \sum_{k=2}^{K}(-2)^{k-2}\sum_{2\leq i_1<\cdots<i_{k-1}\leq K}F_{\eta_{i_1}}\cdots F_{\eta_{i_{k-1}}} \\
& - F_{\eta_1}\left(1 + \sum_{k=2}^{K}(-2)^{k-1}\sum_{2\leq i_1<\cdots<i_{k-1}\leq K}F_{\eta_{i_1}}\cdots F_{\eta_{i_{k-1}}}\right) \\
= {} & 1 - \sum_{k=1}^{K}(-2)^{k-1}\sum_{1\leq i_1<\cdots<i_k\leq K}F_{\eta_{i_1}}\cdots F_{\eta_{i_k}}.
\end{aligned}
\tag{A-6}
$$

The expected value of the output $y_{o,K}$ is

$$
\begin{aligned}
\hat{y}_{out,K} &= 2V\Pr(K) - V \\
&= 2V - 2V\sum_{k=1}^{K}(-2)^{k-1}\left(\sum_{1\leq i_1<\cdots<i_k\leq K}F_{\eta_{i_1}}\cdots F_{\eta_{i_k}}\right) - V \\
&= V + V\sum_{k=1}^{K}(-2)^{k}\sum_{1\leq i_1<\cdots<i_k\leq K}F_{\eta_{i_1}}(\theta_{i_1}-x_{i_1})\cdots F_{\eta_{i_k}}(\theta_{i_k}-x_{i_k}).
\end{aligned}
\tag{A-7}
$$

A-4 Derivation of (3-30)

For Gaussian noise sources, the cumulative distribution function (CDF) can be approximated with

$$F(z) \approx \frac{1}{2} + \frac{1}{\sigma\sqrt{2\pi}}(z). \tag{A-8}$$

Equation (A-6) can be written as

$$\Pr(K) = 1 - \left[\sum_{1 \le i_1 \le K} F_{\eta_{i_1}} - 2 \sum_{1 \le i_1 < i_2 \le K} F_{\eta_{i_1}} F_{\eta_{i_2}} - 4 \sum_{1 \le i_1 < i_2 < i_3 \le K} F_{\eta_{i_1}} F_{\eta_{i_2}} F_{\eta_{i_3}} + \cdots \right.$$
$$\left. (-2)^{K-1} \prod_{k=1}^{K} F_{\eta_k} \right]. \tag{A-9}$$

Substituting (A-8) to (A-9) will result in all possible subproduct of z_k with coefficients that correspond to the combination of K and k. In other words,

$$\Pr(K) \approx 1 - \left[\left(-\frac{1}{2} \sum_{k=1}^{K} \binom{K}{k}(-1)^k \right) + \left(\frac{1}{\sqrt{2\pi}} \sum_{k=0}^{K-1} \binom{K-1}{k}(-1)^k \right) \sum_{1 \le i_1 \le K} z_{i_1} \right.$$
$$+ \left(\frac{1}{(\sqrt{2\pi})^2} \sum_{k=0}^{K-2} \binom{K-2}{k}(-1)^k \right) \sum_{1 \le i_1 < i_2 \le K} z_{i_1} z_{i_2} + \cdots$$
$$+ \left(\frac{1}{(\sqrt{2\pi})^{K-1}} \sum_{k=0}^{1} \binom{1}{k}(-1)^k \right) \sum_{1 \le i_1 < \cdots < i_{K-1} \le K} z_{i_1} \cdots z_{i_{K-1}}$$
$$\left. + \frac{(-2)^{K-1}}{(\sqrt{2\pi})^K} \prod_{k=1}^{K} z_k \right]. \tag{A-10}$$

The term $\sum_{k=1}^{K} \binom{K}{k}(-1)^k$ is equal to -1, while the rest of the term except the last term is equal to zero. The last term can be simplified as $-\frac{1}{2}\left(-\sqrt{\frac{2}{\pi}}\right)^K$. Therefore,

$$\Pr(K) \approx 1 - \frac{1}{2} + \frac{1}{2}\left(-\sqrt{\frac{2}{\pi}}\right)^K \prod_{k=1}^{K} z_k$$
$$= \frac{1}{2} + \frac{1}{2}\left(-\sqrt{\frac{2}{\pi}}\right)^K \prod_{k=1}^{K} z_k. \tag{A-11}$$

The approximation of the expected value of $y_{o,K}$ is

$$\hat{y}_{out,K} = 2V \Pr(K) - V$$
$$\approx 2V\frac{1}{2} + 2V\frac{1}{2}\left(-\sqrt{\frac{2}{\pi}}\right)^K \prod_{k=1}^{K} z_k - V$$
$$= V\left(-\sqrt{\frac{2}{\pi}}\right)^K \prod_{k=1}^{K} \left(\frac{\theta_k - x_k}{\sigma_k}\right). \tag{A-12}$$

A-5   Proof that $(4\text{-}8)$ is equivalent to $(4\text{-}10)$

Substituting (4-5) to (4-8),

$$8V^2 F_{\eta_1}(\theta_1 - x_1) F_{\eta_2}(\theta_2 - x_2)$$

$$
\begin{aligned}
+2V\hat{y}_{out} - \hat{y}_{out}^2 &= 8V^2 F_{\eta_1}(\theta_1 - x_1) F_{\eta_2}(\theta_2 - x_2) \\
&\quad + 2V\Big(2V\big(1 - (F_{\eta_1}(\theta_1 - x_1) + F_{\eta_2}(\theta_2 - x_2))\big)\Big) \\
&\quad - \Big(2V\big(1 - (F_{\eta_1}(\theta_1 - x_1) + F_{\eta_2}(\theta_2 - x_2))\big)\Big)^2 \\
&= 8V^2 F_{\eta_1}(\theta_1 - x_1) F_{\eta_2}(\theta_2 - x_2) \\
&\quad + 4V^2 - 4V^2 F_{\eta_1}(\theta_1 - x_1) - 4V^2 F_{\eta_2}(\theta_2 - x_2) \\
&\quad - 4V^2 + 8V^2 F_{\eta_1}(\theta_1 - x_1) + 8V^2 F_{\eta_2}(\theta_2 - x_2) \\
&\quad - 4V^2 F_{\eta_1}^2(\theta_1 - x_1) - 4V^2 F_{\eta_2}^2(\theta_2 - x_2) \\
&\quad - 8V^2 F_{\eta_1}(\theta_1 - x_1) F_{\eta_2}(\theta_2 - x_2) \\
&= 4V^2\Big(F_{\eta_1}(\theta_1 - x_1) - F_{\eta_1}^2(\theta_1 - x_1) + F_{\eta_2}(\theta_2 - x_2) - F_{\eta_2}^2(\theta_2 - x_2)\Big).
\end{aligned}
$$
$$(\text{A-13})$$

Therefore, (4-8) and (4-10) are equivalent.

A-6   Derivation of $(4\text{-}13)$

Using (4-1) to calculate y_o, the probabilities of y_o are

$$
\begin{aligned}
\Pr(y_o = +2V \mid x_1, x_2) &= \Pr(b_1 = 1 \cap b_0 = 0 \mid x_1, x_2) \\
&= \Pr(y_1 = 1 \cap y_2 = 0 \mid x_1, x_2) \\
&= \Pr(y_1 = 1 \mid x_1, x_2) \Pr(y_2 = 0 \mid x_1, x_2) \\
&= (1 - F_{\eta_1}(\theta_1 - x_1)) F_{\eta_2}(\theta_2 - x_2) \\
&= F_{\eta_2}(\theta_2 - x_2) - F_{\eta_1}(\theta_1 - x_1) F_{\eta_2}(\theta_2 - x_2),
\end{aligned}
$$
$$(\text{A-14})$$

$$
\begin{aligned}
\Pr(y_o = 0 \mid x_1, x_2) &= \Pr(b_1 = 0 \cap b_0 = 1 \mid x_1, x_2) \\
&= \Pr(y_1 = 0 \cap y_2 = 0 \cup y_1 = 1 \cap y_2 = 1 \mid x_1, x_2) \\
&= \Pr(y_1 = 0 \mid x_1, x_2) \Pr(y_2 = 0 \mid x_1, x_2) \\
&\quad + \Pr(y_1 = 1 \mid x_1, x_2) \Pr(y_2 = 1 \mid x_1, x_2) \\
&= F_{\eta_1}(\theta_1 - x_1) F_{\eta_2}(\theta_2 - x_2) + \\
&\quad (1 - F_{\eta_1}(\theta_1 - x_1))(1 - F_{\eta_2}(\theta_2 - x_2)),
\end{aligned}
$$
$$(\text{A-15})$$

and

$$
\begin{aligned}
\Pr(y_o = -2V \mid x_1, x_2) &= \Pr(b_1 = 0 \cap b_0 = 0 \mid x_1, x_2) \\
&= \Pr(y_1 = 0 \cap y_2 = 1 \mid x_1, x_2) \\
&= \Pr(y_1 = 0 \mid x_1, x_2) \Pr(y_2 = 1 \mid x_1, x_2) \\
&= F_{\eta_1}(\theta_1 - x_1)(1 - F_{\eta_2}(\theta_2 - x_2)) \\
&= F_{\eta_1}(\theta_1 - x_1) - F_{\eta_1}(\theta_1 - x_1) F_{\eta_2}(\theta_2 - x_2).
\end{aligned}
$$
$$(\text{A-16})$$

Therefore, $\hat{y}_{out}$ can be calculated as

$$
\begin{aligned}
\hat{y}_{out} = \mathbf{E}\left[y_o \,|\, x_1, x_2\right] &= \Pr\left(y_o = 2V \,|\, x_1, x_2\right)(+2V) + \Pr\left(y_o = 0 \,|\, x_1, x_2\right)(0) \\
&\quad + \Pr\left(y_o = -2V \,|\, x_1, x_2\right)(-2V) \\
&= 2V\left(-\left(F_{\eta_1}\left(\theta_1 - x_1\right) + F_{\eta_2}\left(\theta_2 - x_2\right)\right)\right).
\end{aligned} \tag{A-17}
$$

A-7 **Proof of** $(4\text{-}20)$ **and** $(4\text{-}21)$

Suppose that (4-19) is proven, $y_{o,K}$ is the summation of each individual output of the comparators. In other words,

$$
\begin{aligned}
y_{o,K} &= \sum_{k=1}^{K} y_{k,o} \\
\hat{y}_{out,K} &= \sum_{k=1}^{K} \mathbf{E}\left[y_{k,o} \,|\, x_k\right].
\end{aligned} \tag{A-18}
$$

Substituting (A-1) to (A-18),

$$
\begin{aligned}
\hat{y}_{out,K} &= \sum_{k=1}^{K} \mathbf{E}\left[y_{k,o} \,|\, x_k\right] \\
&= \sum_{k=1}^{K} V\left(1 - 2F_{\eta_k}(\theta_k - x_k)\right) \\
&= \sum_{k=1}^{K} V - 2V \sum_{k=1}^{K} F_{\eta_k}(\theta_k - x_k) \\
&= KV - 2V \sum_{k=1}^{K} F_{\eta_k}\left(\theta_k - x_k\right).
\end{aligned} \tag{A-19}
$$

Approximating (A-19) with (3-6),

$$
\begin{aligned}
\hat{y}_{out,K} &= KV - 2V \sum_{k=1}^{K} F_{\eta_k}\left(\theta_k - x_k\right) \\
&\approx KV - 2V \sum_{k=1}^{K} \left(\frac{1}{2} + \frac{(\theta_k - x_k)}{\sigma_k\sqrt{2\pi}}\right) \\
&= KV - 2V \sum_{k=1}^{K} \frac{1}{2} - 2V \sum_{k=1}^{K} \frac{(\theta_k - x_k)}{\sigma_k\sqrt{2\pi}} \\
&= -2V \sum_{k=1}^{K} \frac{(\theta_k - x_k)}{\sigma_k\sqrt{2\pi}} \\
&= \frac{-2V}{\sqrt{2\pi}} \sum_{k=1}^{K} \left(\frac{\theta_k - x_k}{\sigma_k}\right).
\end{aligned} \tag{A-20}
$$

Appendix B

1-Bit Binary Output Stochastic Resonance-Based Adder

The process of determining a suitable system for the implementation of a stochastic resonance (SR)-based adder begins by examining the binary outcome of the system. Table B-1 shows the outcomes of every possible logic values generated by inputs y_1 and y_2. The outcomes when the inputs are both 1 or both 0 are trivial since the sum of two positive values will be positive while the sum of two negative values will also be negative. However, the problem comes when the inputs have different logic values. In the analog domain, the sum of a positive and negative values will depend on their absolute values, but the value of the sum will always be in-between those values. However, binary systems do not have the symbol that can represent the in-between value. One possible solution for this problem is to let the questionable output be the same as the output of its previous sample. This way, when averaged, it will produce the in-between value that cannot be represented in binary logic.

Table B-1: Truth table of SR-based adder.

y_1	y_2	y_o
1	1	1
1	0	??
0	1	??
0	0	0

B-1 The Proposed System

One of the logic circuits that has the memory property is the gated S-R latch. Based on the truth table of a gated S-R latch, the proposed system for an SR-based adder is shown in Figure B-1 with its truth table presented in Table B-2.
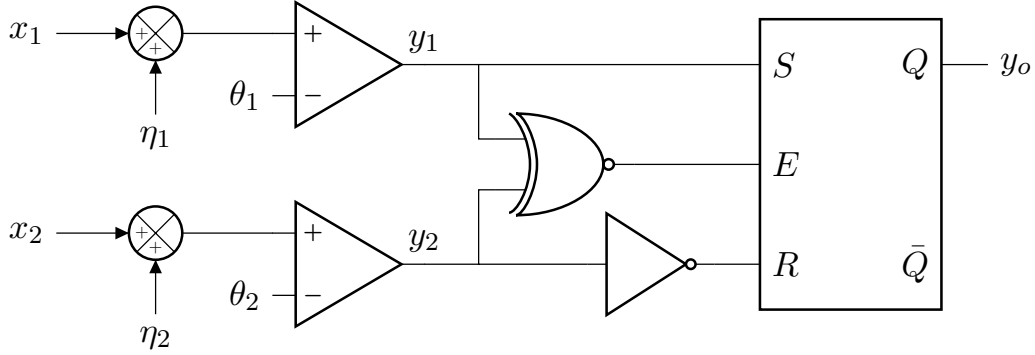
Figure B-1: The proposed SR-based adder using gated S-R latch.

Table B-2: Truth table of the proposed SR-based adder.

y_1	y_2	E	S	R	$y_o(n)$
1	1	1	1	0	1
1	0	0	1	1	$y_o(n-1)$
0	1	0	0	0	$y_o(n-1)$
0	0	1	0	1	0

The probability of $y_o(n) = 1$ given x_1 and x_2 is

$$
\begin{aligned}
\Pr\left(y_o(n) = 1 \,|\, x_1, x_2\right) =& \Pr\left(S = 1 \cap R = 0 \,|\, x_1, x_2\right) + \Pr\left(E = 0 \cap y_o(n-1) = 1 \,|\, x_1, x_2\right) \\
=& \Pr\left(y_1 = 1 \cap y_2 = 1 \,|\, x_1, x_2\right) \\
& + \Pr\left((y_1 = 1 \cap y_2 = 0) \cup (y_1 = 0 \cap y_2 = 1) \,|\, x_1, x_2\right) \\
& \times \Pr\left(y_o(n-1) = 1 \,|\, x_1, x_2\right) \\
=& \left(1 - F_{\eta_1}(\theta_1 - x_1)\right)\left(1 - F_{\eta_2}(\theta_2 - x_2)\right) \\
& + \left(F_{\eta_1}(\theta_1 - x_1) + F_{\eta_2}(\theta_2 - x_2) - 2F_{\eta_1}(\theta_1 - x_2)F_{\eta_2}(\theta_2 - x_2)\right) \\
& \times \Pr\left(y_o(n-1) = 1 \,|\, x_1, x_2\right) \\
=& \left(1 - F_{\eta_1}(\theta_1 - x_2)F_{\eta_2}(\theta_2 - x_2)\right) \\
& + \left(F_{\eta_1}(\theta_1 - x_1) + F_{\eta_2}(\theta_2 - x_2) - 2F_{\eta_1}(\theta_1 - x_2)F_{\eta_2}(\theta_2 - x_2)\right) \\
& \times \left(\Pr\left(y_o(n-1) = 1 \,|\, x_1, x_2\right) - 1\right).
\end{aligned}
\tag{B-1}
$$

The expected value of $y_o(n)$ is

$$
\begin{aligned}
\hat{y}_{out}(n) =& \mathbf{E}\left[y_o(n) \,|\, x_1, x_2\right] \\
=& 2V \Pr\left(y_o(n) = 1 \,|\, x_1, x_2\right) - V \\
=& 2V\Big[\left(1 - F_{\eta_1}(\theta_1 - x_2)F_{\eta_2}(\theta_2 - x_2)\right) \\
& + \left(F_{\eta_1}(\theta_1 - x_1) + F_{\eta_2}(\theta_2 - x_2) - 2F_{\eta_1}(\theta_1 - x_2)F_{\eta_2}(\theta_2 - x_2)\right) \\
& \times \left(\Pr\left(y_o(n-1) = 1 \,|\, x_1, x_2\right) - 1\right)\Big] - V.
\end{aligned}
\tag{B-2}
$$

From (B-2), it can be said that

$$
\begin{aligned}
\hat{y}_{out}(n-1) =& 2V \Pr\left(y_o(n-1)=1 \,|\, x_1, x_2\right) - V \\
\Pr\left(y_o(n-1)=1 \,|\, x_1, x_2\right) =& \frac{1}{2V}\left(\hat{y}_{out}(n-1)+V\right).
\end{aligned}
\tag{B-3}
$$

Substituting (B-3) to (B-2),

$$
\begin{aligned}
\hat{y}_{out}(n) =& 2V - 2V F_{\eta_1}(\theta_1 - x_2) F_{\eta_2}(\theta_2 - x_2) \\
&+ \left(F_{\eta_1}(\theta_1 - x_1) + F_{\eta_2}(\theta_2 - x_2) - 2F_{\eta_1}(\theta_1 - x_2) F_{\eta_2}(\theta_2 - x_2)\right) \\
&\times \left(\hat{y}_{out}(n-1) - V\right) - V \\
=& V - V\left(F_{\eta_1}(\theta_1 - x_1) + F_{\eta_2}(\theta_2 - x_2)\right) \\
&+ \left(F_{\eta_1}(\theta_1 - x_1) + F_{\eta_2}(\theta_2 - x_2) - 2F_{\eta_1}(\theta_1 - x_2) F_{\eta_2}(\theta_2 - x_2)\right) \\
&\times \hat{y}_{out}(n-1).
\end{aligned}
\tag{B-4}
$$

Compared to (4-5), (B-4) differs in its second term. To have an actual adder, σ has to be chosen such that $\mathbf{E}\left[(F_{\eta_2}(\theta_2 - x_2) - 2F_{\eta_1}(\theta_1 - x_2) F_{\eta_2}(\theta_2 - x_2)) \times \hat{y}_{out}(n-1)\right] = 0$.

B-2 Output Noise

Since the output of the adder is a binary signal, (3-10) holds. For parallelization, the formula in (4-9) can predict the output noise, as shown in Figure B-2a. However, due to the second term in (B-4), the output noise is no longer white. In fact, its power spectral density (PSD) resembles a low-pass filter (LPF) (due to $y_o(n-1)$) with a certain cut-off frequency that changes depending on σ and the input signals. Figure B-2b shows that the output noise power changes significantly compared to Figure B-2a.

B-3 Distortion

The distortion behavior is calculated using the exact same formulas that are explained in Chapter 4. From Figure B-3a, it can be seen that $\hat{G}$ for various ρ converge slowly to one value, meaning that as σ increases, the system also becomes more linear. However, the $\hat{G}$ values are relatively smaller than the ones in Figure 4-5a, and comparing distortion power shown in Figure B-3b with the ones in Figure 4-5b, this system is more nonlinear than the SR-based adder proposed in Section 4-1.

(a)

(b)
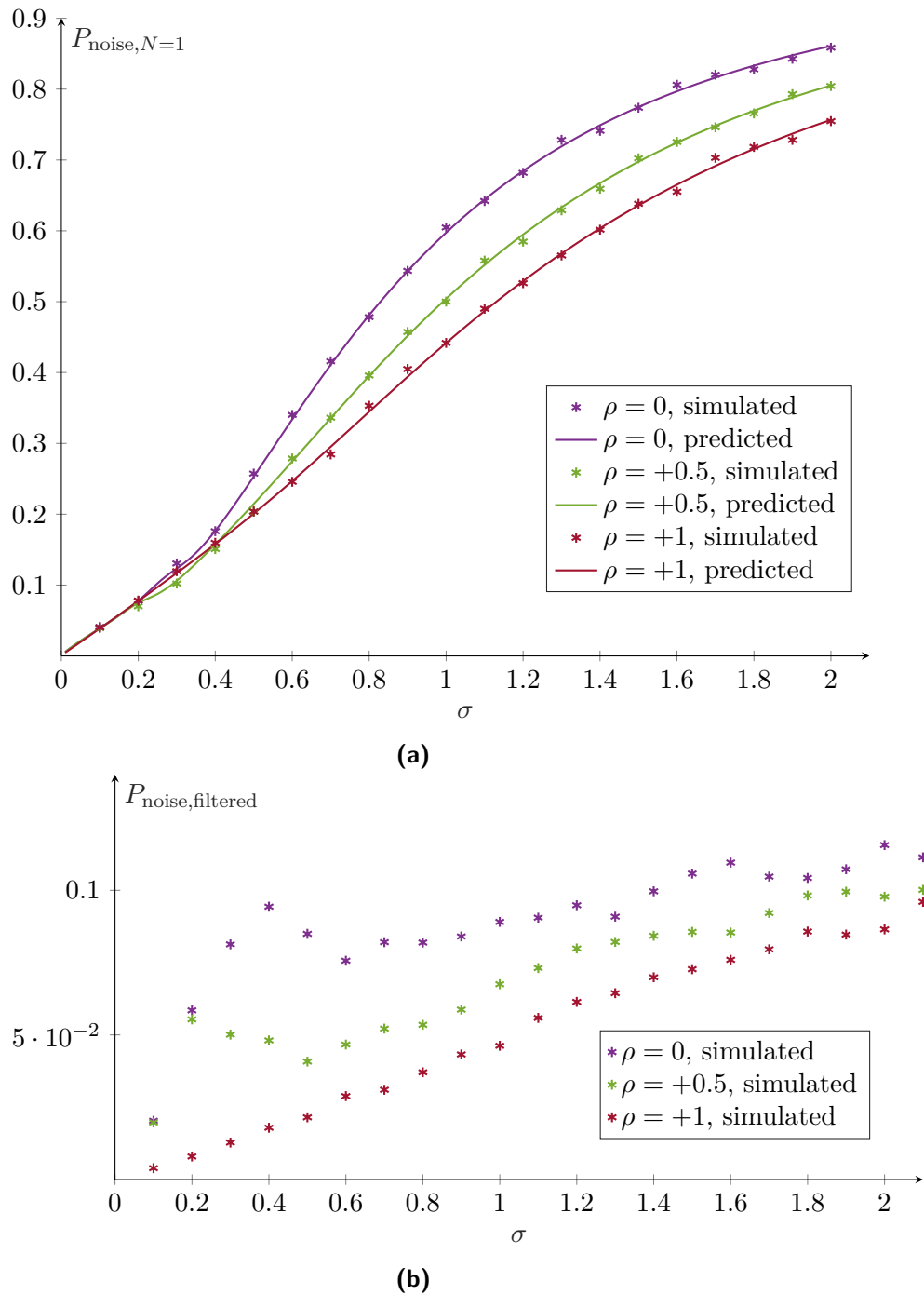
Figure B-2: The output noise for two sinusoidal inputs with unity amplitude, sampled with a sampling frequency of 1 kHz. V is set to 1. The asterisks mark the simulated results and the solid lines are the predicted results based on the formula. (a) The noise power for $N = 1$. (b) The noise power for the output signal LPF with a second order Butterworth LPF with a cut-off frequency of 20 Hz. As σ goes up, the output noise becomes larger.
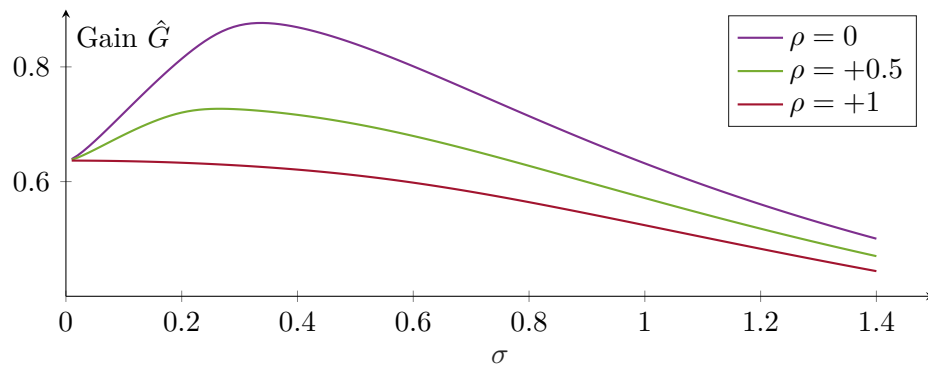
(a)
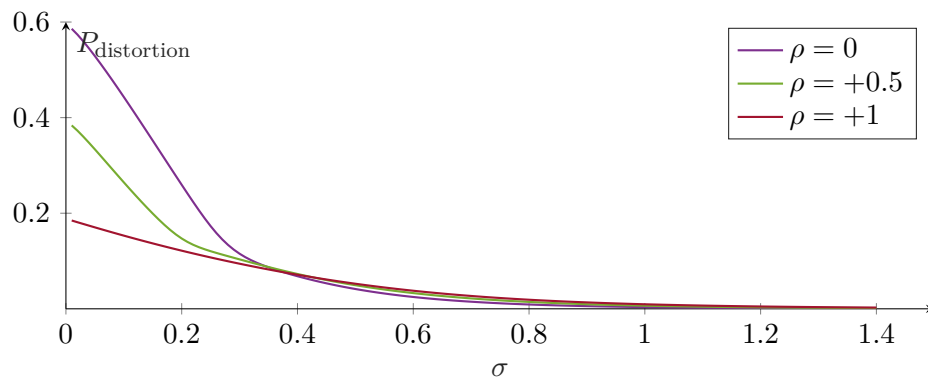
(b)

Figure B-3: The distortion for two sinusoidal inputs with unity amplitude, sampled with a sampling frequency of 1 kHz. V is set to 1. (a) The LSE gain and the predicted linear gain. The gains are the same for sinusoidal inputs regardless of their correlation coefficients. (b) The distortion power. As σ goes up, the output becomes more linear and the distortion power gets closer to zero.

Appendix C

Converting 2-bit Outputs of Stochastic Resonance-Based Adder to Decimal Values

C-1 Conversion Using Analog Multiplexer

It has been discussed in Chapter 4 that the output of a 2 inputs stochastic resonance (SR)-based adder is a 2-bit signal. Therefore, there needs to be a 2-bit to decimal converter that converts b_1 and b_0 to y_o. Such converter can be realized by a 2-to-1 analog multiplexer. The complete block diagram of a converted SR-based adder is shown in Figure C-1. The 2-bit output of the SR-based adder is decoded by a 2-bit to decimal decoder. The decoded signal is used as a control for the corresponding switch.

Ideally, for the 2 inputs adder, it is not possible to have 11 output. Thus, the 11 port of the decoder can be left floating. However, in practice, there is a chance that there is a large noise at the output of the half-adder such that both b_1 and b_0 can generate 1 at the same time. In case this happens, it is better to connect the 11 port to the $+2V$, 0, or $-2V$ switch, depending on the source of incorectness. For example, suppose that it is known that the noise is likely to change the bit of b_0. In this case, The 11 port should be connected to $+2V$ switch because there is a high chance that the logic 11 are actually a corrupted logic 10.

C-2 Alternative of 2 Inputs SR-Based Adder with a Decimal Output

The configuration introduced in Chapter 4 and Section C-1 is convenient because it can be easily generalized to a K inputs SR-based adder. However, it is not the most efficient design. For a 2 inputs adder, the half-adder and 2-bits to decimal decoder can be combined and simplified. The proposed alternative for a 2 inputs SR-based adder with a decimal output is
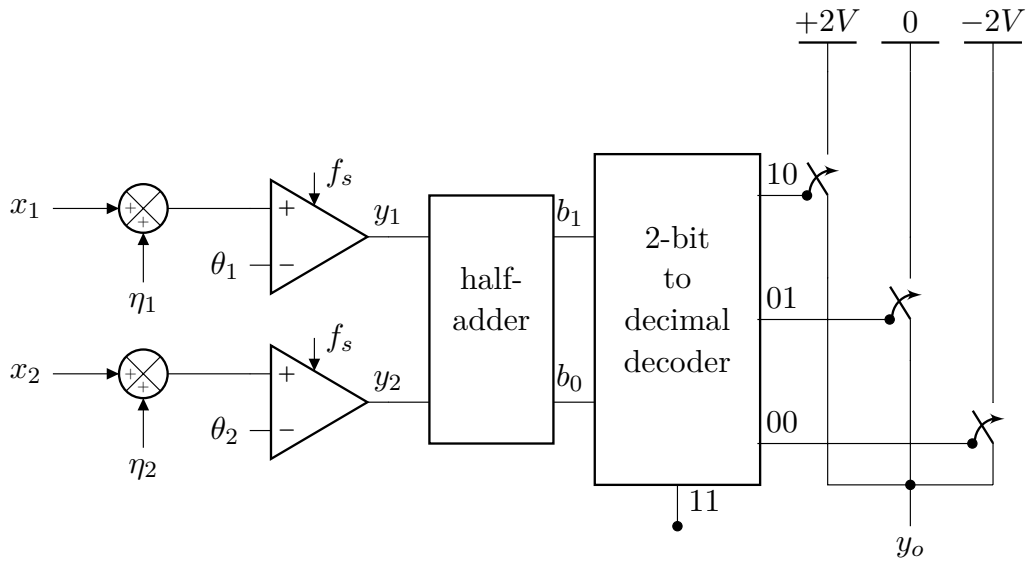
Figure C-1: The complete block diagram of the SR-based adder with a decimal output.

presented in Figure C-2. This alternative only needs three digital gates in addition to the SR fundamental blocks and the switching circuits.
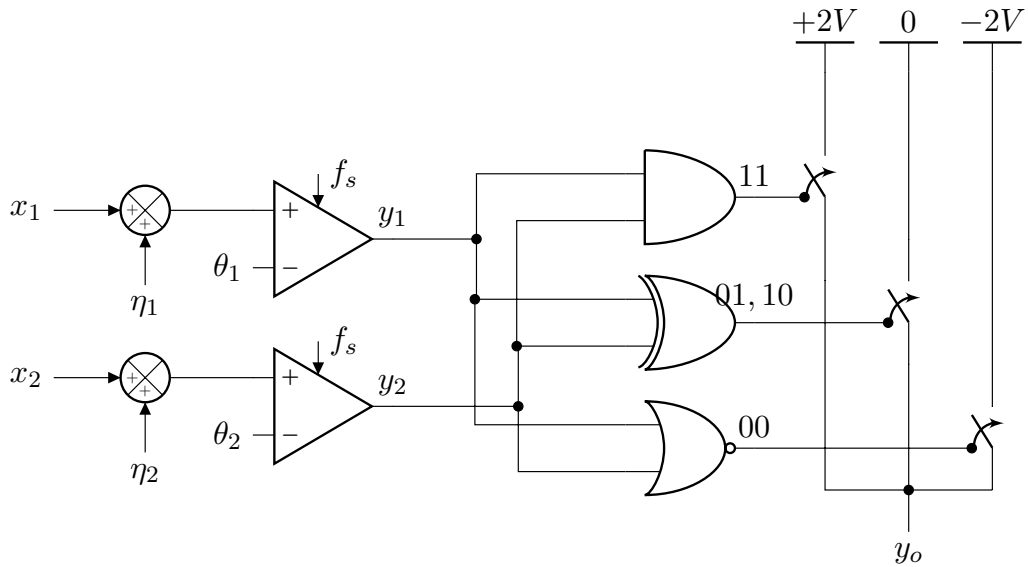
Figure C-2: The proposed alternative for a 2 inputs SR-based adder with a decimal output.

Effects of Noise Distribution to the Performance of Stochastic Resonance-Based Fundamental Building Blocks

Noise can be distinguished based on two characteristics: its distribution and power spectral density. In this thesis, Gaussian white noise is mainly used because a Gaussian distribution is the most abundant in real life, while white noise is usually found in electronics, well-defined, and can be easily simulated. However, this certainly does not mean that a Gaussian white noise is the best noise to use in stochastic resonance (SR)-based systems. In this appendix, two types of white noise distributions, Gaussian and uniform, will be compared.

D-1 Transfer Function of an SR-based Fundamental Building Block Subjected to a Gaussian or Uniformly Distributed Noise

Mathematically, the cumulative distribution function (CDF) of a Gaussian distributed signal is formulated by

$$F(z) = \frac{1}{2}\left(1 + \operatorname{erf}\left(\frac{z}{\sigma\sqrt{2}}\right)\right) \tag{D-1}$$

where $\mathrm{erf}(x)$ is the error function. Consecutively, the CDF of a uniformly distributed signal is

$$
F(z) = \begin{cases} 0 & z < -\sigma\sqrt{3} \\[2mm] \dfrac{1}{2}\left(1 + \dfrac{z}{\sigma\sqrt{3}}\right) & -\sigma\sqrt{3} \le z < \sigma\sqrt{3} \\[2mm] 1 & z \ge \sigma\sqrt{3} \end{cases} \qquad . \tag{D-2}
$$

By substituting (D-1) to (A-1), it can be found that, for $\theta = 0$, the transfer function of the SR-based fundamental building block is equal to the error function [22]. The method applies to all CDFs, therefore it can also be done for the CDF of a uniformly distributed white noise.

Figure D-1 shows the transfer functions of an SR-based fundamental building block. The transfer function of the Gaussian and uniformly distributed noises are plotted in red and blue, respectively. There are several points that can be deduced from the graph. Firstly, around $x = 0$, the slope of the Gaussian distributed noise-induced system is steeper than that of the uniform CDF. This means that the gain produced by an SR-based system subjected to a Gaussian noise will be larger than the one induced to a uniform noise. Secondly, the slope of the uniformly distributed noise-induced system is linear, while the slope of the Gaussian one changes over the range of $-\sigma\sqrt{3} \le x < \sigma\sqrt{3}$. This means that, over the aforementioned range, an SR-based system subjected to a uniform noise will produce constant gain at every value of x, while the same system subjected to a Gaussian noise will amplify the signal with different gains for different values of x. Finally, the uniformly distributed noise-induced system saturates very abruptly once x is outside its linear region, while the Gaussian distributed noise-induced system saturates more smoothly. Moreover, for the same value of σ, the uniformly distributed noise-induced block will saturate faster than the Gaussian one. These three points will affect the distortion behavior, and consequently the output noise of SR-based systems.
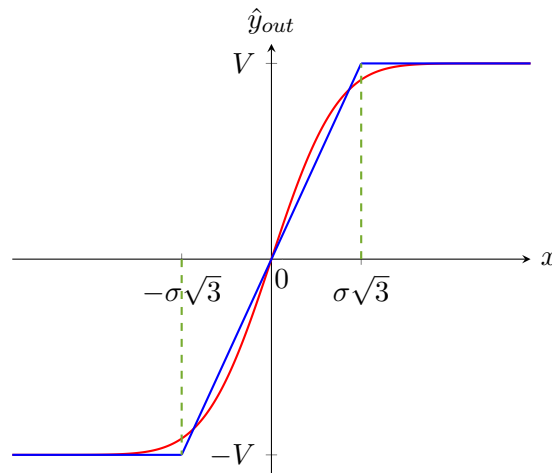
Figure D-1: Transfer function of an SR-based fundamental building block subjected to Gaussian distributed noise (in red) and uniformly distributed noise (in blue).

D-2   Distortion

Figure D-2a shows the least-square error (LSE) gain for SR-based blocks that are subjected to either Gaussian or uniform noise. The input signal is a sinusoid with a unity amplitude. The purple and black dashed lines are the linear gain for each block, respectively. Conforming with the analyses done in the previous paragraph, the Gaussian distributed noise-induced system provides larger gains in the linear region but the uniformly distributed noise-induced block becomes perfectly linear for $\sigma \geq \frac{1}{\sqrt{3}}$. Due to the linearity of the uniformly distributed noise-induced block, its distortion power is always equal to or lower than that of the Gaussian distributed noise-induced block as shown in Figure D-2b.

(a)

(b)
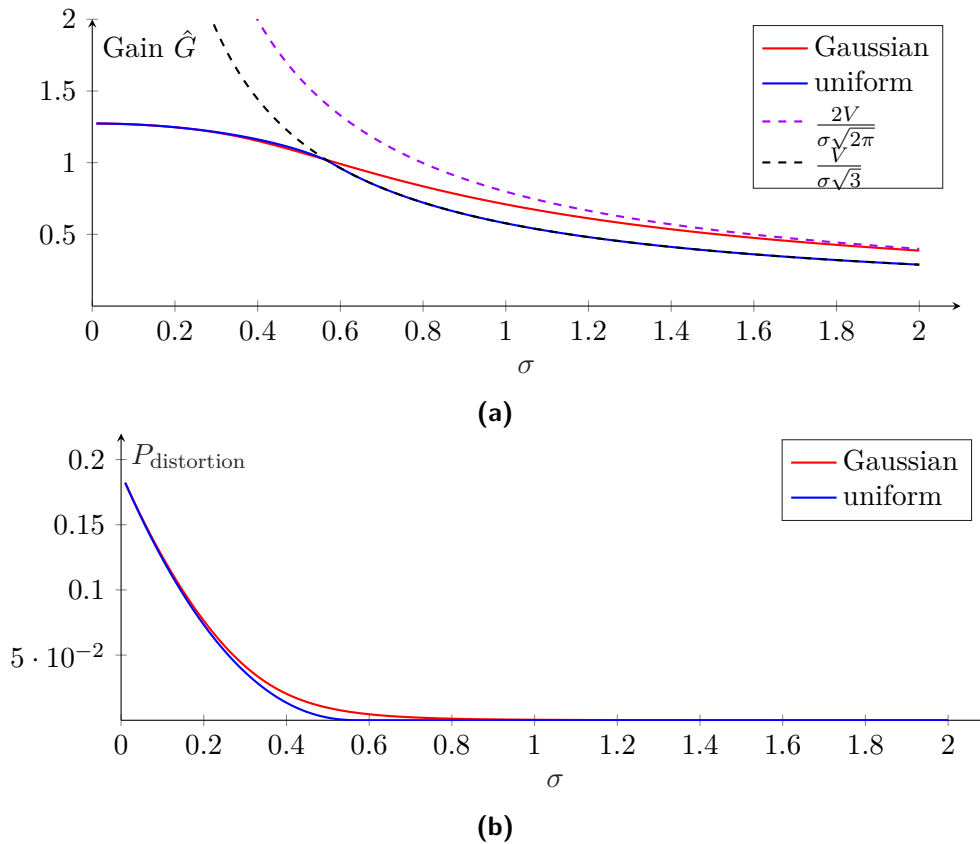
Figure D-2: The distortion for a sinusoidal input with a unity amplitude and frequency. V is set to 1. (a) The LSE gain and the predicted linear gain. (b) The distortion power.

D-3   Output Noise

Since the color of both noises are white, the output noise power can be calculated with (3-14). The noise power depends on the squared value of the output, and because the uniformly distributed noise-induced system provides smaller gains, it will have a larger noise power than that of the Gaussian distributed noise-induced system, as shown in Figure D-3. The higher noise power and smaller gain will make the signal-to-noise ratio (SNR) of a uniformly dis-

tributed noise-induced system smaller than the SNR of a Gaussian distributed noise-induced system, shown in Figure D-4.

D-4   Signal-to-Noise-and-Distortion Ratio (SNDR)

The SNDRs of both systems are presented in Figure D-5. The graph can be divided into two regions: the lower and higher noise regions. In the lower noise region, the uniformly distributed noise-induced system has an SNDR that is higher than or equal to that of the Gaussian one, while the opposite is true in the higher noise region. It is worth noting that the difference of SNDR peaks between the two systems is approximately 2 dB.

For Gaussian noise, a better averaging technique will result in shifting the SNDR peak to the higher noise region. This is because, as the noise power goes down due to the averaging, the system can afford to decrease the distortion power by increasing the noise, although this also means that the signal power will go down.

Meanwhile, for uniform noise, the SNDR peak location will always be found near $\sigma_0 = \frac{\max |x|}{\sqrt{3}}$. At this point, the system is entirely linear and thus, its SNDR is equal to its SNR. Since the SNR goes down as σ increases, better averaging techniques always makes the SNDR peak location get closer to σ_0 .

From these findings, It is relatively easy to determine the noise intensity σ that will provide near-best performance for a uniform white noise. Provided that information about $\max |x|$ can be obtained, it is a safe bet to set $\sigma = \frac{\max |x|}{\sqrt{3}}$ since the SNDR peak location will be around that value.
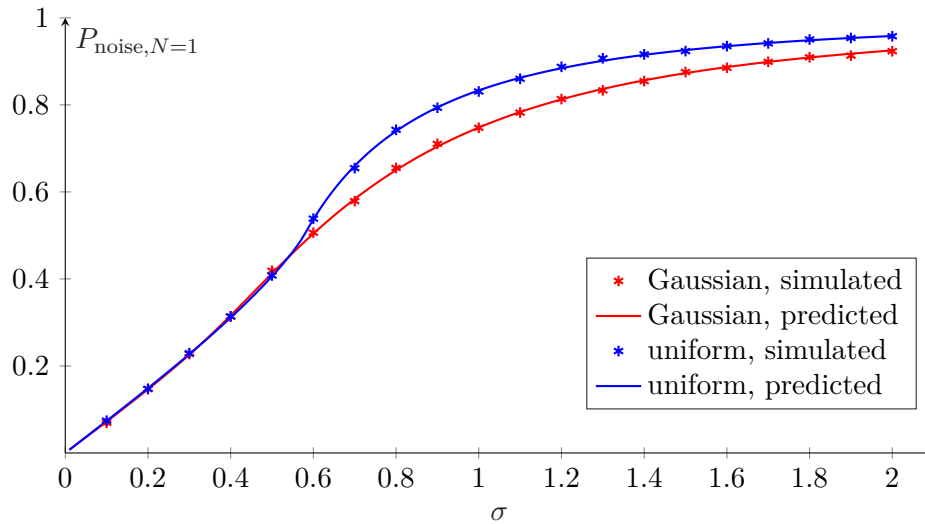
(a)
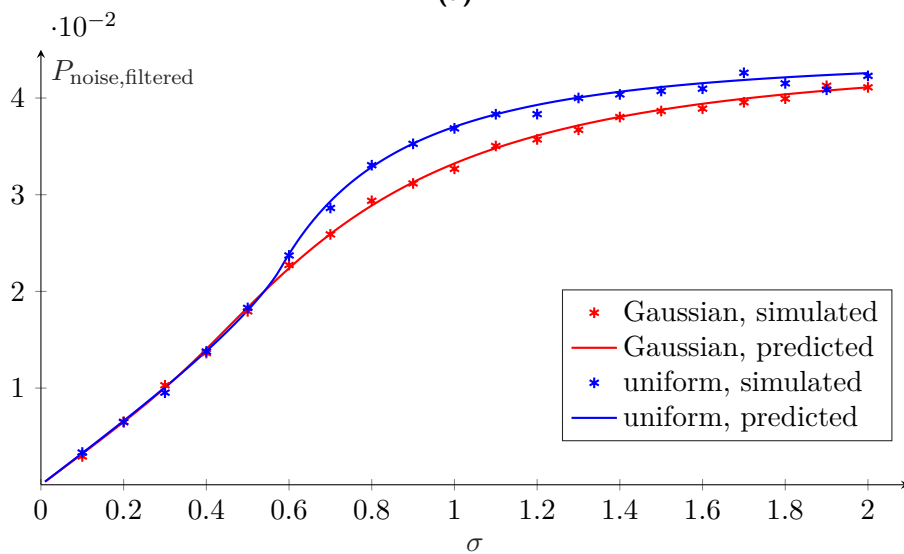
(b)

Figure D-3: The output noise for a sinusoidal input with a unity amplitude and frequency, sampled with a sampling frequency of 1 kHz. V is set to 1. The asterisks mark the simulated results and the solid lines are the predicted results based on the formula. (a) The noise power of the unparalleled system. (b) The noise power of the system filtered by a second order Butterworth LPF with cut-off frequency of 20 Hz.
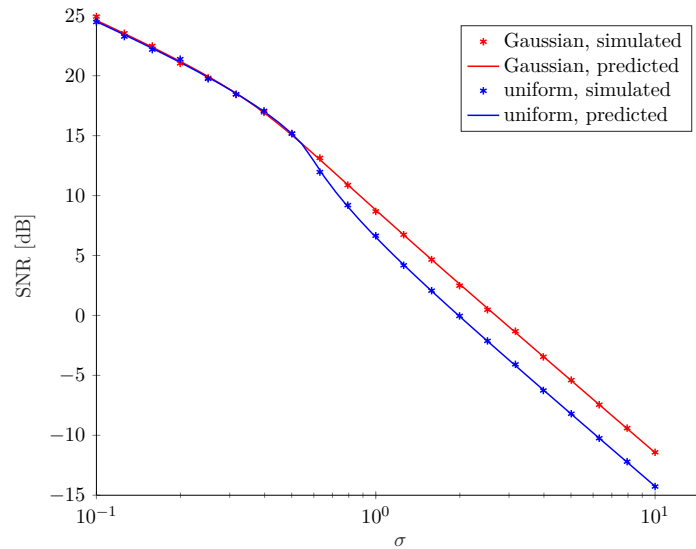
Figure D-4: Signal-to-noise ratio for a sinusoidal input with a unity amplitude and frequency, sampled with a sampling frequency of 1 kHz and filtered by a second order Butterworth LPF with cut-off frequency of 20 Hz. V is set to 1. The asterisks mark the simulated results and the solid lines are the predicted results based on the formula. For the majority of σ, the uniformly distributed noise-induced system has lower SNR.
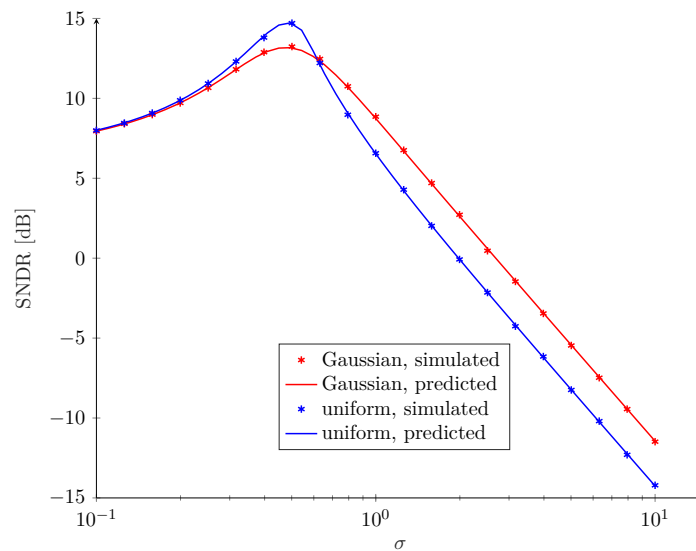
Figure D-5: Signal-to-noise-and-distortion ratio for a sinusoidal input with a unity amplitude and frequency, sampled with a sampling frequency of 1 kHz and filtered by a second order Butterworth LPF with cut-off frequency of 20 Hz. V is set to 1. The asterisks mark the simulated results and the solid lines are the predicted results based on the formula. In the lower noise region, the uniformly distributed noise-induced system has SNDR that is higher than or equal to that of the Gaussian one, while the opposite is true in the higher noise region.

Bibliography

[1] H. A. Hjortland, *Sampled and continuous-time 1-bit signal processing in CMOS for wireless sensor networks.* PhD thesis, University of Oslo, 2016.

[2] M. D. McDonnell, N. G. Stocks, C. E. M. Pearce, and D. Abbott, *Stochastic Resonance: from Suprathreshold Stochastic Resonance to Stochastic Signal Quantization.* Cambridge, UK: Cambridge University Press, 2008.

[3] M. Kawaguchi, H. Mino, K. Momose, and D. M. Durand, "Stochastic resonance with a mixture of sub-and supra-threshold stimuli in a population of neuron models," in *2011 Annual International Conference of the IEEE Engineering in Medicine and Biology Society*, pp. 7328–7331, Aug 2011.

[4] R. Benzi, G. Parisi, A. Sutera, and A. Vulpiani, "Stochastic resonance in climatic change," *Tellus*, vol. 34, pp. 10–16, Feb. 1982.

[5] S. Fauve and F. Heslot, "Stochastic resonance in a bistable system," *Physics Letters*, vol. 97A, pp. 5–7, Aug. 1983.

[6] B. McNamara, K. Wiesenfeld, and R. Roy, "Observation of stochastic resonance in a ring laser," *Physical Review Letters*, vol. 60, pp. 2626–2629, June 1988.

[7] J. K. Douglass, L. Wilkens, E. Pantazelou, and F. Moss, "Noise enhancement of information transfer in crayfish mechanoreceptor by stochastic resonance," *Nature*, vol. 365, pp. 337–340, Sept. 1993.

[8] K. Wiesenfeld, D. Pierson, E. Pantazelou, C. Dames, and F. Moss, "Stochastic resonance on a circle," *Physical Review Letters*, vol. 72, pp. 2125–2129, Apr. 1994.

[9] J. J. Collins, C. C. Chow, and T. T. Imhoff, "Aperiodic stochastic resonance in excitable systems," *Physical Review E*, vol. 52, pp. R3321–R3324, Oct. 1995.

[10] C. Nicolis, "Stochastic aspects of climatic transitions - response to a periodic forcing," *Tellus*, vol. 34, pp. 1–9, Feb. 1982.

[11] M. D. McDonnell and D. Abbott, "What is stochastic resonance? definitions, misconceptions, debates, and its relevance to biology," *PLoS Computational Biology*, vol. 5, pp. 1–9, May 2009.

[12] M. D. McDonnell, D. Abbott, and C. E. M. Pearce, "A characterization of suprathreshold stochastic resonance in an array of comparators by correlation coefficient," *Fluctuation and Noise Letters*, vol. 2, pp. L205–L220, Sept. 2002.

[13] B. Andò and S. Graziani, *Stochastic resonance: theory and applications.* London, UK: Kluwer Academic Publishers, 2000.

[14] N. G. Stocks, "Suprathreshold stochastic resonance in multilevel threshold systems," *Physical Review Letters*, vol. 84, pp. 2310–2313, Mar. 2000.

[15] N. Storey, *Electronics: a Systems Approach.* Essex, England: Pearson Education Limited, fourth ed., 2009.

[16] P. Ivanis and D. Drajic, *Information Theory and Coding: Solved Problems.* Cham, Switzerland: Springer International Publishing, 2017.

[17] D. G. Luchinsky, R. Mannella, P. V. E. McClintock, and N. G. Stocks, "Stochastic resonance in electrical circuits. ii. nonconventional stochastic resonance," *IEEE Transactions on Circuits and Systems II: Analog and Digital Signal Processing*, vol. 46, pp. 1215–1224, Sep 1999.

[18] J. F. Kaiser, "On a simple algorithm to calculate the 'energy' of a signal," in *International Conference on Acoustics, Speech, and Signal Processing*, pp. 381–384 vol.1, Apr 1990.

[19] J. F. Kaiser, "Some useful properties of teager's energy operators," in *1993 IEEE International Conference on Acoustics, Speech, and Signal Processing*, vol. 3, pp. 149–152 vol.3, April 1993.

[20] S. Hiseni, C. Sawigun, and W. A. Serdijn, "Dynamic translinear nonlinear energy operator," in *2009 European Conference on Circuit Theory and Design*, pp. 153–156, Aug 2009.

[21] S. Mukhopadhyay and G. C. Ray, "A new interpretation of nonlinear energy operator and its efficacy in spike detection," *IEEE Transaction on Biomedical Engineering*, vol. 45, pp. 180–187, Feb. 1998.

[22] D. P. N. Mul, "Characterization and design of stochastic resonance analog-to-digital converter for biomedical application," Master's thesis, Technische Universiteit Delft, Delft, the Netherlands, to appear 2017.

[23] D. Leszczyńska-Jasion and P. L. upkowski, "Erotetic search scenarios and three-valued logic," *Journal of Logic, Language and Information*, vol. 25, pp. 51–76, Mar. 2016.

[24] T. N. Alotaiby, S. A. Alshebeili, T. Alshawi, I. Ahmad, and F. E. A. El-Samie, "EEG seizure detection and prediction algorithm: A survey," *EURASIP Journal on Advances in Signal Processing 2014*, vol. 1, pp. 1–21, Dec. 2014.

Glossary

List of Acronyms

SR	stochastic resonance
ADC	analog-to-digital converter
SNR	signal-to-noise ratio
dB	decibel
RMS	root-mean-square
SNDR	signal-to-noise-and-distortion ratio
PDF	probability density function
TEO	Teager Energy Operator
NEO	Nonlinear Energy Operator
AP	action potential
CDF	cumulative distribution function
ENBW	equivalent noise bandwidth
LPF	low-pass filter
LSE	least-square error
LHS	left-hand side
RHS	right-hand side
PSD	power spectral density
FP	false positive
FN	false negative
TP	true positive

List of Symbols

Abbreviations

Δf_{ENBW}	equivalent noise bandwidth
ΔU	height of the potential barrier
erf	error function
η	noise
$\hat{G}$	least-square error gain
$\hat{y}_{out}$	expected value of the output signal
$\lfloor \cdot \rfloor$	floor function
$\mathbf{E}[\cdot]$	expected value
ν_k	Kramers rate
$\oplus$	exclusive OR
$\Pr(\cdot)$	probability
$\prod$	product notation
$\psi(\cdot)$	output of TEO
ρ	correlation coefficient
σ	standard deviation of noise
$\sum$	summation notation
τ	time constant
τ_k	Kramers time
$\mathrm{cov}[\cdot]$	covariance
$\mathrm{sgn}[\cdot]$	signum function
$\mathrm{var}[\cdot]$	variance
θ	threshold level
A	amplitude
$a(n)$	discrete-time signal
$a(t)$	continuous-time signal
$F(\cdot)$	cumulative distribution function
f_0	signal frequency in Hz
f_s	sampling frequency
f_X	probability density function of random variable X
$H(\cdot)$	information entropy
$I(\cdot)$	mutual information
P	power
V	output value of comparators
x	input signal
y	output signal
y_{out}	averaged output signal